SPECTROSCOPIC AND ELECTROCHEMICAL STUDIES OF OPTICALLY ACTIVE BIPYRIDYL COMPLEXES

A thesis submitted to the

UNIVERSITY OF GLASGOW

for the degree of

DOCTOR OF PHILOSOPHY

in the Faculty of Science

by

BRIAN CAMERON NOBLE BSc (Hons) CChem MRSC

Department of Chemistry
University of Glasgow

ProQuest LLC.
789 East Eisenhower Parkway
P.O. Box 1346
Ann Arbor, MI 48106 – 1346

For my family

ACKNOWLEDGEMENTS

I wish to thank my supervisor, Dr Robert D Peacock, for all his advice and encouragement throughout the course of this work.

I would like to thank the members of my family for all their help and support over the past few years. I would also like to thank Susie for her love.

I acknowledge financial support from the Science and Engineering Research Council.

CONTENTS

SUMMARY

The tris(2,2′-bipyridine) complexes of ruthenium(II) and osmium(II) have been synthesised and optically resolved. The singly, doubly and triply reduced complexes have been prepared electrochemically and their circular dichroism and luminescence spectra have been measured. Investigation of the absorption, circular dichroism and luminescence spectra of the complexes and their reduced analogues strongly suggest that the added electrons are localised on the individual bipyridine ligands of the complexes. Hence the complexes are best formulated as $[M(bipy)_n(bipy^-)_{3-n}]^{(n-1)+}$, where M = Ru, Os and n = 0,1,2 and 3. In addition, a chemical reduction technique using lithium metal has been developed. This has enabled the infrared spectra of the triply reduced complexes to be measured. The triply reduced ruthenium complex has been found to racemise in dry acetonitrile but is optically stable in dimethylformamide. This has been attributed to a weakening of the ligand field of bipyridine when it is reduced to the anion.

Lithium 2,2′-bipyridinyl has been synthesised and complexed with the chiral co-ordinating ligands (-)-sparteine and R and S-tetra-N,N,N′,N′-methylpropane-1,2-diamine whereupon its circular dichroism spectra have been measured.

The tris(2,2′-bipyridine)iridium(III) complex has been synthesised and optically resolved and its hitherto unknown circular dichroism spectrum has been measured. The complex has been chemically reduced and in addition to the triply reduced complex the quadruply reduced complex has also been synthesised and their absorption and circular dichroism spectra have been measured. Investigation of the circular dichroism spectra again suggest that the added electrons are localised on the individual bipyridine ligands of the complexes.

CHAPTER 1

INTRODUCTION

SYNOPSIS

Blau[1] first synthesised 2,2′-bipyridine (bipy) (Figure 1) in 1888,

FIGURE 1: 2,2′-bipyridine

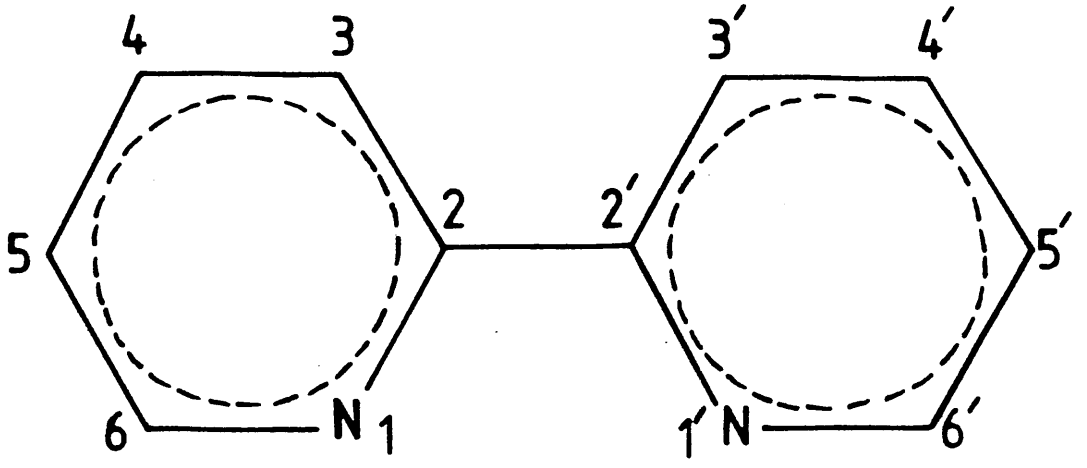

and it was he who first noticed[1] the intense red substance formed in the reaction of the free base with iron(II) salts and subsequently isolated a series of salts of the formula $[Fe(bipy)_3]X_2$[2]. The formation and reactions of $[Fe(bipy)_3]X_2$ compounds were inexplicable by the then current Blomstrand-Jorgensen structural theory but were explained simply and naturally by Werners octahedral model[3] for co-ordination compounds which had been received with widespread scepticism despite the vast array of stereochemical evidence by which it was supported. It was not until nearly 20 years later when Werner[4] demonstrated its correctness by resolving racemic chloro-amine-bis(ethane-1,2-diamine) cobalt(III) chloride with silver d-bromocamphorsulphonate into its two optically active enantiomeric forms, the dissymmetry of which could not have been foreseen without the hypothesis of co-ordination, that the theory received immediate and almost universal recognition. The

prediction and subsequent detection of optical activity in metal complexes sufficed to place the fundamental doctrine of co-ordination beyond the reach of further controversy.

A year after his first resolution, Werner[5] succeeded in resolving Blau's tris(2,2'-bipyridine)iron(II) bromide using ammonium d-tartrate; interest in these chelate molecules then lapsed for nearly 20 years. It was revived by the discovery of Hammett, Walden and Chapman[6] that the iron(II) complex could be used as a valuable redox indicator and by the preparative researches of bipy complexes by Morgan and Burstall, Barbieri, Pfeiffer and Jaeger (reviewed by Brandt et al[7]).

$[Ru(bipy)_3]Cl_2$ was first prepared and resolved by Burstall in 1936[8] and it was found to be appreciably more stable than the analogously constituted ferrous $[Fe(bipy)_3]X_2$ and nickel salts $[Ni(bipy)_3]X_2$. The rate of racemisation of the ruthenium complex was found to be extremely slow; the bromide salts retained their optical activity indefinitely at room temperature not only in the solid state but also in 0.1% solution, whereas the rotations of the iron and nickel salts became negligible after about two hours in aqueous media. $[Os(bipy)_3]Br_2$ was prepared and resolved by Burstall et al[9], and like the Ru(II)[8] analogue, it was found to be optically stable. It was found that the Ru(II) and Os(II) complexes could be easily oxidised to the Ru(III)[10] and Os(III) complexes respectively. When the Ru(III) complex was immediately reduced back to Ru(II), no loss of optical activity was detected[10]. However, on standing the Ru(III) complex lost about half its optical activity in one day whereas the analogous Os(III) complex[9] was completely optically stable.

$[Rh(bipy)_3]Cl_3$ was first prepared in 1935 by Jaeger et al[11], but a suitable method for resolving the complex was not found until 1973[12,13].

The $[Ir(bipy)_3]Cl_3$ complex proved to be the most difficult of the cobalt triad to make. A successful synthesis was not achieved until 1972 by Demas et al[14] and when this work was started the complex had not been resolved.

Much work has been done in characterising and assigning the absorption,[15-20] circular dichroism[13,18,21-25] and luminescence (reviewed by Kalyanasundaram[20]). Spectra of the tris(2,2′-bipyridine)metal complexes and in these contexts, the complex $[Ru(bipy)_3]^{2+}$, has received the most attention.

The luminescence spectrum of $[Ru(bipy)_3]^{2+}$ was first measured in 1959 by Paris and Brandt[26] who initially assigned the emission as due to the $\pi^* \rightarrow$ d charge transfer fluorescence. This was disputed by later authors who assigned it as due to $d^* \rightarrow$ d ligand field phosphorescence,[27] $d^* \rightarrow$ d ligand field fluorescence,[28] charge transfer,[15-29] $\pi^* \rightarrow$ d charge transfer phosphorescence[30] and finally as $\pi^* \rightarrow$ d charge transfer luminescence with no specific multiplicity.[29] The reasons for the shift in assignments are wide, ranging from the identification of certain absorption bands as due to impurities, arguments based on similarity/dissimilarity of the absorption, emission bands of other $\underline{d}^6$ -complexes and long emission lifetimes usually associated with spin-forbidden triplet-singlet transitions. It is now firmly established that the luminescence from the $[Ru(bipy)_3]^{2+}$ complex is essentially of charge transfer type and spin-forbidden in character, at least at 77K.

It was for many years customary to assume that in the thermally equilibrated excited state of $[Ru(bipy)_3]^{2+}$, $[Ru(bipy)_3]^{2+*}$, an electron was transferred from the metal core to an acceptor orbital delocalised over all three ligands [32-35]; that is, that $[Ru(bipy)_3]^{2+*}$ belonged to the same D_3 point group as the ground state complex.[36] As a

consequence there have been difficulties in explaining the photoemission spectrum[37-39] and the behaviour of related mixed ligand complexes, which are asserted to exhibit a higher electronic than molecular geometry.[33,35]

The question as to whether the electrons located on the ligands were delocalised in a molecular orbital extending over all three ligands or whether they were localised in the orbitals of the individual ligands remained to be solved. Localised in this text means the electrons remain on the ligands within the absorption timescale. Resonance Raman studies of the excited state indicated that $[Ru(bipy)_3]^{2+*}$ contained an identifiable reduced bipy ligand ($bipy^-$),[40,41] but it was still to be demonstrated unequivocally that bipy and $bipy^-$ exist simultaneously as distinct ligands in $[Ru(bipy)_3]^{2+*}$. This was recently accomplished by Woodruff and co-workers[42] in further resonance Raman studies. The formulation of $[Ru(bipy)_3]^{2+*}$ as $[Ru(III)(bipy)_2(bipy^-)]^{2+}$ established by resonance Raman studies, was independently confirmed by a series of flash-photolysis studies[43-46] which culminated in a detailed assignment[46] of the excited-state absorption spectrum based on the localised charge-transfer formulation above.

Evidence for symmetry reduction in the excited states was also found for the tris(2,2′-bipyridine)complexes of iridium[38] and osmium[42,47] indicating that the ruthenium complex was not unique in its properties.

After the controversy of localisation versus delocalisation in the excited state of $[Ru(bipy)_3]^{2+}$ had appeared to have been resolved, Ferguson et al[48,49] performed a series of experiments on these complexes in the solid state. From these experiments it was concluded that there was no evidence to support a complete localisation of

charge as an intrinsic property of the excited state, either singlet or triplet and it was shown that a D_3 model accounted for all of the essential features of the luminescence. Yersin et al[50,51] also found that a description of the emitting states of single crystals of $[Ru(bipy)_3](PF_6)_2$, within the D_3' double group, also accounted very well for the symmetry properties of the excited states detected in the temperature dependent polarised emission spectra. It was therefore concluded that the symmetry reduction was not an intrinsic property of the excited state complex, but might originate from the interaction of polar solvent molecules inducing distortion in the excited-state complex. However, it has since been pointed out that the interpretation of these results using a localised excited state model would be equally as valid.[52]

Further experiments on the time-resolved luminescence[53] and the magnetic circularly polarised luminescence spectra[54] of $[Ru(bipy)_3]^{2+}$ by Ferguson et al, led them to the conclusion that there may be a relaxation from an initial delocalised state to a localised state which takes place rapidly in fluid solutions but is inhibited in rigid media. These results have since been questioned by Kliger and co-workers[55] who suggest that the excitation in the MLCT triplet-state remains single ligand localised regardless of the rigidity of the solvent.

The debate on localisation versus delocalisation in the excited state of $[Ru(bipy)_3]^{2+}$, still goes on.

Around the time that the experiments were being performed on the excited state properties of the tris(2,2'-bipyridine) metal complexes, interest developed in the electrochemistry of the complexes when it was found that in addition to a reversible one-electron oxidation, $[Ru(bipy)_3]^{2+}$ also possessed three consecutive, reversible one-electron

reductions.[56,57] The three reductions were originally assigned[56,57] as metal based, corresponding to Ru(I) for the first reduction, Ru(0) for the second reduction and Ru(-1) for the third reduction. The reductions were later assigned as ligand based[58] and interest grew as to whether the electrons were localised on the individual bipy ligands implying a symmetry lower than D_3 for the first two reduction products, as in the excited state complex, or delocalised over all three. Evidence from electrochemical measurements,[59] e.s.r.,[60-62] absorption[63] and Raman spectroscopy[64,65] all suggested that the reduced compounds contained both bipy and $bipy^-$ ligands so that, for example, the first reduction product was formulated as $[Ru(bipy)_2(bipy^-)]^+$, the second as $[Ru(bipy)(bipy^-)_2]$ and the third as $[Ru(bipy^-)_3]^-$.

The electron spin resonance (e.s.r.)[60-62] of the reduced products of $[Fe(bipy)_3]^{2+}$,[60] $[Ru(bipy)_3]^{2+}$ [60,61] and $[Os(bipy)_3]^{2+}$ [62] suggested that the added electrons were localised on the individual ligands rather than delocalised over all three. In the singly and doubly reduced products it was found that the electrons hop from one ligand to another, broadening the e.s.r. line, whereas in the triply reduced species, one electron is on each ligand and no hopping was observed. Further evidence for this electron hopping came from the observation of a ligand-ligand intervalence charge transfer (IVCT)[66] absorption band at 4000 cm^{-1} for the singly and doubly reduced products in agreement with the e.s.r. results.[60] The resonance Raman spectra of the singly and doubly reduced species of $[Ru(bipy)_3]^{2+}$ [64] and $[Fe(bipy)_3]^{2+}$ [65] show the presence of both shifted and unshifted bipy vibrational energies indicating that there are two distinct chromophores in the reduced complex consistent with a localised model of the redox orbital. Recently a ^1H n.m.r. study[67] of the reduced paramagnetic tris(2,2′-bipyridine) complexes of Fe(II), Ru(II) and Os(II) has been

done by Hanck and co-workers from which it was concluded that the unpaired electrons existed in spatially isolated orbitals that were close in proximity but had minimal interaction and consideration of the line widths of $[M(bipy)_3]^+$ (M = Fe, Ru, Os) indicated that the ^1H n.m.r. permitted measurement of the electron hopping rate constants for the species $[M(bipy)_3]^+$ and $[M(bipy)_3]$ which were in agreement with the e.s.r. data.[60]

Notice that the localised description implies, perhaps unexpectedly, that the charge distribution in the singly and doubly reduced complexes is asymmetric, unless rapid electron hopping makes the two models converge.

These two separate lines of research on the excited state of $[Ru(bipy)_3]^{2+}$ and on the reduced complexes of $[Ru(bipy)_3]^{2+}$ have recently been bridged by Braterman et al.[68] As is pointed out, the emitting state of $[Ru(bipy)_3]^{2+}$, $[Ru(III)(bipy)_2(bipy^-)]^{2+}$, is formally derivable from the singly reduced complex $[Ru(II)(bipy)_2(bipy^-)]^+$ by the removal of a single $d(a_1)$ electron, therefore the excited state of $[Ru(bipy)_3]^{2+}$ could be semiquantitatively modelled on the singly reduced complex of $[Ru(bipy)_3]^{2+}$.

In summary, the work that has been done on the reduced tris(2,2′-bipyridine complexes of ruthenium and osmium (reviewed by DeArmond et al[69]) has been mainly confined to the cyclic voltammetry, e.s.r., n.m.r. and resonance Raman studies. The absorption spectra of the ruthenium complexes had been measured but this had not been accomplished for the osmium complexes. For the analogous iridium complexes, only the cyclic voltammetry and the absorption spectra of the reduced complexes had been previously measured. This left a large gap in the experimental studies of these reduced complexes, so the work in this thesis was undertaken in an attempt

to fill the void and gain more information on the reduced complexes and more evidence to support either the localised or delocalised model of the reduced complexes.

As there was evidence of charge localisation in the luminescent states of $[Ru(bipy)_3]^{2+*}$,[37,39] an obvious experiment was to measure the luminescence spectra of the reduced complexes to see if this could give any evidence that the added electrons were localised on the individual bipy ligands. The luminescence spectra of the reduced complexes of $[M(bipy)_3]^{2+}$ (M = Ru, Os, Ir) were measured and as shall be demonstrated later, the spectra gave conclusive evidence that charge localisation occurs in the luminescent states of the reduced complexes.

In the past, all the literature preparations of the reduced complexes of $[Ru(bipy)_3]^{2+}$ were performed electro-chemically which does not give a convenient method for isolation of the reduced complexes. So a chemical method for preparing the reduced complexes was developed. This has allowed the infra-red spectra of the triply-reduced complexes to be measured, which had hitherto not been possible.

It has been shown[21] that the magnitudes of the effects due to π-electron delocalisation throughout the tris(2,2′-bipyridine)metal complexes are not large. It has been concluded that the absorption of the ligands in the tris-complexes can be thought of as arising from slightly perturbed transitions of the free ligand. Similarly, in the reduced complexes the added electrons have been shown to be localised on the individual bipy ligands. π-electron delocalisation between the ligands must therefore be small and the reduced ligands in the complex could also be thought of as the slightly perturbed "free" reduced ligands. This means that many of the properties of the "free" reduced ligand should be very

similar to those of the reduced ligand in the complex. The "free" reduced ligand has been examined in the past[70-74] but again there are gaps in the experimental knowledge of the compound. Therefore, to help in the interpretation of the experimental results for the reduced complexes, "free" reduced bipy was examined in more detail and the measurement of its infra-red, Raman, luminescence and circular dichroism spectra have been accomplished.

The circular dichroism spectra for the reduced complexes of ruthenium and osmium tris(2,2´bipyridine) had not been examined in the past and for the analogous iridium complex, the parent ion $[Ir(bipy)_3]^{3+}$ had not even been resolved before. It was not even known whether the reduced complexes were optically stable and so examination of the circular dichroism spectra of the complexes was undertaken.

Mason and co-workers[21-23] had earlier successfully applied the exciton theory of optical activity to explain the c.d.spectra in the region of the ligand $\pi \rightarrow \pi^*$ absorption of the tris-(2,2´-bipyridine) complexes of osmium and ruthenium. The circular dichroism studies in this thesis were carried out in order to see if the exciton theory of optical activity could distinguish between the localised and delocalised theories for the reduced complexes and to extend the studies to include the analogous iridium complexes. Now in the simplest form of the exciton theory it is assumed that there is no π-electron delocalisation between the individual bipy ligands in a tris-chelated complex, so in theory the exciton model should be able to distinguish between a triply reduced complex in which the electrons are localised on the individual bipy ligands from that in which they are delocalised over all three.

In singly and doubly reduced complexes, if the electrons were delocalised

over all three ligands, they could be formulated as $[M(bipy^{\frac{1}{3}-})_3]^+$ and $[M(bipy^{\frac{2}{3}-})_3]$,(M = Os, Ru), respectively, hence all three ligands would be identical, the complex would have D_3 symmetry and they could be described as homo-trischelated complexes. In the localised theory, the complexes could be formulated as $[M(bipy)_2(bipy^-)]^+$ and $[M(bipy)(bipy^-)_2]$ for the singly and doubly reduced complexes respectively. In this case, the complexes would have at the most C_2 symmetry and they could be described as hetero-trischelated complexes. Now the exciton theory of optical activity predicts characteristic spectra for hetero-trischelated complexes as demonstrated by Mason[75-77] and Bosnich[78,79] for the mixed bipy/phenanthroline complexes of osmium and ruthenium, and so in theory, the exciton model should distinguish between singly and doubly reduced complexes in which the electrons are delocalised over all three ligands from that in which they are localised on the individual ligands.

Exciton Theory

The essentials of Fresnel's[80] classical helical model carry over into the quantum mechanical theory of optical rotation in which a charged particle displaced through a helical path undergoes a translatory motion, generating an electric dipole moment, and a rotatory motion, producing a magnetic dipole moment, the two moments being co-linear. In the quantum theory the absorption of light by a dissymmetric molecule promotes a valence electron from one stationary molecular energy state to another and the reorganisation of the electronic charge distribution generates transient electric and magnetic dipole moments. The scalar product of the electric dipole and magnetic dipole transition moment is the rotational strength R_{no} of the transition between the

electronic states Ψ_o and Ψ_n so that,

$$R_{no} = Im\langle o|\underset{\sim}{\mu}|n\rangle\langle n|\underset{\sim}{m}|o\rangle \qquad (1)$$

where $\underset{\sim}{\mu}$ and $\underset{\sim}{m}$ are the electric and magnetic dipole operators respectively, and Im signifies that the imaginary part of the product is to be taken. The rotational strength R_{no} is obtained experimentally from the band area of the circular dichroism absorption due to the transition $\Psi_o \rightarrow \Psi_n$.

The detailed quantum theory of optical activity at present assumes one of three distinct forms, depending upon the particular electronic structure of the molecule and the type of electronic transition considered. In one limiting case, that of molecules containing an inherently dissymmetric chromophore such as the helicenes,[81] each electronic excitation has an intrinsic electric and magnetic dipole transition moment. Calculation of the sign and magnitude of the rotational strength (Equation 1) of a particular transition for a given enantiomer gives, unambiguously, the absolute stereochemical configuration of the enantiomer from its circular dichroism spectrum, providing the electronic transitions are correctly assigned.

The second limiting case is that of the symmetric chromophore in a dissymmetric molecular environment where the substituent groups are virtually inert spectroscopically, absorbing radiation only in the vacuum ultraviolet; for example, saturated carbonyl compounds.[82,83] Here the electronic transitions of the chromophore, which has one or more secondary elements of symmetry, are generally either electric - or magnetic - dipole allowed, or the two moments are orthogonal. No electronic transition of the molecule has a zero-order rotational

strength, but the electric and magnetic dipole transitions of the chromophore are mixed by the static perturbing field, V, due to the dissymmetric substituents, and each resulting transition acquires a first-order rotational strength.

If the symmetric chromophore has two main transitions from the ground state, Ψ_o, one magnetic-dipole allowed to the state, Ψ_a, and the other electric-dipole allowed to the state, Ψ_b, the first order rotational strengths are,

$$R_{ao} = \mathrm{Im}\langle a|\underset{\sim}{m}|o\rangle \langle o|\underset{\sim}{u}|b\rangle \langle b|\underset{\sim}{V}|a\rangle/(E_b - E_a) \qquad (2)$$

and

$$R_{bo} = \mathrm{Im}\langle a|\underset{\sim}{m}|o\rangle \langle o|\underset{\sim}{u}|b\rangle \langle b|\underset{\sim}{V}|a\rangle/(E_a - E_b) \qquad (3)$$

where E_a and E_b are the respective transition energies. These two rotational strengths are equal in magnitude and opposite in sign, and an equivalent sum rule applies in the general case where equation (2) is summed over all electric-dipole transitions of the chromophore and equation (3) over all magnetic-dipole transitions.[84,85]

These two limiting approaches are bridged by the coupled chromophore treatment, due in its classical form to Kuhn,[86-88] developed quantum-mechanically by Kirkwood[89] and modified within the formalism of the exciton theory by Moffitt.[90]

In the classical coupled oscillator theory,[86,87] a dissymmetric molecule contains two or more elastically-bound electrons which are constrained to oscillate along axes with no common origin and no

common plane, and the separation (d) between any given pair of oscillators is small compared to the wavelength of light, so that they experience the same radiation field. If there is no coupling between the two electrons each oscillates independently of the other; if they are coupled the overall charge displacement is helical and there is an in-phase and an out-of-phase coupling mode for each pair of oscillators, the one mode involving a left-handed and the other a right-handed helical charge displacement (Figure 2).

FIGURE 2: The classical coupled oscillator

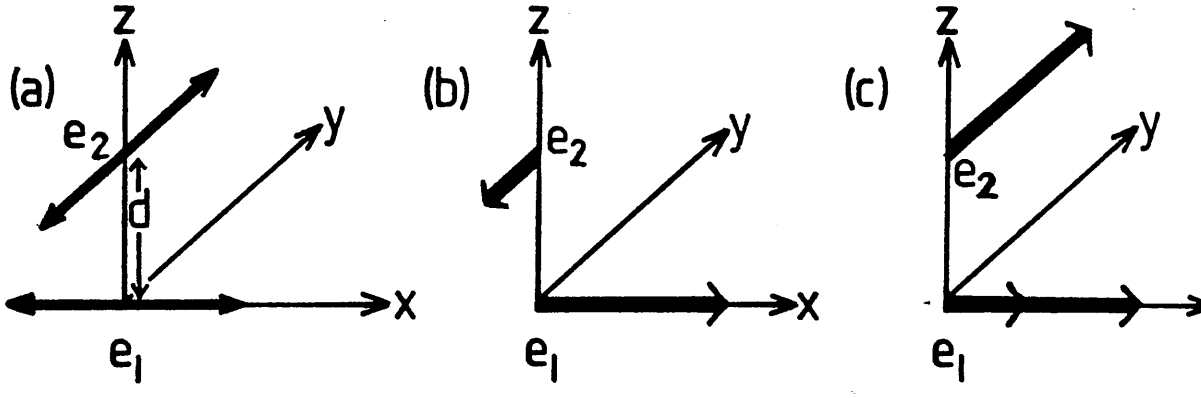

a) No coupling; e_1 and e_2 oscillate independently of each other.

b) e_1 oscillation with coupling; resultant left-handed helical charge displacement.

c) e_2 oscillation with coupling; resultant right-handed helical charge displacement.

For a molecule containing an isolated pair of coupled electronic oscillators the optical activity in the absorption region consists of two circular dichroism bands with equal areas and opposite signs.

More generally the pairs of electronic oscillators in an optically-active molecule interact amongst themselves, redistributing the positive and negative circular dichroism over the frequency range of absorption, but over the spectrum as a whole the sum of the classical equivalents of the rotational strength vanish.

In the quantum mechanical form of the coupled oscillator model the classical oscillators are replaced by the electronic transition moments of the two or more chromophores of the dissymmetric molecule and the exciton optical activity is due to the coupling of the electronic transition moments by Coulombic interaction. The optically-active molecule is regarded as a dissymmetric ensemble of symmetric groups, each with its own characteristic electronic properties and when this multi-chromophoric system absorbs radiation, the excitation energy is not localised in one particular light-absorbing group. The exciton energy transfers rapidly from one chromophore to another during the lifetime of the excited state, and is effectively delocalised over the molecule as a whole. If two or more of the excitation moments of the individual chromophores in the molecule are neither perpendicular nor coplanar, the resultant transition is optically active since the overall charge displacement has a helical form.

At one extreme of the exciton treatment the individual chromophores have allowed electric-dipole transitions which are close in energy or are degenerate, the groups being chemically similar or equivalent and the coupling is then strong. When electron exchange between pairs of groups becomes appreciable, this extreme of the coupled-chromophore model merges with that of the inherently dissymetric chromophore, as in the case of the sterically-hindered

bianthryls.[91]

In a bis- or tris-chelated co-ordination compound containing unsaturated ligands a major source of optical activity is the Coulombic coupling of the allowed $\pi \rightarrow \pi^*$ excitations in the individual ligands, each involving a linear charge displacement, to give an overall resultant helical charge displacement. It is assumed in the simplest treatment, involving degenerate exciton theory, that there is no π-electron delocalisation between the individual ligands, either through the co-ordinated central atom or between nearest-neighbour atoms of different ligands and that the main coupling arises from the instantaneous Coulombic interaction between the electric dipoles of the $\pi \rightarrow \pi^*$ excitations with the same energy in the different ligands of the complex. The former assumption is a good approximation in the case of co-ordination compounds containing unsaturated ligands and a central ion with a closed-shell electronic configuration, such as the tris(acetylacetonato)silicon(IV)[92] ion or tris(catchetyl)arsenic(V) ion[93], as the electron exchange between the π-systems of different ligands is small. In quantitative terms the latter assumption is generally a poor approximation for the transition energies of co-ordination compounds since the dipole moment lengths of the ligand $\pi \rightarrow \pi^*$ transitions are generally of the same order as the distance between the ligands, but qualitatively the point dipole approximation gives the correct energy order for the principal coupling modes of the ligand excitations.[92]

In the case of co-ordination compounds containing a central ion with an open-shell electronic configuration, notably for the phenanthroline and 2,2′-bipyridine complexes of transition-metal ions, both assumptions give rise to uncertainties in the simple exciton analysis of the circular dichroism spectra.[75,94] From investigations[19,21,25] of the spectra of

the tris(2,2′-bipyridine)complexes of osmium(II) and ruthenium(II) it has been concluded that the intense absorption bands in the visible region of the complexes are due to metal-to-ligand charge transfer (MLCT) transitions. The large intensity of the visible absorption implies that charge transfer configurations make an important contribution to the electronic ground state of these complexes[95,96] and so there will be some π-electron exchange between the metal d-orbitals and the π-orbitals of the ligands. An x-ray diffraction study[36] of tris(2,2 -bipyridine) ruthenium(II) hexafluorophosphate revealed a Ru^{II} - N bond length of some 2.056 Å which is shorter than Ru^{III} bond lengths in similar compounds. This is contrary to an expected increase in bond length resulting from a larger ionic radius of Ru^{II} and hence considerable π-bonding between delocalised π* orbitals on the bipy ligands and the metal d-orbitals of the Ru^{II} core was postulated.[36] However the magnitudes of these effects cannot be large as the dipole strength of the absorption bands at 284 nm for $[Ru(bipy)_3]^{2+}$ is approximately three times as large as that of the free ligand[21], so that mixing of these ligand transitions with other ligand excitations or with MLCT transitions cannot be extensive and the effects of π-electron delocalisation can be considered[21] as perturbations to the principal exciton states.

Homo-trischelated Complexes

Consider a trischelated metal complex $[ML_aL_bL_c]^{n+}$ where M is a transition metal ion and L is a symmetrical bidentate ligand (for example $[Ru(bipy)_3]^{2+}$) such that the complex ion has D_3 symmetry (Figure 3). Each ligand has a ground-state and an excited state electronic wave function, x and x′ respectively, and the electric moment of the transition $x \longrightarrow x'$ may be directed along either the long (l) or short (s) in-plane molecular axis (Figure 4). In the absence of electron-exchange

FIGURE 3: Structure of Δ-tris(2,2´-bipyridine)ruthenium(II)

Δ-$[Ru(bipy)_3]^{2+}$

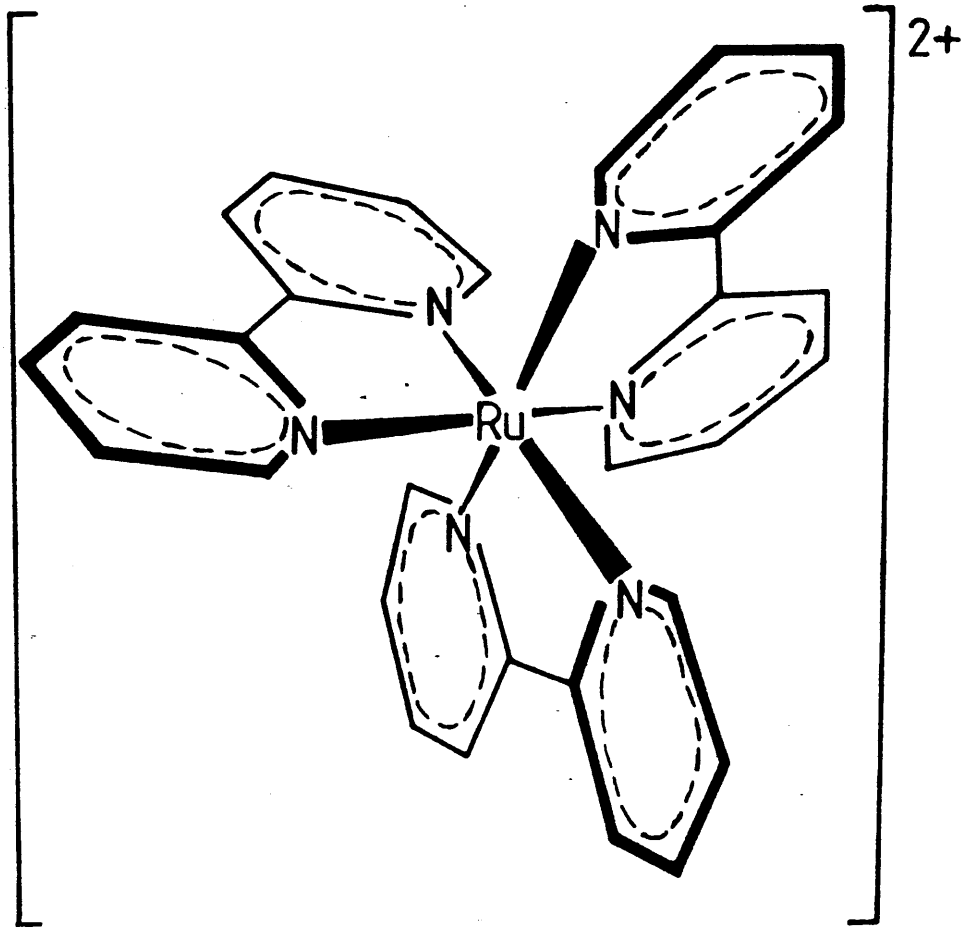

FIGURE 4: The long (l) and short (s) in-plane molecular axes of 2,2′-bipyridine

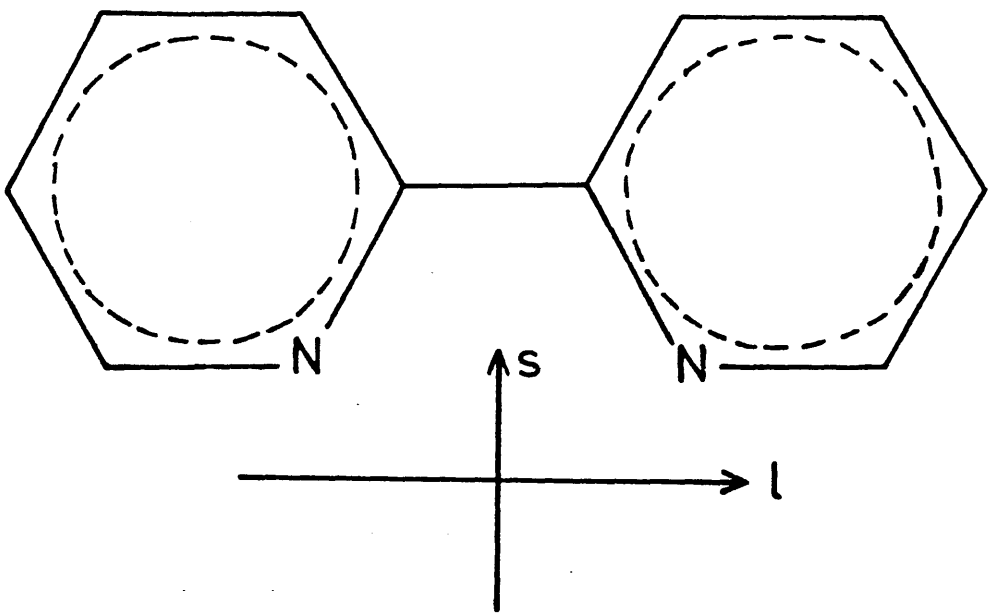

between the ligands, and between the metal ion and the ligands, the ground-state wave function of the complex is represented by the simple product,

$$\Psi_o = x_1 x_2 x_3 \tag{4}$$

and supposing that only one excited state of the individual chromophores of the assembly need be considered, the (singly) excited state wave functions, Φ_i, of the system can be written in the following way,

$$\Phi_1 = x_1' x_2 x_3, \qquad \Phi_2 = x_1 x_2' x_3 \qquad \text{and} \qquad \Phi_3 = x_1 x_2 x_3' \tag{5}$$

where the primes represent excited state wave functions of the long-axis polarised $\pi \rightarrow \pi^*$ transitions. The total wave function, Ψ_j, corresponding to the jth excited state of the assembly, may therefore be expressed as a linear combination of the unperturbed singly excited-state wave functions, Φ_i, with apposite mixing coefficients, C_{ij}, referring to the ith function of the jth level.

$$\Psi_j = C_{1j}\Phi_1 + C_{2j}\Phi_2 + C_{3j}\Phi_3 \tag{6}$$

where j = 1, 2, 3. The application of the variation theorem (Appendix 1) leads to the set of 3 simultaneous equations which may be represented by,

$$\sum_{i=1}^{3} C_i(H_{ij} - ES_{ij}) = 0 \tag{7}$$

where $H_{ij} = \langle \Phi_i | H | \Phi_j \rangle$, H being the Hamiltonian of the system, $S_{ij} = \langle \Phi_i | \Phi_j \rangle$, and E is the appropriate energy. For non-trivial solutions to the simultaneous equations the secular determinant is set to zero and the allowed energies found by solving for E,

$$|H_{ij} - ES_{ij}| = 0 \qquad (8)$$

where, provided normalised basis functions are used, $S_{ij} = 1$ when $i = j$, and assuming zero overlap, $S_{ij} = 0$ when $i \neq j$. Now substituting in equation 8 and simplifying, the secular determinant of the system becomes,

$$\begin{vmatrix} H_{11} - H_{00} - E & H_{12} & H_{12} \\ H_{12} & H_{11} - H_{00} - E & H_{12} \\ H_{12} & H_{12} & H_{11} - H_{00} - E \end{vmatrix} = 0 \qquad (9)$$

where, so that energies may be expressed as transition energies, the term $H_{00} = \langle \Psi_o | H | \Psi_o \rangle$ has been included. The solution to this problem gives 3 eigenfunctions and, correspondingly, 3 eigenvalues and allows for the calculation of the dipole and rotational strengths of the system in terms of the empirically known spectroscopic properties of the individual constituent chromophores. Solving the secular determinant for E gives the three solutions,

$$E = H_{11} - H_{00} - H_{12} \text{ (twice)} \quad \text{and} \quad E = H_{11} - H_{oo} + 2H_{12} \qquad (10)$$

If it is assumed that, to a first approximation, the tris(2,2′-bipyridine) metal complex ion can be described as a weakly coupled system where only electrostatic coupling of the chromophores need be considered, the total

Hamiltonian, H, of the system may be split in the following way:

$$H = H_1 + H_2 + H_3 + \sum_{i<j}^{3} \theta_{ij} \qquad (11)$$

where H_1, H_2 and H_3 are the appropriate Hamiltonians for the 2,2′-bipyridine ligands and the operator θ_{ij} refers to the electrostatic multipole interaction between the ith and jth ligand molecules of the system. By making this assumption H_{11}, H_{00} and H_{12} can be written (Appendix 1),

$$H_{11} = \langle x_1' \, x_2 x_3 | H_1 + H_2 + H_3 + \sum_{i<j}^{3} \theta_{ij} | x_1' \, x_2 x_3 \rangle$$

$$= \langle x_1' \, | H_1 | x_1' \rangle + \langle x_2 | H_2 | x_2 \rangle + \langle x_3 | H_3 | x_3 \rangle + \langle x_1' \, x_2 | \theta_{12} | x_1' \, x_2 \rangle +$$
$$\langle x_1' \, x_3 | \theta_{13} | x_1' \, x_3 \rangle + \langle x_2 x_3 | \theta_{23} | x_2 x_3 \rangle \qquad (12)$$

provided orthonormal functions are used. In Equation 12, the first term, $\langle x_1' \, | H_1 | x_1' \rangle = E_1'$, represents the excited-state energy of the long-axis polarised $\pi \rightarrow \pi^*$ transition of 2,2′-bipyridine molecule 1, the terms $\langle x_2 | H_2 | x_2 \rangle = E_2$ and $\langle x_3 | H_3 | x_3 \rangle = E_3$ are the ground-state energies of 2,2′-bipyridine molecules 2 and 3, the terms $\langle x_1' \, x_2 | \theta_{12} | x_1' \, x_2 \rangle$ and $\langle x_1' \, x_3 | \theta_{13} | x_1' \, x_3 \rangle$ represent the interactions of the static excited-state multipole moment of molecule 1 with the static ground-state multipole moments of molecules 2 and 3 respectively, and, finally, the last term, $\langle x_2 x_3 | \theta_{23} | x_2 x_3 \rangle$, represents the interaction of the static ground-state multipole moments of molecules 2 and 3. By similar methods,

$$H_{00} = \langle x_1 | H_1 | x_1 \rangle + \langle x_2 | H_2 | x_2 \rangle + \langle x_3 | H_3 | x_3 \rangle + \langle x_1 x_2 | \theta_{12} | x_1 x_2 \rangle +$$
$$\langle x_1 x_3 | \theta_{13} | x_1 x_3 \rangle + \langle x_2 x_3 | \theta_{23} | x_2 x_3 \rangle \qquad (13)$$

and,

$$H_{12} = \langle x_1' \, x_2 x_3 | H_1 + H_2 + H_3 + \sum_{i<j}^{3} \theta_{ij} | x_1 x_2' \, x_3 \rangle$$
$$= \langle x_1' \, x_2 | \theta_{12} | x_1 x_2' \rangle$$
$$= V_{12} \qquad (14)$$

where V_{12} represents the interaction between the transition dipole moments of 2,2′-bipyridine molecules 1 and 2, where $\langle x_1 | H_1 | x_1 \rangle = E_1$ is the ground-state energy of 2,2′-bipyridine molecule 1, and where the last three terms in Equation 13 refer to the ground-state multipole interactions. The solutions of the secular determinant (Equation 10) can now be rewritten (Appendix 1) to give the eigenvalues E_{A_2}, E_E^1 and E_E^2 (where E_E^1 and E_E^2 are degenerate in D_3 symmetry),

$$E_{A_2} = \Delta E_1 + 2V_{12}, \qquad E_E^1 = \Delta E_1 - V_{12} \qquad \text{and} \qquad E_E^2 = \Delta E_1 - V_{12} \qquad (15)$$

where $\Delta E_1 = E_1' - E_1$ is the transition energy of the long-axis polarised $\pi \rightarrow \pi^*$ transition of 2,2′-bipyridine molecule 1. It has been assumed that the difference between the static multipole moments of the excited states of the molecules and the static multipole moments of the ground states of the molecules is small and can be neglected. This is a usual assumption although the justification for it is not always strong. However, it will not affect the outcome of the semiquantitative arguments pursued here.

The corresponding eigenfunctions for E_{A_2}, E_E^1, and E_E^2 are,

$$\Psi_{A_2} = \frac{1}{\sqrt{3}} \left(x_1' x_2 x_3 + x_1 x_2' x_3 + x_1 x_2 x_3'\right)$$

$$\Psi_E 1 = \frac{1}{\sqrt{6}} \left(2x_1' x_2 x_3 - x_1 x_2' x_3 - x_1 x_2 x_3'\right)$$

$$\Psi_E{}^2 = \frac{1}{\sqrt{2}} \left(x_1 x_2' x_3 - x_1 x_2 x_3'\right)$$

It has so far been shown that the long-axis polarised transitions of the three 2,2′-bipyridine molecules in a tris-chelated complex interact electrostatically to give an A_2 coupling mode and two E coupling modes which are degenerate in D_3 symmetry. These coupling modes together with the short-axis polarised coupling modes are schematically represented in Figure 5 for a tris-chelate complex with the Δ-absolute configuration. The ligand excitations which are long-axis polarised couple in the tris-chelated complex to give resultant transitions which involve helical charge displacements and are thus strongly optically-active. The non-degenerate transition of the complex ion, $\Psi_0 \rightarrow \Psi_{A_2}$, resulting from the coupling of long-axis ligand excitations, gives rise to a right-handed helical charge displacement along and around the C_3 axis of the complex (Figure 5). The transition $\Psi_0 \rightarrow \Psi_E{}^2$ of the complex, shown on the right of Figure 5 involves a left-handed helical charge displacement along and around a C_2 axis of the complex, and the combination in the centre, $\Psi_0 \rightarrow \Psi_E 1$, is of mixed chirality which may be seen by taking the arrows in pairs. The pairs 1, 2 and 2, 3 involve left-handed helical charge displacements along and around C_2 axes of the complex, while the pair 1, 3 involves a right-handed helical displacement of charge along and around the C_3 axis of the complex. For the particular absolute configuration shown in Figure 5 (the Δ-enantiomer) it has been shown that the screw sense of the $\Psi_0 \rightarrow \Psi_{A_2}$ transition is right-handed and hence this transition should give positive circular dichroism, while the

FIGURE 5: Schematic representation of the long- and short-axis polarised transition coupling modes in a tris-chelated complex with the Δ-absolute configuration

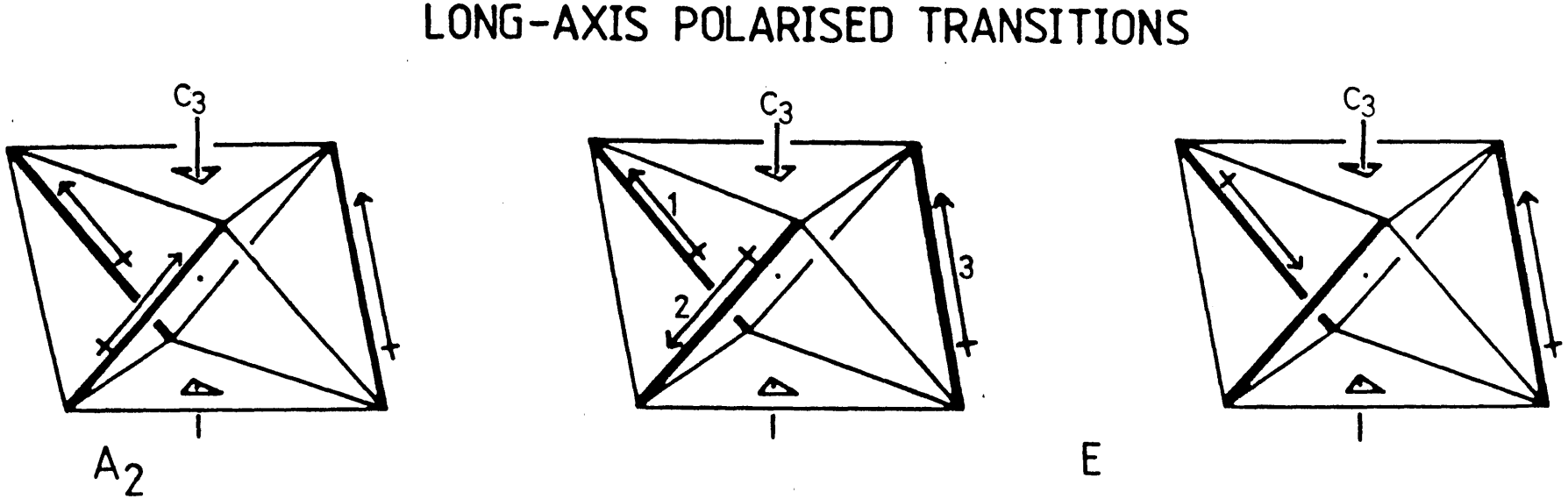

combinations of the degenerate E coupling modes involve a net left-handed helical displacement, and thus the total $\Psi_0 \rightarrow \Psi_E$ transition should give negative circular dichroism.

It can be shown that the rotational strength of the $\Psi_0 \rightarrow \Psi_{A_2}$ transition is equal but opposite in sign to the $\Psi_0 \rightarrow \Psi_E$ excitation, and, were these two transitions of the same energy, the exciton rotational strength would vanish. The energies of the two transitions, however, are different because the interactions of the dipoles in the two coupling modes are different. This can be seen in the following way. The Ψ_{A_2} coupling mode involves the dipole vectors in an arrangement where they are essentially "head-to-head", whereas the $\Psi_E{}^2$ coupling mode (which is the same energy as $\Psi_E 1$) involves the dipoles in an essentially "head-to-tail" arrangement. Intuitive electrostatic considerations will suggest that the "head-to-head" arrangement is of higher energy than the "head-to-tail" arrangement. Thus for the particular absolute configuration shown in Figure 5, the $[M(bipy)_3]^{n+}$ systems should show negative circular dichroism at lower energies and equal positive circular dichroism to higher energies in the regions of the long-axis polarised $\pi \rightarrow \pi^*$ transition of bipy. In addition, it can be shown that the isotropic absorption of the $\Psi_0 \rightarrow \Psi_{A_2}$ transition should be twice as strong as that of the $\Psi_0 \rightarrow \Psi_E$ transition.

The areas of the circular dichroism bands measure experimentally the rotational strengths R of the transitions in the complex ion, which are given in the point-dipole approximation for the Δ-$[M(bipy)_3]^{n+}$ configuration of the complex by,

$$R(A_2)_1 = - R(E)_1 = \sqrt{2}\, n\bar{\nu}_o r_{ML} p_{o1}{}^2 \qquad (16)$$

where $\bar{\nu}_0$ and $p_{01}{}^2$ are, respectively, the frequency and the dipole strength of a long-axis polarised excitation in the free ligand, and r_{ML} is the distance in the complex from the metal ion to the assumed location of the point excitation dipole in a ligand, that is, the centre of the internuclear bond in 2,2′-bipyridine. The dipole strengths of the transitions of the complex ion resulting from long-axis ligand excitations are related by,

$$p^2(A_2)_1 = 2p^2(E)_1 = 2p_{01}{}^2 \qquad (17)$$

The electronic transitions of a tris-chelated complex ion deriving from ligand excitations which are short-axis polarised (Figure 5) are not optically-active in the exciton approximation. The transition $\Psi_0 \rightarrow \Psi_{A_1}$, of the complex is forbidden, since the component excitation moments have a vanishing resultant and in the corresponding degenerate transitions of the complex $\Psi_0 \rightarrow \Psi_E$, the component excitation moments are coplanar. The resultant absorption intensity is concentrated in the degenerate E transition which has the dipole strength,

$$p^2(E)_S = 3p_{0S}{}^2 \qquad (18)$$

where $p_{0S}{}^2$ is the dipole strength of the short-axis excitation of the free ligand. However, if there were to be appreciable electron exchange between the three bipy ligands in the complex, the coupled chromophore model of the exciton theory, merges with that of the inherently dissymmetric chromophore as in the case of the sterically-hindered bianthryls[91] and the benzo[c] phenanthrenes.[97,98] In this case the short-axis polarised transitions with a finite dipole strength have an intrinsic non-zero rotational strength, owing to the displacement of charge through a helical path determined by the dissymmetric nuclear framework of the complex.

But even if the delocalisation of π-electrons from one ligand to another and to the co-ordinated metal ion does not occur, the short-axis polarised excitations of one ligand may interact Coulombically with the long-axis directed transitions of the other, mixing the two types. In particular, the doubly-degenerate coupling modes (Figure 5) mix on symmetry grounds, both transforming under the E representation of the group D_3 to which the complex belongs, whereas the non-degenerate modes mix neither with each other nor with the degenerate modes, as they are spanned by the A_2 and the A_1 representation respectively. Accordingly complexes of the type $[M(bipy)_3]^{n+}$ would be expected to show a weak second-order circular dichroism in the wavelength region of the absorption due to an electronic transition which is short-axis polarised in the free bipy ligand.

These expectations of the degenerate exciton theory are in good accord with the observed absorption and circular dichroism spectra of the tris(2,2′-bipyridine) and tris(phenanthroline) complexes of transition metal ions.[21] In the triply reduced complex, if the electrons were localised on the individual bipy ligands, a similar exciton couplet to those observed for the tris(2,2′-bipyridine) and tris(1,10-phenanthrolene) complexes would be expected. If, on the other hand, the electrons were completely delocalised over all three ligands, the complex might be expected to show a circular dichroism spectrum with the characteristic one-electron structure as is seen for the inherently dissymmetric chromophores such as the helicenes[81] and the benzo [c] phenanthrenes.[97,98] Therefore the exciton theory of optical activity should be able to distinguish between a triply reduced tris(2,2′-bipyridine) complex in which the electrons are localised on the individual bipy ligands from that in which the electrons are completely delocalised over all three.

Hetero-trischelated Complexes

If the symmetry of a tris-chelated complex is reduced from D_3 to C_2 by replacing one of the bidentate ligands with another of a different type the predictions of the exciton theory of optical activity are diversified, permitting a more detailed comparison of the theory with experiment.[75-79] In a hetero-trischelated complex with C_2 symmetry the exciton modes which are doubly degenerate in the analogous homo-trischelated D_3 complex are split and give rise in principle to distinct circular dichroism bands. Thus the ligand transitions with long-axis polarisation produce three circular dichroism bands in hetero-trischelated complexes if the energy difference between the excitations of the dissimilar ligands is not too large, whereas the corresponding excitations in homo-trischelated complexes with D_3 or C_3 symmetry give rise to only two circular dichroism bands.

The general formalism of the non-degenerate case follows closely that used for the degenerate system. Consider a hetero-trischelated complex $[M(L_aL_bL_c)]^{n+}$ where M is a transition metal ion and L is a symmetrical bidentate ligand with $L_a = L_b \neq L_c$, the only element of symmetry, apart from the identity, is the two-fold rotation axis of the ligand L_c, and the electronic states belong to either the A or the B representation. In the absence of electron-exchange between the ligands, and between the metal ion and the ligands, the ground-state wavefunction of the complex is represented by the simple product,

$$\Psi_0 = x_1 x_2 \emptyset_3 \qquad (19)$$

where x_1 and x_2 refer to the ground-state wavefunctions of the complexed, identical ligands 1 and 2, and where $\emptyset_3$ refers to the ground-state wave

function of the odd complexed ligand. Supposing that only one excited state of the individual chromophores of the assembly need be considered, the (singly) excited state wavefunctions, Φ_i, of the system can be written in the following way,

$$\Phi_1 = x_1' x_2 \phi_3, \qquad \Phi_2 = x_1 x_2' \phi_3 \qquad \text{and} \qquad \Phi_3 = x_1 x_2 \phi_3' \tag{20}$$

where the primes represent the excited-state wave functions of the long-axis polarised $\pi \longrightarrow \pi^*$ transitions. As before the total wave function, Ψ_j, corresponding to the jth excited state of the assembly, may be expressed as a linear combination of the unperturbed singly excited-state wave functions, Φ_i, with apposite mixing coefficients, C_{ij}, (Equation 6) and the application of the variation theorem leads to the set of simultaneous equations as in Equation 7. For non-trivial solutions to the simultaneous equations, the secular determinant is set to zero (Equation 8) and the allowed energies found by solving for E. By recognising the symmetry (C_2) of the system and substituting in Equation 8, the secular determinant for the system becomes, (Appendix 2),

$$2(H_{11} - H_{00} - E - H_{12}) \begin{vmatrix} 2(H_{11} - H_{00} - E + H_{12}) & 2H_{13} \\ 2H_{13} & H_{33} - H_{00} - E \end{vmatrix} = 0 \tag{21}$$

Assuming that, to a first approximation, the complex ion can be described as a weakly coupled system where only electrostatic coupling of the chromophores need be considered. This allows the total Hamiltonian, H, of the system to be split as in Equation 11. By making this assumption the determinant in Equation 21 may be simplified, and as an example H_{11}, H_{12} and H_{00} can be written (remembering the orthonormality of the ligand wavefunctions),

$$H_{11} = \langle x_1' \, x_2 \phi_3 | H_1 + H_2 + H_3 + \sum_{i<j}^{3} \theta_{ij} | x_1' \, x_2 \phi_3 \rangle$$

$$= \langle x_1' | H_1 | x_1' \rangle + \langle x_2 | H_2 | x_2 \rangle + \langle \phi_3 | H_3 | \phi_3 \rangle + \langle x_1' \, x_2 | \theta_{12} | x_1' \, x_2 \rangle$$
$$+ \langle x_1' \, \phi_3 | \theta_{13} | x_1' \, \phi_3 \rangle + \langle x_2 \phi_3 | \theta_{23} | x_2 \phi_3 \rangle \qquad (22)$$

$$H_{12} = \langle x_1' \, x_2 \phi_3 | H_1 + H_2 + H_3 + \sum_{i<j}^{3} \theta_{ij} | x_1 x_2' \, \phi_3 \rangle$$

$$= \langle x_1' \, x_2 | \theta_{12} | x_1 x_2' \rangle = V_{12} \qquad (23)$$

and

$$H_{00} = \langle x_1 | H_1 | x_1 \rangle + \langle x_2 | H_2 | x_2 \rangle + \langle \phi_3 | H_3 | \phi_3 \rangle + \langle x_1 x_2 | \theta_{12} | x_1 x_2 \rangle$$
$$+ \langle x_1 \phi_3 | \theta_{13} | x_1 \phi_3 \rangle + \langle x_2 \phi_3 | \theta_{23} | x_2 \phi_3 \rangle \qquad (24)$$

where V_{12} represents the interaction between the transition dipole moments of the two identical ligands. The first term of (21) thus reduces to,

$$H_{11} + H_{12} - H_{00} - E = \Delta E_1 + V_{12} - E$$

making the same assumptions as before. With these assumptions and carrying out the calculations for the other terms, the determinant in Equation 21 reduces to,

$$(\Delta E_1 - V_{12} - E) \begin{vmatrix} 2(\Delta E_1 + V_{12} - E) & 2V_{13} \\ 2V_{13} & \Delta E_3 - E \end{vmatrix} = 0 \qquad (25)$$

where an obvious extension of the symbolism has been employed. Thus

the eigenvalues E_A, E_B^+ and E_B^- can be found,

$$E_A = \Delta E_1 - V_{12} \tag{26}$$

$$E_B^+ = \frac{\Delta E_1 + \Delta E_3 + V_{12} + [(-\Delta E_1 - \Delta E_3 - V_{12})^2 - 4(\Delta E_1 \Delta E_3 + \Delta E_3 V_{12} - 2V_{13}^2)]^{\frac{1}{2}}}{2} \tag{27}$$

$$E_B^- = \frac{\Delta E_1 + \Delta E_3 + V_{12} - [(-\Delta E_1 - \Delta E_3 - V_{12})^2 - 4(\Delta E_1 \Delta E_3 + \Delta E_3 V_{12} - 2V_{13}^2)]^{\frac{1}{2}}}{2} \tag{28}$$

The corresponding eigenfunctions for E_A, E_B^+ and E_B^- respectively, are,[78]

$$\Psi_A = \frac{1}{\sqrt{2}} (\Phi_1 - \Phi_2) \tag{29}$$

$$\Psi_B^+ = C_1^+ [\frac{1}{\sqrt{2}} (\Phi_1 + \Phi_2)] + C_2^+ \Phi_3 \tag{30}$$

$$\Psi_B^- = C_1^- [\frac{1}{\sqrt{2}} (\Phi_1 + \Phi_2)] + C_2^- \Phi_3 \tag{31}$$

where the subscripts A and B refer to the irreducible representations of C_2 under which the functions transform. The constants C_1^+, C_2^+, C_1^- and C_2^- are the mixing coefficients which, when the wavefunctions are orthonormal, have the values,[78]

$$C_1^+ = -C_2^- = \frac{-\sqrt{2}\, V_{13}}{(2V_{13}^2 + L^2)^{\frac{1}{2}}} \tag{32}$$

and,

$$C_2^+ = C_1^- = \frac{L}{(2V_{13}^2 + L^2)^{\frac{1}{2}}} \tag{33}$$

where,

$$L = \frac{\Delta E_1 + V_{12} - \Delta E_3 - [(-\Delta E_1 - \Delta E_3 - V_{12})^2 - 4(\Delta E_1 \Delta E_3 + \Delta E_3 V_{12} - 2V_{13}^2)]^{\frac{1}{2}}}{2} \tag{34}$$

Note that, $|C_1^+| = |C_2^-| > |C_2^+| = |C_1^-|$ and that C_2^+ and C_1^- are always negative,[78] and that the two originally degenerate ligand transitions are split by exciton interaction, and the energies of the final upper states lie in the following decreasing order $E_B^+ > E_A > E_B^-$.

For the transition from the totally symmetric ground-state function, Ψ_0, to the excited-state wavefunction, Ψ_A, which is polarised along the twofold axis of the hetero-trischelated complex, the dipole strength, D_A, and the rotational strength, R_A, for the Δ absolute configuration shown in Figure 5, are given by,[78]

$$D_A = \frac{1}{2} p_1^2 \tag{35}$$

and,

$$R_A = -\frac{1}{\sqrt{2}} \pi \bar{v}_1 r_1 p_1^2 \tag{36}$$

where $\bar{v}_1$ is the frequency in wave numbers of the long-axis polarised $\pi \rightarrow \pi^*$ transition of the unperturbed (complexed) ligand molecule 1. Note that, $r_1 = r_2$, $\bar{v}_1 = \bar{v}_2$ and $p_1 = p_2$. The transition $\Psi_0 \rightarrow \Psi_B^+$, which is polarised in the directions normal to the twofold axis, has,

for the absolute configuration shown in Figure 5, a dipole strength, D_B^+, and a rotational strength, R_B^+, given by,

$$D_B^+ = (C_1^+)^2 \frac{3}{2} p_1^2 + (C_2^+)^2 p_3^2 + C_1^+ C_2^+ \sqrt{2} p_1 p_3 \qquad (37)$$

and

$$R_B^+ = (C_1^+)^2 \frac{1}{\sqrt{2}} \pi \bar{\nu}_1 r_1 p_1^2 + C_1^+ C_2^+ \pi \bar{\nu}_1 r_1 p_1 p_3 + C_1^+ C_2^+ \pi \bar{\nu}_3 r_3 p_1 p_3 \qquad (38)$$

where $\bar{\nu}_3$ is the frequency in wave numbers at which the isolated (complexed) hetero-ligand $\pi \rightarrow \pi^*$ transition occurs. For the $\Psi_0 \rightarrow \Psi_B^-$ transition, which is also polarised in the directions normal to the twofold axis, a similar expression obtains for the dipole strength, D_B^-, and the rotational strength, R_B^-, for the absolute configuration shown in Figure 5, namely,

$$D_B^- = (C_1^-)^2 \frac{3}{2} p_1^2 + (C_2^-)^2 p_3^2 + C_1^- C_2^- \sqrt{2} p_1 p_3 \qquad (39)$$

and

$$R_B^- = (C_1^-)^2 \frac{1}{\sqrt{2}} \pi \bar{\nu}_1 r_1 p_1^2 + C_1^- C_2^- \pi \bar{\nu}_1 r_1 p_1 p_3 + C_1^- C_2^- \pi \bar{\nu}_3 r_3 p_1 p_3 \qquad (40)$$

Note that the conservation laws for both dipole strength and rotational strength hold, as shown by, (Appendix 2),

$$D_A + D_B^+ + D_B^- = 2p_1^2 + p_3^2 = p_1^2 + p_2^2 + p_3^2 \qquad (41)$$

and

$$R_A + R_B^+ + R_B^- = 0 \qquad (42)$$

Thus the exciton theory of optical activity predicts that, for a hetero-trischelated complex in the Δ absolute configuration, the transition $\Psi_0 \rightarrow \Psi_A$ should carry negative circular dichroism and, since C_1^+ and C_2^+ are both negative quantities, [78] the $\Psi_0 \rightarrow \Psi_B^+$ transition should carry positive circular dichroism. Despite the fact that C_1^- and C_2^- are of opposite sign, the $\Psi_0 \rightarrow \Psi_B^-$ transition will also carry negative circular dichroism.

This treatment of the non-degenerate exciton theory allows the theoretical dipole and rotational strengths of a hetero-trischelated complex to be readily calculated. The unknown quantities, ΔE_1, ΔE_3, p_1, p_3, r_1, r_3, R_{12}, R_{13}, $\bar{\nu}_1$ and $\bar{\nu}_3$ in the equations can easily be

found from experiment. The only other unknown quantities in the equations are V_{12} and V_{13}, both of which can be calculated from the monopole exciton energy.[76] The monopole exciton energy for the transitions of the complex ion resulting from an excitation between the molecular orbitals π_i and π_j in the free ligand is obtained by expanding the molecular orbitals over the atomic orbitals contributing to the π-system of the ligands, giving the summation,

$$V_{ab} = 2 \sum_{s(a)} \sum_{t(b)} (C_{si}C_{sj})_a (C_{ti}C_{tj})_b \gamma_{st} \qquad (43)$$

where C_{si} is the atomic orbital coefficient of the atom s in the molecular orbital π_i of the ligand L_a, and γ_{st} is the repulsion integral between an electron on atom s and on atom t, the sums being taken over all of the atoms s of the ligand L_a and all of the atoms t of the ligand L_b. Alternatively, V_{12} and V_{13} can be readily calculated using the point-dipole approximation,[60] however, the point-dipole approximation is unlikely to be quantitatively sufficient in the present system, since the dipole length and the distance between the chromophores are the same order of magnitude; it leads to large discrepancies in the order of magnitude of the splittings compared either with observation or with the monopole value. However, it generally gives the correct sense of the splittings which is sufficient for some purposes. It is found that using this approximation and using the choice of phases shown in Figure 6 that,

$$V_{12} = \frac{1}{4} \frac{p_1 p_2}{R_{12}^3} \qquad (44)$$

and,

$$V_{13} = \frac{1}{R_{13}^3} \left\{ \frac{p_1 p_3}{2} - \frac{3 p_1 p_3 r_1}{4(r_1 + r_3)^2} \right\} \qquad (45)$$

FIGURE 6: The geometry of $[M(L_aL_bL_c)]^{n+}$ complex ions and definitions of the various geometric parameters used in the calculations.

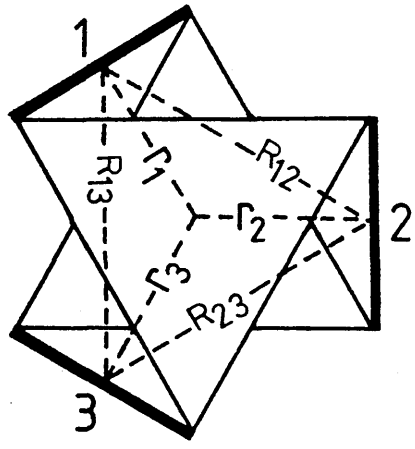

where R_{12} is the distance between the "centres" of the excitation moments of the two identical ligand molecules, and R_{13} is the distance between the "centres" of the excitation moments of two different ligand molecules, r_1 and r_3 are the distances between the centre of the metal ion and the "centres" of the two types of ligand molecules and p_1 and p_3 refer to the values of the transition dipole moments of the long-axis polarised $\pi \rightarrow \pi^*$ transitions of the two types of ligand molecules. Note that $p_1 = p_2$, $r_1 = r_2$, $R_{12} = \sqrt{3}\, r_1$, $R_{13} = \sqrt{r_1^2 + r_3^2 + r_1 r_3}$ and $R_{13} = R_{31}$ (Figure 6). Also V_{12} can be estimated from experiment[76] as,

$$hc\,[\bar{\nu}(A_2) - \bar{\nu}(E)] = 3V_{12} \qquad (46)$$

although this method may give answers different from those calculated using the point-dipole approximation and the monopole method.

The application of the non-degenerate exciton theory of optical activity to hetero-trischelated complexes predicts three characteristic coupling

modes at different energies of the long-axis polarised $\pi \rightarrow \pi^*$ transitions of the ligand molecules in the complex. So for a hetero-trischelated complex with C_2 symmetry, for example the localised models of the singly and doubly reduced complexes, $[Ru(bipy)_2(bipy^-)]^+$ and $[Ru(bipy)(bipy^-)_2]$ respectively, in principle, three exciton circular dichroism bands in the region of the ligand long-axis polarised $\pi \rightarrow \pi^*$ transitions are predicted. In the singly and doubly reduced complexes of $[M(bipy)_3]^{2+}$, (M = Ru, Os), if the added electrons were delocalised over all three bipy ligands, the complexes could be formulated as $[M(bipy^{\frac{1}{3}-})_3]^+$ and $[M(bipy^{\frac{2}{3}-})_3]$ for the singly and doubly reduced complexes respectively, and so in effect, the complexes could be described as homo-trischelated complexes with D_3 symmetry. It has been shown that the exciton theory of optical activity predicts completely different spectra for the homo- and hetro-trischelated complexes, so it should be an excellent method to distinguish between the localised and delocalised theories for the reduced tris(2,2´-bipyridine)metal complexes.

CHAPTER 2

EXPERIMENTAL

INSTRUMENTATION

CYCLIC VOLTAMMETRY

All voltammetric experiments were performed in a conventional cell (Princeton Applied Research) fitted with a three-electrode configuration consisting of a working electrode, an auxiliary electrode (both platinum wire) and a Ag/Ag^+ reference electrode. The reference electrode (Figure 7) consisted of a silver wire in a 0.1M solution of silver nitrate in an air-tight compartment with a porous Vycor glass frit. This electrode compartment was placed in a salt bridge compartment which was separated from the bulk electrochemical solution by a porous Vycor frit. The salt bridge compartment was used to minimise junction potentials[99] and contained the electrolyte solution (0.1M n-Bu_4NBF_4 in CH_3CN). The electrochemical cell was air-tight and had inlet and outlet valves to allow degassing of the solutions by argon which had been previously dried by passing it through a cold trap followed by columns of 3A and 4A molecular sieves. Solutions were purged with argon for twenty minutes prior to use.

Cyclic voltammograms were recorded using an EG & G Princeton Applied Research Model 175 Universal Programmer coupled to an EG & G Princeton Applied Research Model 173 Potentiostat/Galvanostat with a JJ 'XY' Plotter type PL51. Scan rates were in the range 20 to 200 mV/s with routine measurements at 100 mV/s, and concentrations of I, II and III were approximately $10^{-4} mol l^{-1}$.

SPECTROELECTROCHEMISTRY

The spectroelectrochemistry was performed using an optically transparent

thin layer electrode (O.T.T.L.E.) (Figure 7) mounted in the spectrometer beam. The O.T.T.L.E. consisted of a conventional 1 mm u.v. cell which was modified to hold the three electrode arrangement shown. The reference electrode used was identical to that used in the cyclic voltammetry experiments. The working electrode was a piece of platinum gauze which fitted snugly into the 1 mm u.v. cell where the new species were electrogenerated. The auxiliary electrode was a piece of platinum gauze in a compartment separated from the bulk solution by a porous Vycor frit to minimise reactions between reduced and non-reduced species. Constant potentials were applied using an EG & G Princeton Applied Research Model 173 Potentiostat/Galvanostat. Concentrations of I, II and III were varied to optimise the different spectral regions.

The O.T.T.L.E. used in the luminescence experiments was identical to that shown in Figure 7, except that the 1 mm u.v. cell was bent at an angle of 90° to the bulk solution compartment to allow it to lie horizontally in the laser beam.

In all experiments the starting complexes I, II and III were regenerated after each reduction stage to check for decomposition and racemisation.

LOW TEMPERATURE CELL

Low temperature (-41°C) spectroelectrochemistry experiments were performed by mounting the O.T.T.L.E. in a teflon block which was divided into three compartments by four strain-free quartz windows (Figure 8). The O.T.T.L.E. was inserted into the central compartment and cold, dry nitrogen was blown around the cell, maintaining the temperature at -41°C. Dry nitrogen at room temperature was blown through the outer compartments which maintained the outer windows at room temperature and prevented condensation from forming on the quartz

FIGURE 7: Schematic diagram of the O.T.T.L.E.

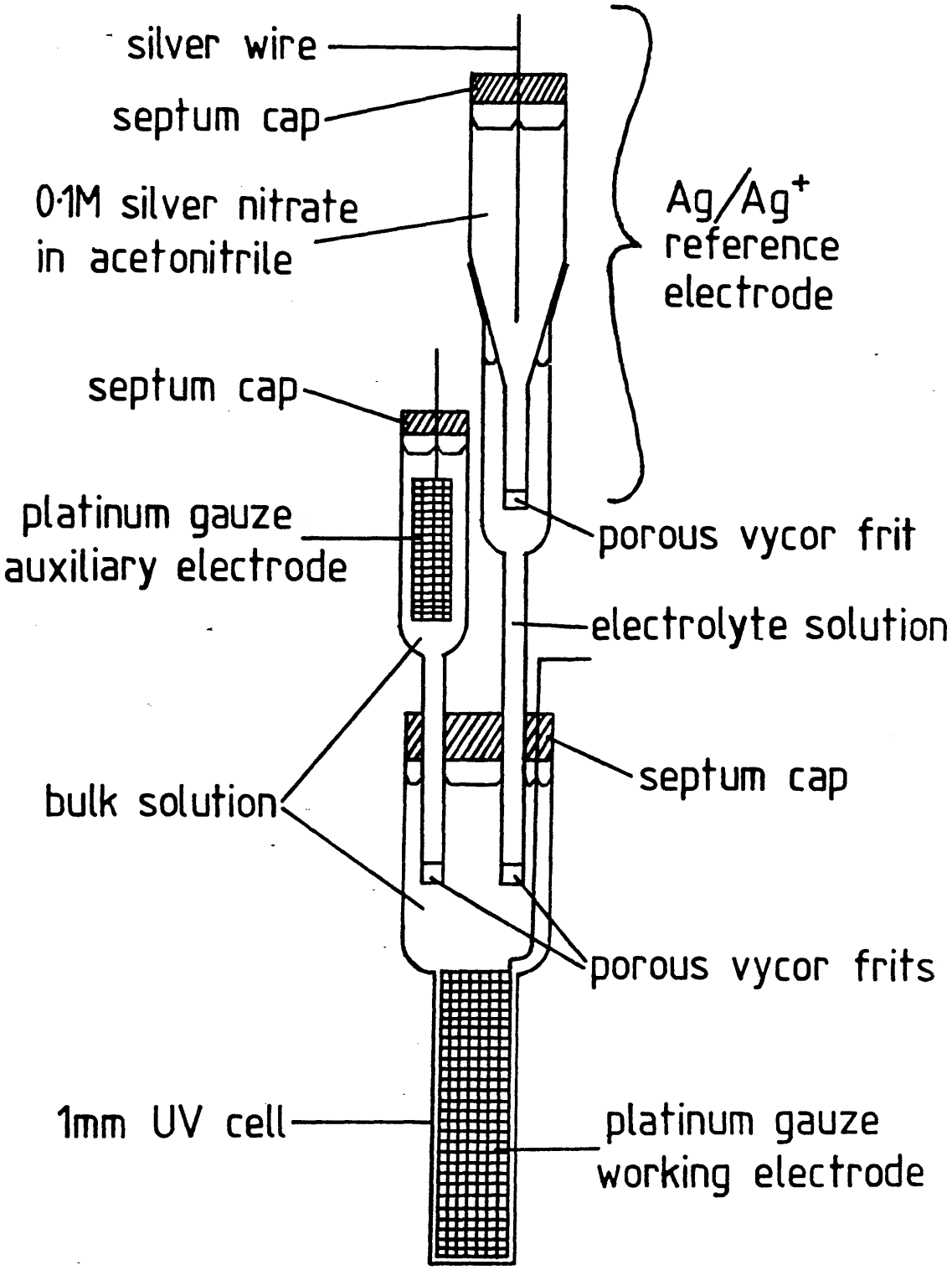

FIGURE 8: Schematic diagram of the low temperature cell

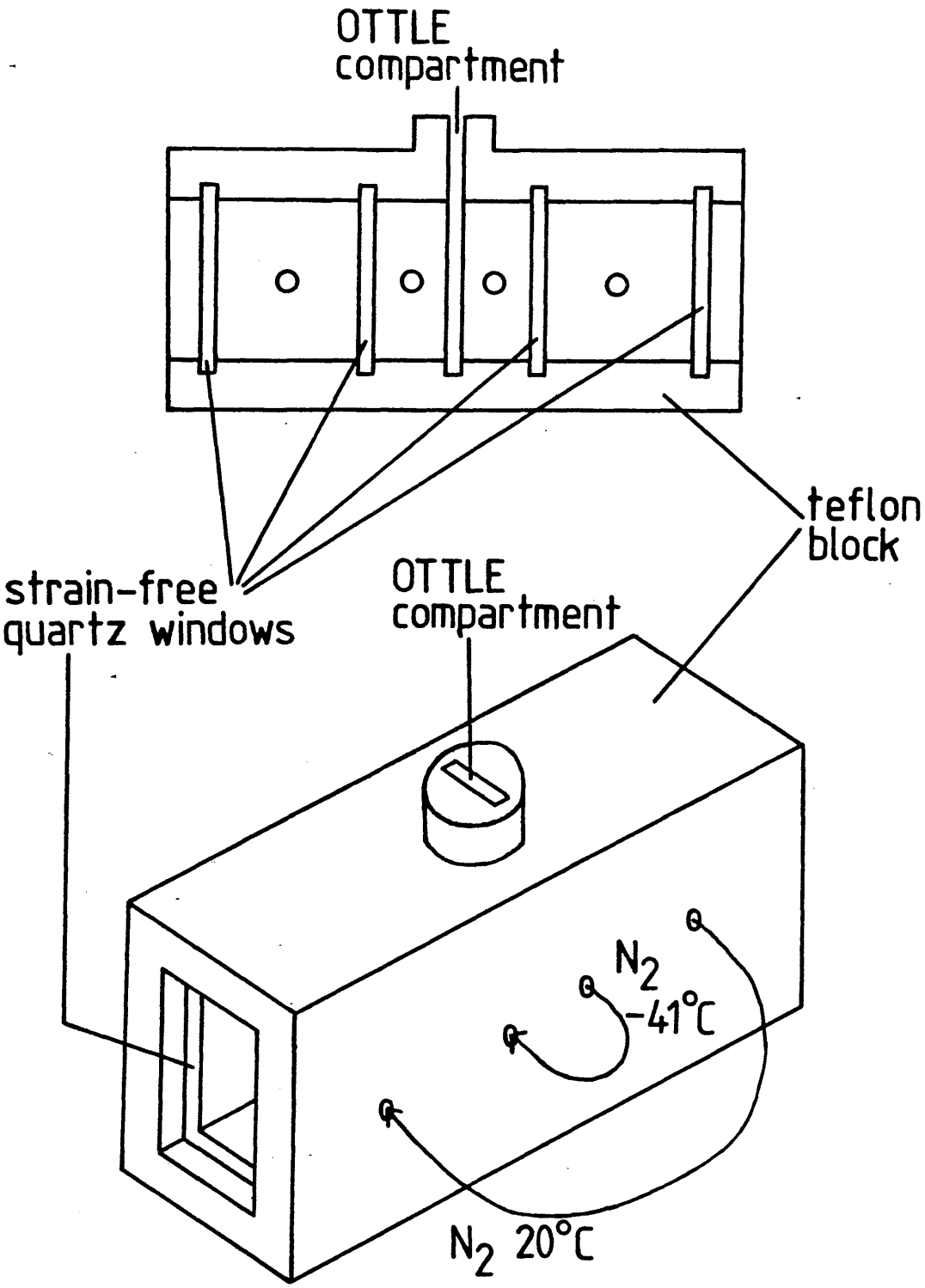

windows. The temperature inside the cell was monitored at all times using a thermocouple which was inserted into the cell.

CIRCULAR DICHROISM MEASUREMENT

The c.d. spectrometer (Figure 9) was constructed around a Jobin-Yvon 0.6 m monochromator. The source was a 150W horizontally mounted xenon arc lamp (powered by a PRA M303 Lamp Supply) which was focussed by means of a parabolic reflector. The light energy from the single grating monochromator was passed through a filtering system and then was plane-polarised in the vertical plane by a quartz Rochon prism. The plane-polarised light was then circularly-polarised by passing it through a silica photo-elastic modulator (powered by a PEM-80 Photoelastic Modulator System Controller) held at 45° to its optic axes. The circularly-polarised light passed through the sample and was collected by an EMI model 9558QB photomultiplier. The modulated signal was measured using a synchronous lock-in amplifier (Bentham) referenced to the photo-elastic modulator vibration frequency of 50 KHz. The lock-in amplifier detected the periodic difference in light intensity due to the presence of an optically active sample. The lock-in output was plotted on a Belmont Instruments chart recorder as the monochromator was scanned in wavelength, producing a spectrum of ΔA varying with wavelength, where ΔA is the fractional circular dichroism absorbance.

OPERATION OF THE PHOTO-ELASTIC MODULATOR

The photo-elastic modulator consists of a bar-shaped crystal of calcium fluoride or fused silica which is driven into oscillation by mechanical coupling to a bonded-on piezoelectric transducer made of crystal quartz. The stretching and compression of the optical element results in an oscillating birefringence ($n_x - n_y$). This is due to a time-varying

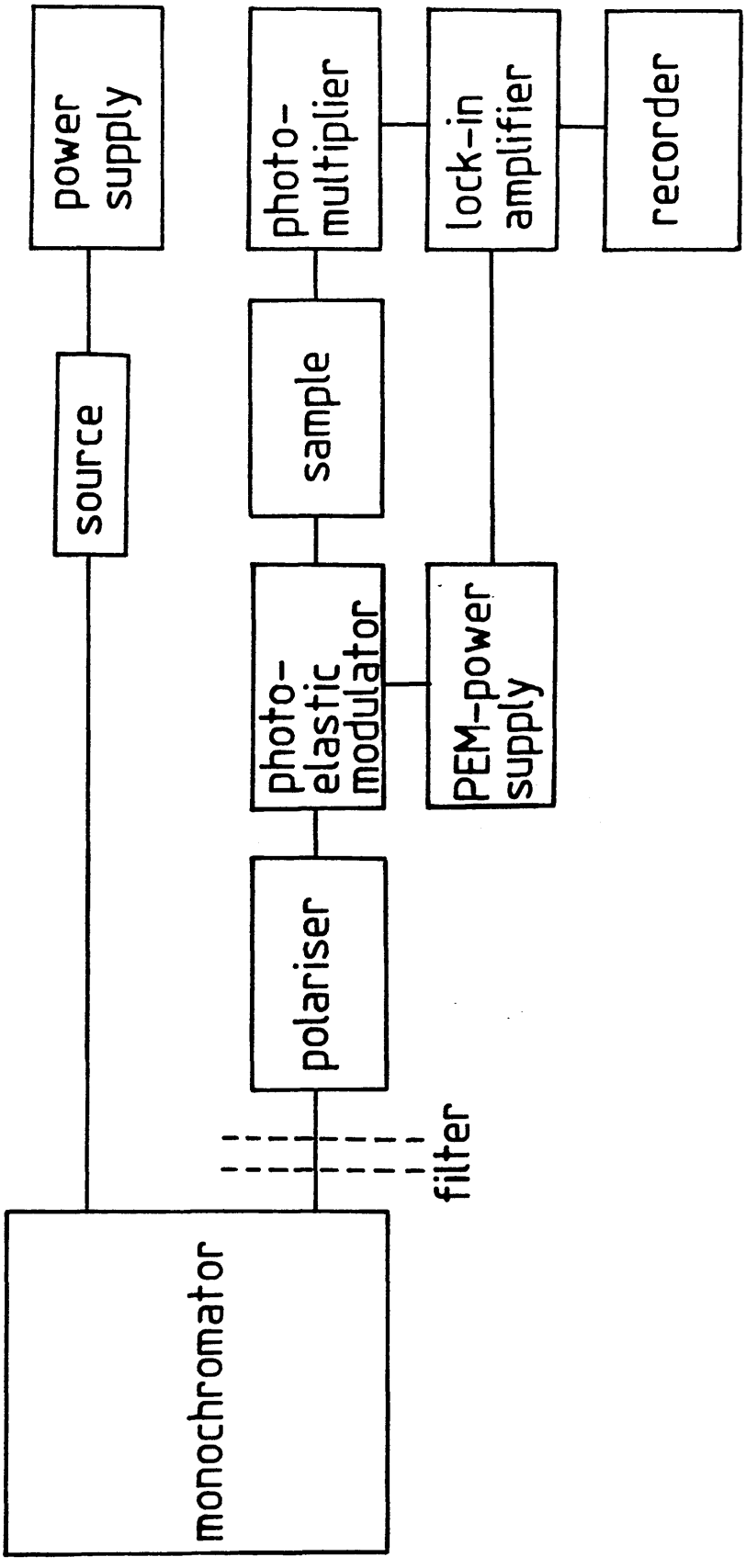

FIGURE 9: Schematic diagram of the c.d. spectrometer

difference between the two refractive indices, n_x and n_y, applying to light polarised parallel or perpendicular to the x and y axes in Figure 10.

The extensional displacements along the x-axis of the bar are given by,

$$\delta = \delta_0 \sin(2\pi x/\lambda)\sin\omega t \qquad (2.1)$$

where δ_0 is the maximum extension, λ is the wavelength of the incident light, ω is the oscillating frequency and t is the time. The corresponding strain is proportional to $(\partial\delta/\partial x)$, that is, to $\cos(2\pi x/\lambda)$ and is a maximum at the bars centre. The birefringence $(n_x - n_y)$ is proportional to the strain and varies with time as $\sin(\omega t)$.

Consider a linearly polarised light beam which is the resultant of two linear components abc and a′b′c′ (Figure 10). This light beam, with its resultant linear axis orientated at 45° to the pressure axes, now passes through a block of isotropic fused silica rendered linearly birefringent by pressure exerted along the x or y axis. The induced differential refractive index $(n_x \neq n_y)$ causes one of the linear components of the light beam (abc or a′b′c′) to travel through the silica faster than the other. If $n_x > n_y$ then the x component (abc) will travel more slowly than the y component (a′b′c′), that is it will be retarded. As drawn in Figure 10 (a), an x-component retardation of exactly ¼ wave ($\lambda/4$) leads to right-circular polarisation ($^{-}\lambda/4$, $^{3}\lambda/4$, $^{7}\lambda/4$ ... etc retardation will give left-circular polarisation) (Figure 10 (b)). A half wave retardation, plus or minus, will cause a 90° rotation of the original plane of linear polarisation. Zero $(n_x = n_y)$ of full-wave retardation leaves the polarisation of the incident beam unchanged. The general phase retardation, δ, leads to elliptically

FIGURE 10: Polarisation modulation: (a) $n_x > n_y$, $\delta = \lambda/4$, right-circular polarisation;
(b) $n_x < n_y$, $\delta = \lambda/4$, left-circular polarisation

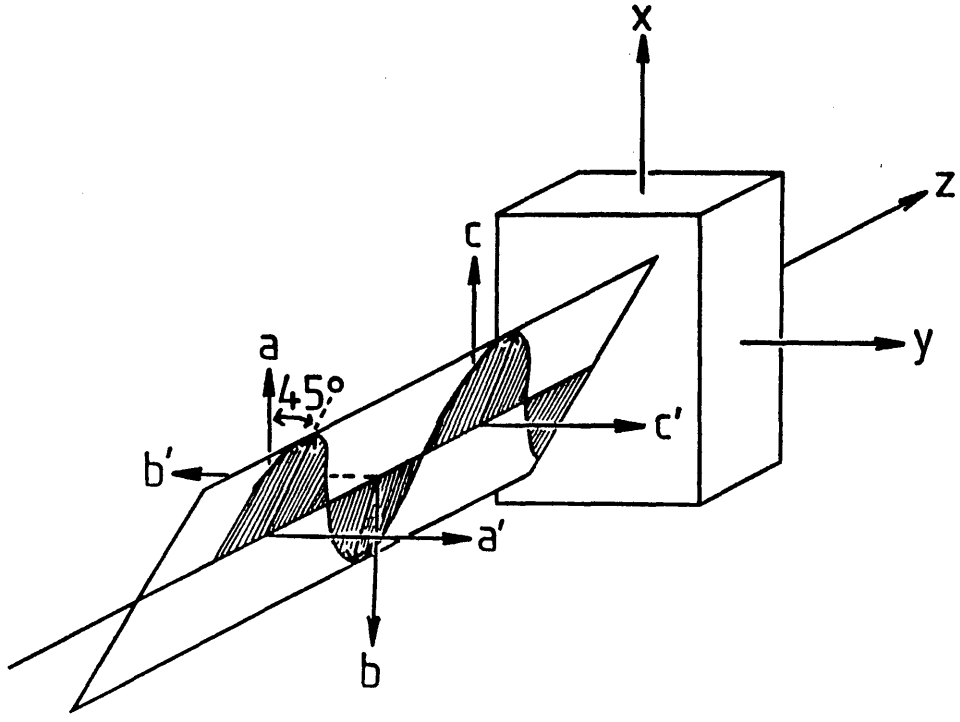

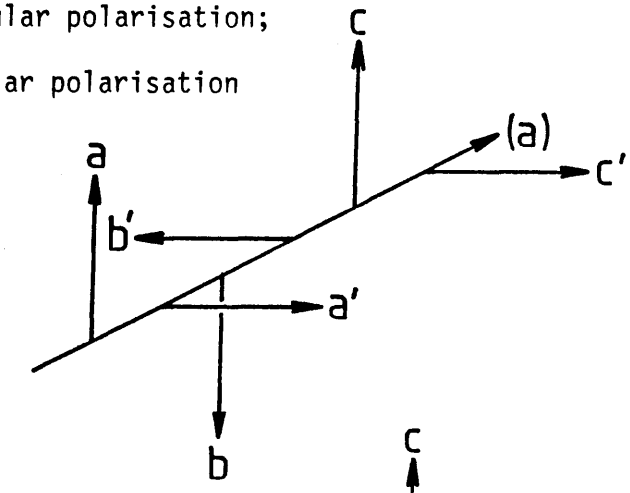

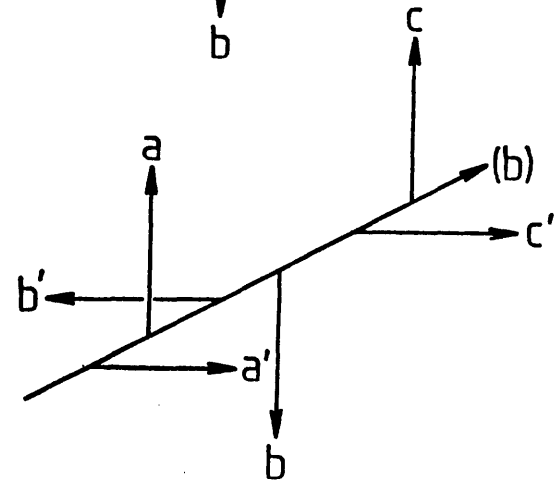

polarised light. A programmed variable pressure on the optical block is the basis of a device to generate a controllable polarisation. This is polarisation modulation.

ELECTRONIC ABSORPTION SPECTROSCOPY

Electronic absorption spectra were recorded on a Beckman U.V. 5270 u.v.-visible-N.I.R. spectrophotometer, using standard or vacuum line 1 mm quartz cells or the 1 mm quartz O.T.T.L.E.

LUMINESCENCE SPECTROSCOPY

Coherent 52G Kr^+ and Ar^+ ion lasers were used as excitation sources for recording the luminescence spectra. The emitted light was collected at 180°C to the incident beam and was analysed with a Spex Ramalog 4 double monochromator. The rotating sample technique was employed with solid samples to prevent burning in the laser beam.

INFRA-RED SPECTROSCOPY

Infra-red spectra were recorded on a Perkin Elmer 983 Infra-red Spectrophotometer with a 3600 Data Station. Samples were prepared in a dry box as fluorolube and nujol mulls between potassium bromide and silver chloride discs respectively.

RAMAN SPECTROSCOPY

Coherent 52G Kr^+ and Ar^+ ion lasers were used as light sources for recording Raman spectra. The rotating sample technique was employed

with solid samples to prevent burning in the laser beam. The scattered light was collected at 180° to the incident beam and was analysed with a Spex Ramalog 4 double monochromator. Spectra were calibrated using a neon lamp.

EXPERIMENTAL PROCEDURE

CHEMICALS

Table 1 lists the methods of purification for the solvents used in this work. Table 2 lists some of the chemicals used in this work, along with the suppliers and purity of the materials.

ELECTROLYTE

The electrolyte used in all electrochemical experiments was tetra-n-butylammonium tetrafluoroborate, purchased from Aldrich (99% pure) and Fluka (>99% pure). This was further purified as follows; 50 g of the electrolyte was added to 400 ml of water and heated to 50°C with stirring for two hours. The electrolyte was then filtered and washed with a further 100 ml of water. This was then dried overnight at room temperature under vacuum. The dry electrolyte was then recrystallised twice from ethylacetate/pentane and finally dried under vacuum and stored in a vacuum dessicator.

VACUUM LINE AND GLOVE BOX PROCEDURES

Conventional high vacuum techniques, using a Pyrex glass vacuum line

TABLE 1: Methods of purification of solvents

SOLVENT	PURIFICATION METHOD
Diethyl ether	Refluxed over sodium metal and distilled from sodium/potassium almagam, then transferred to a vacuum line vessel and degassed. Stored in the dark over activated 3A molecular sieves.
Toluene) Pentane)	Distilled from sodium then transferred to a vacuum line vessel and degassed. Stored in the dark over activated 5A molecular sieves.
Acetonitrile	Acetonitrile (Rathburn Chemicals HPLC Grade) was purified using the method of Winfield,[100] then stored in the dark over activated 3A molecular sieves.
Dimethylformamide	Method of purification was that of Coetzee,[101] then stored in the dark over activated 4A molecular sieves.
Methanol) Ethanol)	Distilled from CaH_2 and stored over activated 3A molecular sieves.
Methylenechloride	Dried over $CaCl_2$ and distilled from P_2O_5. Stored in the dark over activated 3A molecular sieves.
Ethylacetate) 1,2-dichlorobenzene) Ethylene glycol)	Stored over activated 4A molecular sieves.

TABLE 2: List of Chemicals

CHEMICAL	SUPPLIER	PURITY
2,2´-bipyridine	B.D.H.	99.5%
2,2´-bipyridine	Aldrich	99.5%
tetra-n-butylammonium tetrafluoroborate	Fluka	>99%
tetra-n-butylammonium tetrafluoroborate	Aldrich	99%
iridium(III) chloride trihydrate	Aldrich	99%
ruthenium(III) chloride trihydrate	Aldrich	99%
ammonium hexabromoosmate(IV)	Alpha	99%
(-)sparteine sulphate pentahydrate	Aldrich	99%
tetrafluoroboric acid	Riedel-de Haën	97%
lithium	Hopkin & Williams	99.8%
hydrochloric acid	May & Baker	>99%
nitric acid	B.D.H.	AnalaR
silver nitrate	Johnson Matthey	pure
potassium iodide	Riedel-de Haën	99.5%
propane-1,2-diamine	Hopkin & Williams	99%
formic acid	May & Baker	98%
sodium hydroxide	Formachem	96%
cobalt(II) chloride	Hopkin & Williams	99%
triethylorthoformate	May & Baker	98%
hydrogen peroxide	May & Baker	99%
trifluoromethanesulponic acid	Fluka	>98%
1,10-phenanthroline hydrate	Koch-Light Ltd	≥98%

and utilising a Genevac GDN3 rotary vane vacuum pump and a Jencons mercury diffusion pump, were employed for some reactions in this work. Pressures were measured using an Edwards Model 2G Vacustat Gauge, and minimum pressures were in the range 10^{-3}m bars or lower. Standard glass joints were greased with Dow Corning high vacuum grease, and reaction vessels were fitted with Rotaflo stopcocks. All vessels employed in vacuum line procedures were pre-dried by heating with an oxygen/methane torch while pumping. All solvents were purified before use and were degassed on the vacuum line by using a minimum of three, freeze-pump-thaw cycles, before storing over activated molecular sieves in the dark. Reactions were carried out in Pyrex double limb vessels (Figure 11), the reaction products being isolated in the second limb of the vessel, or alternatively, reactions were carried out in a vessel fitted with a 1 mm quartz u.v. cell (Figure 12) so that the electronic spectra could be monitored as the reactions proceeded.

Manipulations involving involatile compounds and materials were carried out in an argon atmosphere glove box (Lintott Engineering Company Limited), in which, typical moisture levels were in the range 2-12 ppm. Molecular sieves and manganese oxide were used for the removal of moisture and oxygen respectively from the box.

ANION EXCHANGE COLUMN PROCEDURE

The anion exchange resin used was Amberlite IRA-400 (Cl) purchased from BDH, evenly packed into a 2 x 30 cm column. To convert the resin from the chloride form into the tetrafluoroborate form, the column was eluted with 4 litres of 0.2 M tetrafluoroboric acid until testing

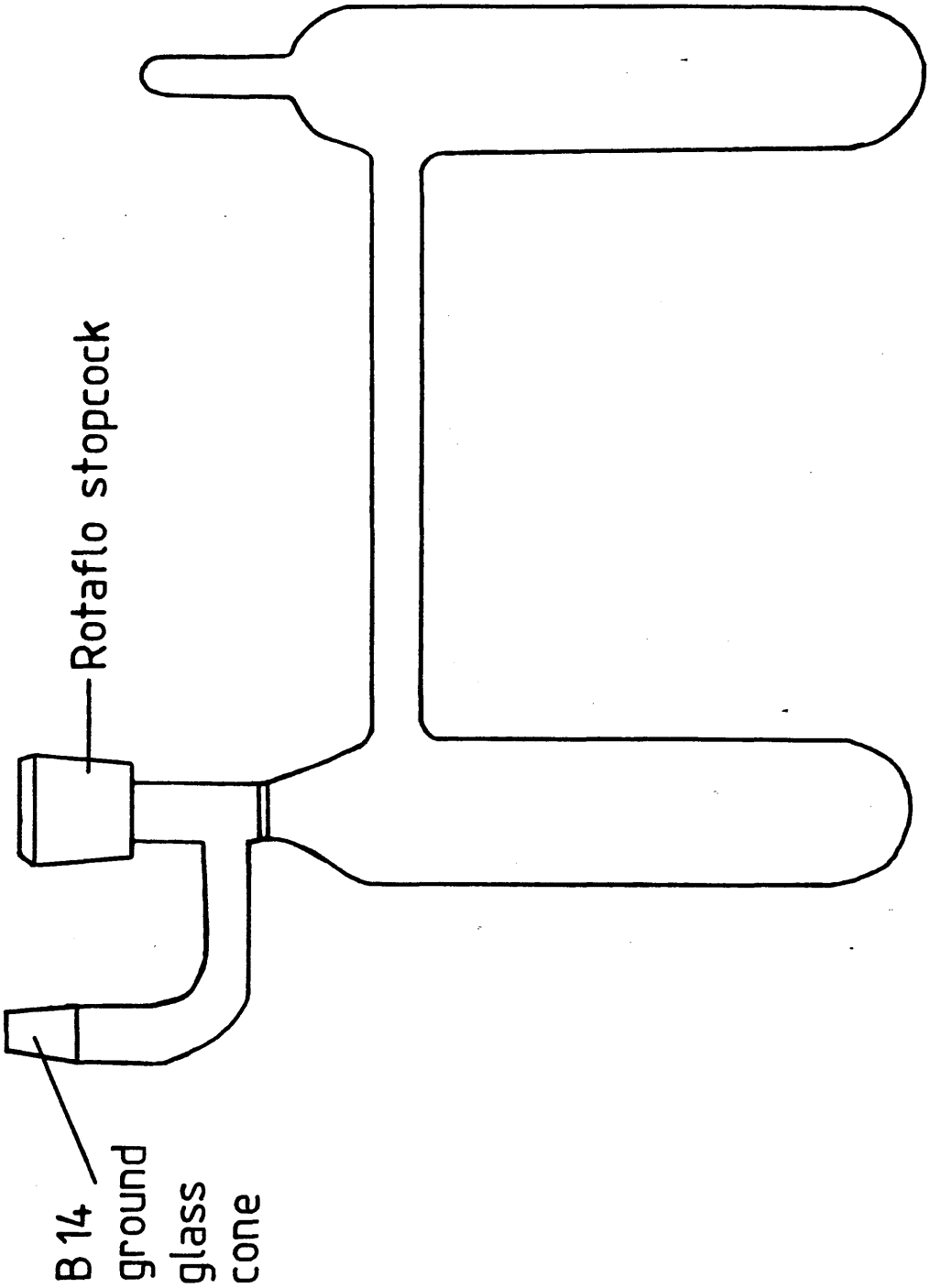

FIGURE 11: Double-limbed reaction vessel

FIGURE 12: Evacuable Cell for Electronic Spectroscopy

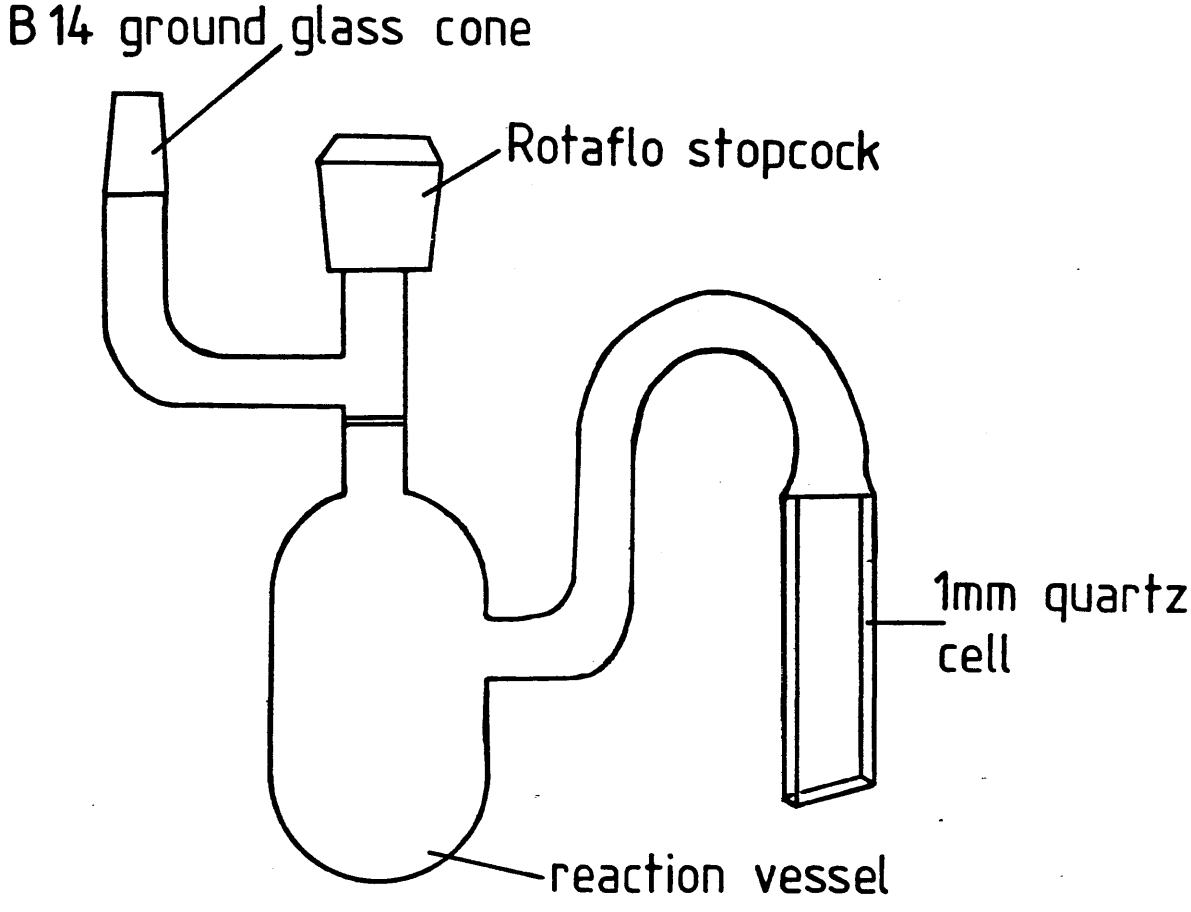

with silver nitrate solution showed no trace of chloride ions. The column was then eluted with 1 litre of distilled water to remove excess tetrafluoroboric acid. A dilute aqueous solution of the required compound could then be run down the column to convert it into the tetrafluoroborate salt.

SYNTHETIC PREPARATIONS

Preparation of tris(2,2´-bipyridine)ruthenium(II) iodide

Tris(2,2´-bipyridine)ruthenium(II) iodide was prepared using the method of Burstall.[8] Ruthenium trichloride (3.0 g) and 2,2´-bipyridine (9.0 g) were heated slowly with stirring to 220°C. The flask was then stoppered and the temperature raised to 280°C on a sandbath and was stirred vigorously for 5 hours. The cooled melt was then extracted with hot water into a separating funnel, and the solution was extracted with 3 x 50 ml of diethylether. The remaining solution was filtered from insoluble material and evaporated to crystallising point. The bright orange crystals were collected and dissolved in hot water to form a concentrated solution, to which a concentrated aqueous solution of potassium iodide was added. The red crystalline precipitate was recrystallised from hot water to yield 5.3 g of the complex iodide.

Resolution of tris(2,2´-bipyridine)ruthenium(II) iodide

Tris(2,2´-bipyridine)ruthenium(II) iodide was resolved using the method of Dwyer and Gyarfas.[10] The racemic iodide (2.0 g) was converted into the antimonyl(+)tartrate, by shaking with silver antimonyl(+)tartrate (0.9 g),

the silver iodide produced was removed by filtration. The solution was concentrated on a rotary evaporator and then cooled in ice, whereupon the antimonyl(+)tartrate salt crystallised out. The red crystals were washed with a small quantity of ice cold ethanol to remove traces of the more soluble salts. The red crystals were then dissolved in hot water and fractionally precipitated by addition of potassium iodide solution. The (-) or Δ-enantiomer was found in the least soluble fractions, and this was purified by recrystallisation from hot water.

The Δ-iodide was converted into the tetrafluoroborate salt on an anion exchange column as described earlier. The tetrafluoroborate salt was recrystallised from ethanol to give the pure complex I. The chloride salt was prepared in an analogous procedure.

Preparation of lithium Δ-tris(2,2′-bipyridinyl)ruthenate(II)

Δ-tris(2,2′-bipyridine)ruthenium(II) chloride, I, was dried under vacuum at 90-100°C before being added to a dry twin-limb vacuum line vessel. Lithium metal was cleaned of parafin using 1,1,1-trichloroethane and the outer coating was cut off in the glove box. Excess lithium metal was then added to the vessel containing the complex chloride. Purified dimethylformamide was distilled into the vessel and the solution was cooled in ice as the exothermic reaction proceeded. Occasionally the reaction was enhanced by placing the vessel in an ultrasonic bath.[102] Once the solution had changed from bright orange to dark red in colour and no further reaction occurred, the red solution could be decanted from the lithium chloride precipitate and excess lithium metal, and the solvent removed to leave the solid complex, I^{3-}. Pure complex I^{3-} could not be isolated as some residual lithium chloride always remained

with the solid.

Preparation of tris(2,2′-bipyridine)osmium(II) iodide trihydrate

Tris(2,2′-bipyridine)osmium(II) iodide trihydrate was prepared following the method of Burstall et al.[9] Ammonium hexabromoosmium(IV) (3.46 g) and 2,2′-bipyridine (8.00 g) were mixed intimately and heated carefully, the temperature being raised slowly to 220°C over a period of 1 hour, whereupon the resulting melt was a red/brown colour. Then under a nitrogen atmosphere the temperature was increased to 280°C using a sandbath and the mixture was stirred vigorously overnight. The black solution was allowed to cool and was then extracted with 400 ml of hot water. After filtration from traces of a black insoluble material the solution was taken to dryness on a rotary evaporator and the solid extracted with 4 x 50 ml of benzene to remove excess bipyridine. The remaining green solid was dissolved in 300 ml of hot water to which a saturated solution of potassium iodide was added to precipitate the iodide salt. The dark green solid was recrystallised from water with the addition of potassium iodide solution (yield 5.51 g). The remaining brown solution was discarded.

Resolution of tris(2,2′-bipyridine)osmium(II) iodide trihydrate

Tris(2,2′-bipyridine)osmium(II) iodide trihydrate was resolved using the method of Burstall et al.[9] Tris(2,2′bipyridine)osmium(II) iodide trihydrate (5.51 g) was dissolved in 400 ml of hot water, to which silver antimonyl(+)tartrate (2.25 g) was added. After filtration the solution was concentrated until approximately half of the compound crystallised on cooling in ice. The dark green platlets were filtered and washed with small quantities of ice cold ethanol, to remove traces of the more

soluble salts. This was then dissolved in warm water and fractionally precipitated repeatedly with potassium iodide solution, to give 0.41 g of the optically pure (-) or Δ-enantiomer. The mother liquors from the various crystallisations were combined and repeatedly crystallised by fractional precipitation with potassium iodide solution. Fractions of racemic material were combined and fractions of the (+) or Λ-enantiomer were combined until the Λ-enantiomer was fully resolved (yield 0.21 g) leaving 1.80 g of the pure racemic iodide.

The samples were checked for purity by chromatographing them on a Sephadex LH-20 column and eluting with methanol. In most cases only one dark green band was collected, occasionally a red band preceded the dark green band; this red band was discarded. Some of the optically resolved iodide was converted into the tetrafluoroborate salt on the anion exchange column as described earlier. The tetrafluoroborate salt was then recrystallised from ethanol to give the pure complex II. The chloride salt was prepared using an analogous procedure.

Preparation of lithium Δ-tris(2,2′-bipyridinyl)osmate(II)

Δ-lithium tris(2,2′-bipyridinyl)osmate(II), II^{3-}, was prepared in an analogous procedure to I^{3-}. The reaction proceeded with the green starting solution turning the dark red colour of the reduced complex. Pure complex II^{3-} could not be isolated as some residual lithium chloride always remained with the solid.

Preparation of cis-dichlorobis(2,2′-bipyridine)iridium(III) chloride

Cis-dichlorobis(2,2′-bipyridine)iridium(III) chloride was prepared using the method of Watts and co-workers.[103] Iridium trichloride (1.06 g)

and 2,2′-bipyridine 2.51 g were placed in a 25 ml round-bottomed flask with glycerol (10 ml). The flask was heated in a sand bath with stirring at 180°C for 2 hours, then left to cool overnight. Water (20 ml) was added to the resulting black solution, which was then extracted with 3 x 25 ml of diethylether to remove excess 2,2′-bipyridine. The remaining brown solution was cooled in ice and filtered. The brown solid was then dissolved in methanol, concentrated on a steam bath and the solution allowed to crystallise. The resulting yellow crystals were collected and washed with ice cold methanol and dried to yield 0.58 g of the product.

Preparation of cis-ditrifluoromethanesulphonatebis(2,2′-bipyridine)-iridium(III) trifluoromethanesulphonate

Cis-ditrifluoromethanesulphonatebis(2,2′-bipyridine)iridium(III) trifluoromethanesulphonate was prepared using the method of Sullivan et al.[104] Cis-dichlorobis(2,2′bipyridine)iridium(III) chloride (0.58 g) was placed in a flask with 30 ml of methylenechloride. Trifluoromethanesulphonic acid (10 ml) was added, whereupon the yellow solid dissolved to give a golden yellow solution which was allowed to evaporate overnight eliminating HCl. The resulting yellow solution was checked for the absence of free chloride with silver nitrate. A further 2 ml of trifluoromethanesulphonic acid was added to this solution which was then refluxed in 1,2-dichlorobenzene (20 ml) for 3 hours, then left to cool overnight. Diethylether (50 ml) was added to the cooled solution and the yellow crystals of cis-$[Ir(bipy)_2(OSO_2CF_3)_2](F_3CSO_3)$ were collected and washed with 200 ml of diethylether then dried to yield 0.25 g of the product. Anal Calcd for $[Ir(C_{10}H_8N_2)_2(CF_3SO_3)_2](CF_3SO_3)$: C, 29.02; H, 1.70; N, 5.89; S, 10.10. Found: C, 29.02; H, 1.56; N, 5.82; S, 9.91.

Preparation of tris(2,2′-bipyridine)iridium(III) chloride

Tris(2,2′-bipyridine)iridium(III) chloride was prepared using the method of Sullivan et al.[104] Cis-$[Ir(bipy)_2(OSO_2CF_3)_2](F_3CSO_3)$, (0.20 g), and 2,2′-bipyridine (0.70 g) were refluxed in ethyleneglycol (5 ml) for 6 hours, after which time the solution had turned brown in colour. Water (20 ml) was added to this and then extracted with 3 x 30 ml of diethylether to remove excess 2,2′-bipyridine. The solvent was evaporated off under vacuum and the remaining brown solid was dissolved in 30 ml of hot methanol. This solution was then concentrated to 4 ml on a rotary evaporator and the solution run down a 2.5 x 30 cm Sephadex LH-20 column, eluting with methanol. Three fractions were collected, the 2nd fraction was yellow and fluoresced green under a 365 nm u.v. lamp; this fraction contained the $[Ir(bipy)_3](CF_3SO_3)_3$. This was converted to the chloride salt by running a dilute aqueous solution down an anion exchange column as described earlier. (Yield 0.19 g)

Preparation of potassium (+)-tris(L-cysteinesulphinato(2-)-SN)cobaltate(III)

Potassium (+)-tris(L-cysteinesulphinato(2-)-SN)cobaltate(III) was prepared using the method of Dollimore et al.[12] $[Co(NH_3)_6]Cl_3$ (2.0 g) in water (50 ml) was deoxygenated using a nitrogen bubbler and then L-cystein (4.5 g) and potassium hydroxide (6.0 g) were added. The mixture was heated with stirring to 70°C and, when no further evolution of ammonia could be detected (4 hours), ethanol (50 ml) was added to precipitate the green potassium tris(L-cysteinato-SN)cobaltate(III). After cooling in ice and filtering, the solid was washed with 50 ml of ethanol. This was then added slowly to hydrogen peroxide (100 vol, 10 ml) cooling in an ice bath, to give a bright yellow solution. The complex

$K_3(+)$-[Co(L-cysu)$_3$] was precipitated by the addition of ethanol (60 ml) and was collected and washed with ethanol (50 ml). The complex was recrystallised from water/ethanol and dried to yield 2.3 g of product.

Resolution of tris(2,2′-bipyridine)iridium(III) chloride

Tris(2,2′-bipyridine)iridium(III) chloride was resolved by selective precipitation of the more insoluble diastereomer formed with the (+)-[Co(L-cysu)$_3$]$^{3-}$ complex ion.[12] The racemic [Ir(bipy)$_3$]Cl$_3$, (0.1850 g) was dissolved in hot water (5 ml) and an aqueous solution of $K_3(+)$-[Co(L-cysu)$_3$], (0.0880 g in 5 ml of H_2O) (2 mole racemate: 1 mole $K_3(+)$-[Co(L-cysu)$_3$]) was added to this. The solution was then fractionally crystallised, the optical activity of each fraction was tested and fractions of the same diastereomer were combined and the process repeated five times. The fractions were converted back to the chloride salts by anion exchange chromatography as described earlier (p 52). The solution of the more insoluble diastereomer rendered the pure complex (+) or Λ-[Ir(bipy)$_3$]Cl$_3$, III. The solution of the more soluble diastereomer was purified by chromatographing it on a Sephadex - LH-20 column in methanol to remove traces of a red compound. (NB neither enantiomer is likely to be fully resolved due to difficulty in crystallising the small amount of material available).

Preparation of Λ-tris(2,2′-bipyridinyl)iridium(III)

Λ-tris(2,2′-bipyridinyl)iridium(III), III^{3-}, was prepared in an analogous procedure to I^{3-} and II^{3-}. The reaction proceeded with the yellow solution turning the dark red red colour of the reduced complex.

Preparation of lithium 2,2´-bipyridinyl

2,2´-bipyridine was dried under vacuum then added to a dry twin-limb vacuum line vessel. Excess lithium metal (prepared as described earlier) was added to the vessel and solvent (either diethylether or toluene) was distilled in. The reaction proceeded with the colourless solution turning the dark red colour of the reduced compound. At this stage the solution was decanted off the excess lithium to prevent formation of the dark green dilithium 2,2´bipyridinyl. The solvent was back-distilled to leave the black solid salt, IV.

Preparation of R(+)-tetra-N,N,N´,N´-methylpropane-1,2-diamine

R(-)-propane-1,2-diamine (6.8 g) dissolved in water (60 ml) was added slowly to ice cold formic acid (65 ml). To this, formaldehyde (40%, 60 ml) was added and the mixture refluxed for 7 hours then cooled overnight. 10M hydrochloric acid (55 ml) was added to the cooled solution which was then evaporated on a rotary evaporator, the receiver being cooled in ice, to give a yellow oil. Sodium hydroxide (16 g) dissolved in water (100 ml) was added to the oil and the solution was extracted with 3 x 150 ml of diethylether. The ether was removed on a rotary evaporator to leave a yellow liquid which was then fractionally distilled off a 20 cm column under vacuum. The fraction which distilled at 34°C was collected and stored over activated 5A molecular sieves in the dark. The 90 MHz n.m.r. of the liquid in $CDCl_3$ confirmed it was R(+)-tetra-N,N,N´,N´-methylpropane-1,2-diamine with 2 singlets at 2.23 and 2.20 ppm and a doublet at 0.91 ppm (integral 2:2:1) corresponding to the 5 methyl groups, and weaker signals between 2.90 and 1.85 ppm (integral 1) corresponding to the 3 single protons.

Preparation of S(-)-tetra-N,N,N′,N′-methylpropane-1,2-diamine

S(-)-tetra-N,N,N′,N′-methylpropane-1,2-diamine was prepared using the above method, starting from S(+)-propane-1,2-diamine.

Optical purity of R(+) and S(-)-tetra-N,N,N′,N′-methylpropane-1,2-diamine

The optical purity of the R and S enantiomers could be checked by preparing the cobalt(II) chloride complexes.[105] Cobalt(II) chloride (0.15 g) was dissolved in ethanol (10 ml) to which triethyloroformate (1 ml) had been added. Tetra-N,N,N′,N′-methylpropane-1,2-diamine (1 ml) and triethylorthoformate (1 ml) were dissolved in ethanol (10 ml) and this solution was slowly added to the solution of cobalt(II) chloride. The resulting solution was refluxed for ¼ hour then boiled to remove most of the ethanol. When cool, diethylether was added and the bright blue crystals were collected and washed with cold ethanol/diethylether 1:1) then dried in a vacuum dessicator. (Yield 0.20 g)

The differential extinction coefficients of the two enantiomeric complexes were compared with literature values.[105] The S(-) enantiomer had $\Delta\varepsilon_{575nm}$ = 0.17 (lit 0.21) and so the S(-) enantiomer was 80% resolved. The R(+) enantiomer was found to be optically pure.

Preparation of 2,2′-bipyridinyl(R(+)-tetra-N,N,N′,N′-methylpropane-1,2-diamine)lithium(I)

All manipulations were executed using vacuum line and glove box techniques. Lithium metal (excess) and 2,2′-bipyridine were added to a dry vacuum line vessel. R(+)-tetra-N,N,N′,N′-methylpropane-1,2-diamine (excess) was distilled into the vessel followed by the solvent (either diethylether or toluene). The lithium was left in

the vessel until the dark red colour of the product had formed and was then removed to prevent any further reaction.

The S(+) complex was prepared in an analogous procedure.

Preparation of (-)-sparteine

(-)-sparteine sulphate dissolved in water was basified with aqueous sodium hydroxide until the solution turned milky white and a colourless oil formed on the surface. The oil was extracted 3 times with diethylether and the ether was removed on a rotary evaporator. The remaining liquid was distilled under vacuum, the fraction which distilled at 101°C was retained and was stored over 5A molecular sieves.

Preparation of 2,2′-bipyridinyl((-)-sparteine)lithium(I)

All manipulations were executed using vacuum line and glove box techniques. Lithium metal (excess) 2,2′-bipyridine and (-)-sparteine (excess) were added to a dry vacuum line vessel. The solvent (either toluene or diethylether) was distilled in and the reaction allowed to proceed until the dark red colour of the product had formed, then the lithium was removed to prevent any further reaction.

CHAPTER 3

LITHIUM- BIPYRIDINYL

The 2,2′-Bipyridinyl Anion

The 2,2′-bipyridinyl anion ($bipy^-$) was first synthesised in 1958 as the sodium and lithium salts by Elschner and Herzog[106] who reported the e.s.r. spectrum of the anion. From the e.s.r. spectra it was proposed that both the lithium and sodium cations were co-ordinated to both nitrogen atoms of $bipy^-$ (that is, $bipy^-$ assumed the planar cis-configuration) and that the unpaired electron resided in the π-orbitals of the aromatic compound. However no detailed analysis of the hyper-fine structure of the e.s.r. spectrum was given. Since then the e.s.r. spectrum of the compound has been reported in more detail by several authors[71-74, 107-109] and as well as the sodium and lithium salts, the potassium,[72-74, 107] rubidium[73,107] and more recently, organometallic cation salts[108,109] have also been prepared.

Other spectroscopic studies on $bipy^-$ have since been reported, including absorption,[70,110-112] infrared[113] and Raman spectra[41,42] but in some cases arbitrary[112] or inaccurate[110,111] units were used and only a limited spectral range was covered.[110-112,41,42] In this work an attempt has been made to correlate the existing information and to extend the studies on the compound in an attempt to gain more information on the structure, bonding and properties of the $bipy^-$ anion.

Electronic Spectroscopy of $Bipy^-$

2,2′-bipyridine can be considered to have twelve Hückel molecular orbitals[114] (designated π 1 to π 12) the first six of which are bonding orbitals and will be completely filled for the neutral molecule (Figure 13). The lowest energy $\pi \rightarrow \pi^*$ excitation will be from π 6 (HOMO) to π 7 (LUMO) which occurs at 278 nm for free bipy. When the mono anion

of bipy (bipy$^-$) is formed as in Li^+bipy^-, the added electron will enter the π 7 antibonding orbital. The lowest energy $\pi \rightarrow \pi^*$ transition in bipy$^-$ will still be the π 6 $\rightarrow$ π 7 transition[70] as the π 7 orbital is not completely filled. However this will not be the lowest energy transition as now transitions from the π 7 orbital to π 8, π 9 and π 10 are now available. The occupancy of the π-orbitals of both bipy and bipy$^-$ are shown in Figure 13.

The electronic absorption spectrum of bipy$^-$ in the region between 200 and 1600 nm consists of four main absorption bands (Figure 14). Konig and Kremer[70] assigned the bands centred on approximately 261 nm as π 6 $\rightarrow$ π 8,9 transitions, the band centred on 393 nm was assigned as a π 6 $\rightarrow$ π 7 transition, the band centred on 534 nm was assigned as a π 7 $\rightarrow$ π 10 transition and the band at 816 nm was assigned as π 7 $\rightarrow$ π 8,9 transitions. The experimental data in this work is, on the whole, in agreement with the assignments of Konig and Kremer, however on careful examination of the absorption bands and vibrational intervals, several differences do arise. The experimentally observed wavelengths and energies of the electronic transitions and vibronic lines and the assignments of these bands are given in Table 3.

Individual assignments of the bands in the high energy region between 200 and 300 nm has not been possible and these are collectively assigned as in reference 70 as π 6 $\rightarrow$ π 8,9, π 4 $\rightarrow$ π 7 and π 5 $\rightarrow$ π 7 transitions. The two weaker bands at 230 and 286 nm have no visible vibronic structure but the strongest band which has its origin at 267.5 nm has a vibrational progression of 948 cm^{-1} which is quite low in energy.

The most intense band centred on approximately 380 nm at first glance seems to have a regular vibrational progression and has been assigned

TABLE 3

Wavelength (nm)	Energy (cm^{-1})	(Progression) Energy Difference (cm^{-1})	Assignment
230	43,478	-	
237.5	42,105		
		953	$\pi 4 \rightarrow \pi 7$
243.0	41,152	937	$\pi 5 \rightarrow \pi 7$
248.6	40,225	927	$\pi 6 \rightarrow \pi 8,9$
254.4	39,308	950	
260.7	38,358	975	Average
267.5	37,383		948 cm^{-1}
286	34,965	-	
325.8	30,694		
		976	
336.5	29,718	1,081	$\pi 6 \rightarrow \pi 7$
349.2	28,637	782	$\pi 7 \rightarrow \pi 11$
359.0	27,855	1,153	
374.5	26,702	762	
385.5	25,940	-1,902	(origin)
416.0	24,038		(hot band)
483	20,704		
		1,249	$\pi 7 \rightarrow \pi 10$
514	19,455	1,240	Average
549	18,215		1245 cm^{-1}
671	14,903		
		1,389	$\pi 7 \rightarrow \pi 9$
740	13,514	1,383	Average
825	12,121	1,391	1388 cm^{-1}
932	10,730		
1,048	9,545		
		1,363	$\pi 7 \rightarrow \pi 8$
1,222	8,182	1,364	Average
1,467	6,818		1364 cm^{-1}

FIGURE 13: The occupancy of the π-orbitals of bipy and bipy$^-$

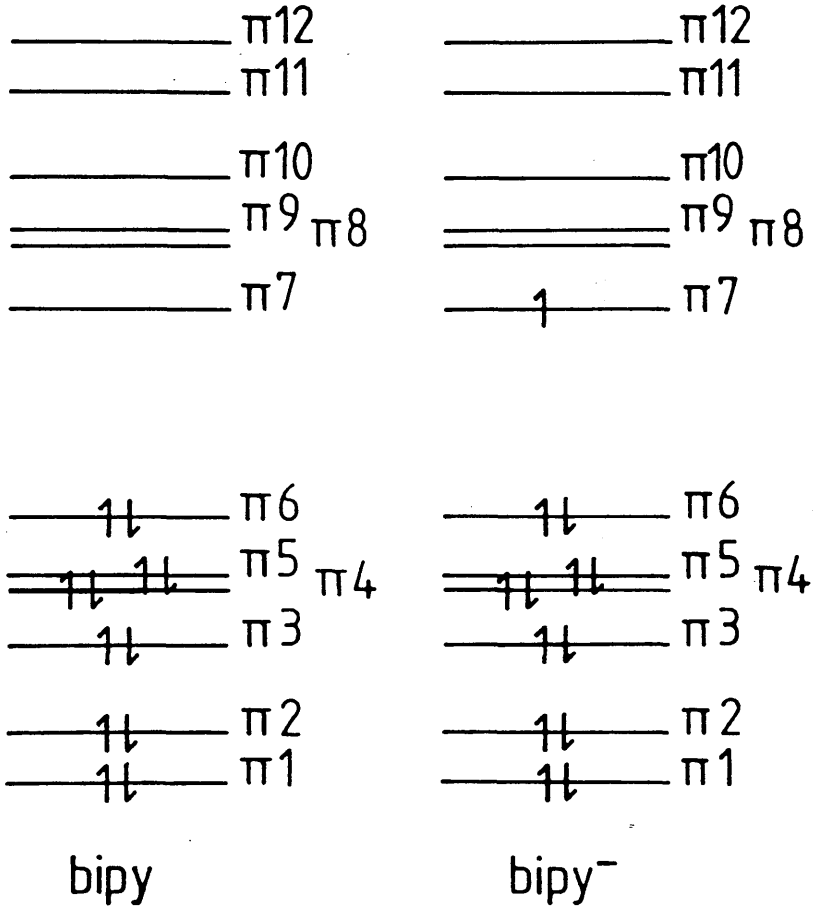

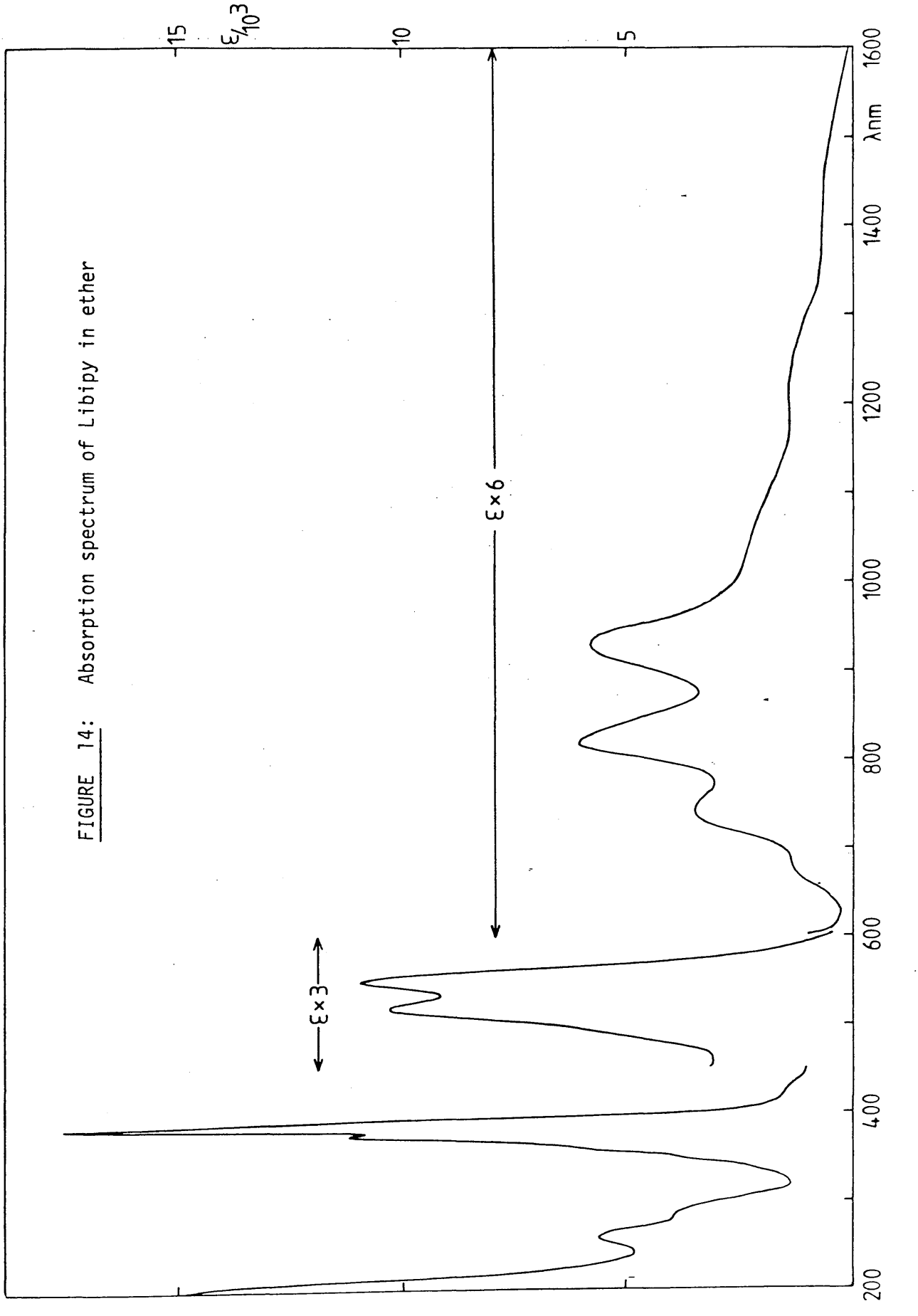

FIGURE 14: Absorption spectrum of Libipy in ether

as the π 6 $\rightarrow$ π 7 transition by Konig and Kremer.[70] However on careful measurements of the energy differences between individual absorptions, an extremely irregular pattern emerges (Table 3). Ignoring the band at 416 nm, the energy differences between the bands fluctuate between approximately 800 cm^{-1} and 1100 cm^{-1}. The possibility of having two vibronic progressions on one electronic transition can be ruled out because the lower in energy of the two progressions would be an average of 800 cm^{-1} from an origin band at 385.5 nm or 1100 cm^{-1} from an origin at 374.5 nm. However the higher energy progression would then be approximately 1900 cm^{-1}, which is far too high an energy to be of vibrational origin in this compound. Now from the calculations of Konig and Kremer[70], the π 7 $\rightarrow$ π 11 band of $bipy^-$ is predicted to occur at 356 nm which is in the region of this band. The dipole strength of this transition was calculated as only 0.02$\mathring{A}^2$ compared to 1.46$\mathring{A}^2$ for the π 6 $\rightarrow$ π 7 band and so has been ignored by Konig and Kremer.[70] However if the theoretically calculated dipole strengths are compared to the experimental values there is very little agreement. It may therefore be possible that the experimental dipole strength of the π 7 $\rightarrow$ π 11 band is actually far greater than the theoretical value. Accordingly, this band is tentatively assigned as being due to both the π 6 $\rightarrow$ π 7 and the π 7 $\rightarrow$ π 11 transitions of $bipy^-$.

The band between 450 and 600 nm has been assigned, in agreement with Konig and Kremer,[70] as the π 7 $\rightarrow$ π 10 transition of $bipy^-$. Measured from the origin band at 549 nm, it has a vibrational progression of 1245 cm^{-1}.

The lowest energy band was collectively assigned as the π 7 $\rightarrow$ π 8,9 transition of $bipy^-$ by Konig and Kremer.[70] On examination of the shape

of the band, from an origin at 1,467 nm there is a gentle increase in intensity to 1,000 nm followed by a sharp increase in the intensity of the band which is not a normal Frank-Condon profile. Furthermore, when the vibrational intervals are measured between 1,467 and 1,048 nm the interval is 1364 cm^{-1} but between 932 and 671 nm it is 1388 cm^{-1} and so clearly it is possible to distinguish between the two transitions. Hence the lower energy and less intense band with its origin at 1,467 nm and a vibrational progression of 1364 cm^{-1} is assigned as the π 7 $\rightarrow$ π 8 transition of $bipy^-$. The higher energy and more intense band with its origin at 932 nm and a vibrational progression of 1388 cm^{-1} is assigned as the π 7 $\rightarrow$ π 9 transition of $bipy^-$.

Comparing the vibrational progressions for the π 7 $\rightarrow$ π 8,9 and 10 transitions of $bipy^-$, the π 7 $\rightarrow$ π 8 and 9 progressions are very similar, being 1364 and 1388 cm^{-1} respectively whilst that of the π 7 $\rightarrow$ π 10 progression is considerably lower in energy at 1245 cm^{-1}. To help reconcile the differences, MNDO molecular orbital calculations were performed on bipy and the schematic molecular orbitals for π 7 to π 10 are shown in Figure 15.

The molecular orbital diagrams have been simplified to show the schematic bonding in the π 7,8,9 and 10 orbitals of $bipy^-$ in Figure 16. The π 7 orbital is found to have considerable double bond character in both the rings and a double bond between the rings. Both the π 8 and π 9 orbitals on the other hand appear to have very little double-bond character, either in the rings, or in the bond between the rings. So in a π 7 $\rightarrow$ π 8 or π 9 transition of $bipy^-$ the double-bond character of the rings is reduced and the strength of the central bond would be reduced. The similarity of the π 7 $\rightarrow$ π 8 and the π 7 $\rightarrow$ π 4 transitions suggests that it is likely that the vibration in both cases is of the

FIGURE 15: Schematic molecular orbitals of bipy

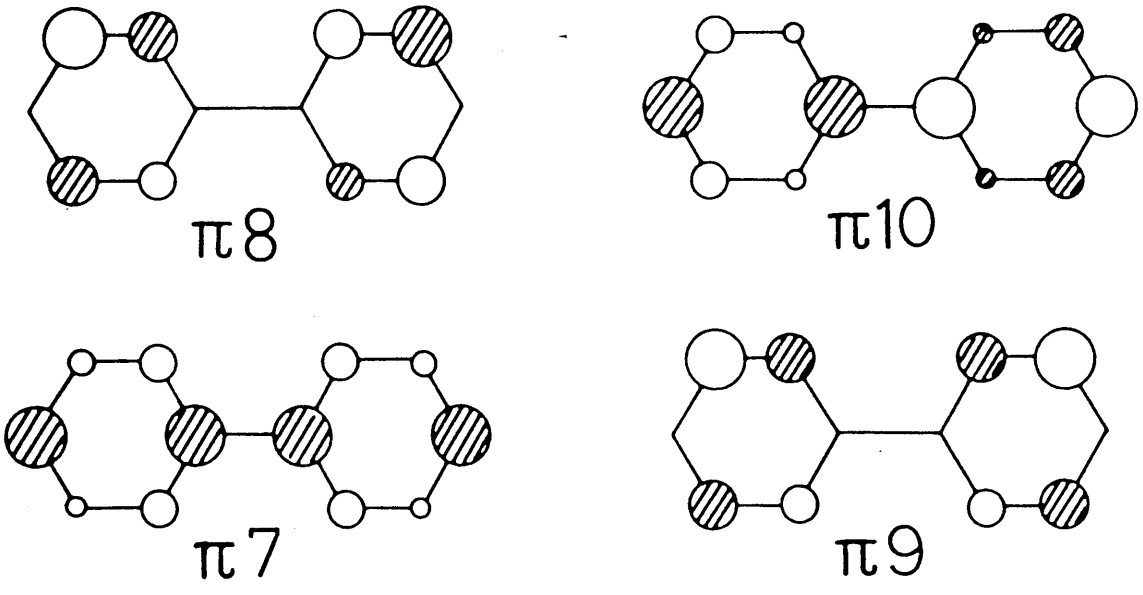

same type (possibly a ring stretching mode) and this would be consistent with the similar values of the vibrational progressions of 1364 and 1388 cm^{-1} for the π 7 $\rightarrow$ π 8 and π 7 $\rightarrow$ π 9 transitions respectively.

Comparing the π 7 and the π 10 orbitals of $bipy^-$, it is immediately obvious that the only difference between the bonding character of the two orbitals is that π 7 has a central double bond whilst π 10 does not. It is therefore possible that the vibration of 1245 cm^{-1} in the π 7 $\rightarrow$ π 10 transition is due to the symmetric inter-ring stretching mode of $bipy^-$. This would explain the difference in energies between the π 7 $\rightarrow$ π 10 and the π 7 $\rightarrow$ π 8 and π 9 vibrational progressions in $bipy^-$.

FIGURE 16: Schematic bonding diagrams of π-orbitals of bipy$^-$.

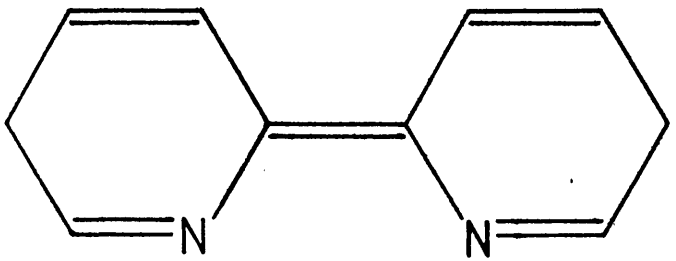

π7

π7 → π8

π7 → π9

π7 → π10

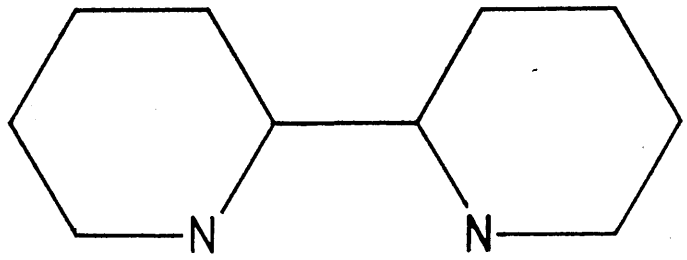

π8

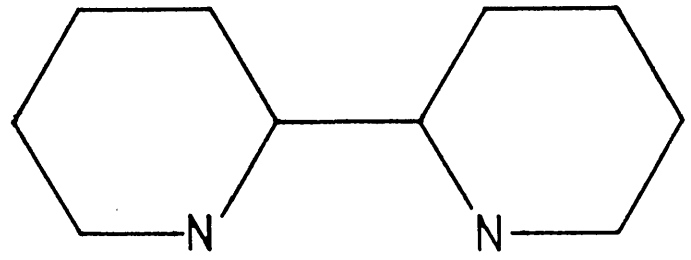

π9

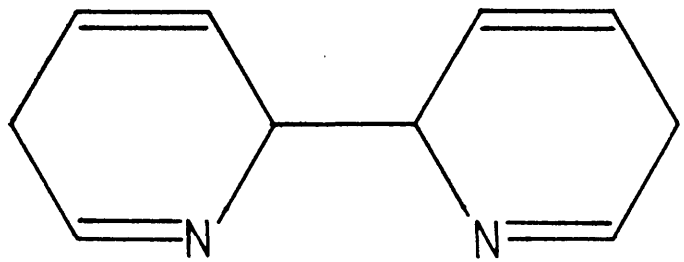

π10

Infra-red and Resonance Raman Spectra

In the solid state, 2,2′-bipyridine is trans-coplanar with essentially C_{2h} symmetry. It has a centre of symmetry, making the Raman and infra-red modes mutually exclusive, thus eliminating approximately half of the vibrational degrees of freedom from infra-red activity. On reduction with lithium the 2,2′-bipyridinyl anion assumes the cis-configuration (symmetry C_{2v}) thus increasing the number of infra-red active modes and only disallowing some of the out-of-plane modes. For example four i.r. active C-H vibrations are expected and observed in the 3100-3000 cm^{-1} region of 2,2′-bipyridine whereas in the bipyridinyl anion, eight stretching modes are expected.[113]

The infra-red spectrum of $Libipy^-$ in both nujol and fluorolube mulls are shown in Figure 17 and the infra-red and Raman wavenumbers are given in Table 4 along with the literature values for comparison together with their empirical assignments.[113] The solid and solution infra-red wavenumbers are in good agreement between 1600 and 400 cm^{-1} with only small differences between the values of the comparable frequencies. However in the C-H stretching region there are major differences in the spectra. The literature spectrum has only two frequencies at 3120 and 3078 cm^{-1} which are both higher in energy than any of the solid phase frequencies. It is possible that these two frequencies correspond to the 3060 and 3018 cm^{-1} bands in the solid state spectra and have been shifted by 60 cm^{-1} to higher energy by some sort of solvent interaction. This is a feasible explanation as solvent shifts of up to 100 cm^{-1} are not uncommon.[115] The other difference is that there is no report of any C-H stretching bands below 3000 cm^{-1} in the literature whereas the solid state spectrum gives three bands. It is possible that any such bands in the solution spectrum were very weak and may have gone unnoticed but it

FIGURE 17: Infra-red spectra of Libipy in fluorolube and nujol mulls

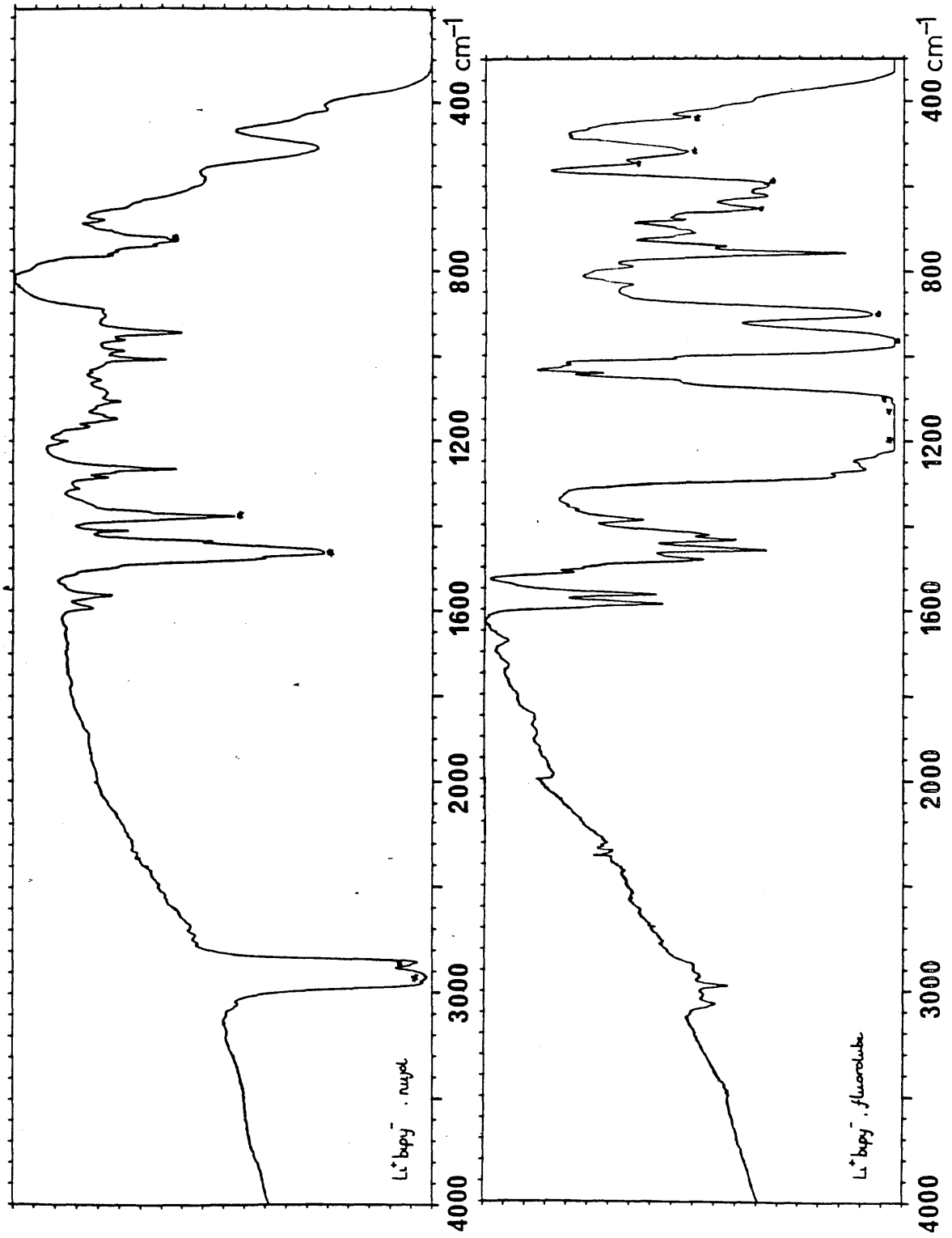

TABLE 4: Infrared and Raman frequencies of Libipy with empirical assignments

INFRARED (cm^{-1})		RAMAN (cm^{-1})		EMPIRICAL ASSIGNMENTS
Nujol/Fluorolube	tetrahydrofuran	d_8-Dioxan	tetrahydrofuran[42]	
3060	3120	3014		C-H stretch
3018	3078	2983		
2972		2949		
2930		2854		
2880				
1588	1597			ring stretch (C = C and C = N)
1563	1585	1555	1554	
1512	1570			
1495	1490			
1480	1460	1488	1486	ring stretch (C = C and C = N) + C-H bend
1459				
1433				
1421				
1410	1415		1412	
1389	1354			
1311		1353	1350	ring stretch (C = C and C = N)
1283				
1272	1277	1276	1275	
1265				
1200	1208	1205	1206	resonant dependant ring stretch
1165	1162	1164		
1148	1145			ring-H in-plane bend
1139				
1107				
1060				ring stretch
1041				
1021				
1008	1009		1019	ring H out-of-plane bend
988	991	995	992	
961	954			ring stretch (breathing)
944				
	806			ring-H out-of-plane bend
759	764			
742	745			
720				ring-H out-of-plane bend
711	713			
708				
699				
680	681			
623	646			ring bend
	621			
	484			inter-ring deformation
	440			
414	421			ring torsion
400	402			

is not possible to confirm this as the spectrum in this region was not included in the literature. The possibility that the C-H stretching bands below 3000 cm^{-1} are due to co-ordinated diethylether can be discounted. This is because although diethylether does have C-H stretching bands which are similar to those in the Libipy spectrum, it also has other very strong characteristic bands between 1500 and 1340 cm^{-1} and between 1190 and 1020 cm^{-1}. These strong bands are not present in the Libipy spectrum and other characteristic weaker bands of diethylether at 2600 cm^{-1} and 1970 cm^{-1} are also not present in the Libipy spectrum. Hence the C-H stretching bands below 3000 cm^{-1} must be assigned to Libipy. The presence of aromatic C-H stretching vibrations at lower energy than 3000 cm^{-1} is quite unusual in itself. 2,2′-bipyridine does have extremely weak vibrations at 2977, 2922 and 2875 cm^{-1} but these are more likely to be due to combination bands than C-H stretching frequencies. Other aromatic anions such as the cyclopentadienyl anion in ferrocene[116] has its C-H stretching vibrations at higher energy than 3000 cm^{-1} although this may be due to the near covalent bonding in this compound but even in cyclopentadienylthalium where the bonding is thought to be largely ionic, the C-H stretching modes are still at a higher energy than 3000 cm^{-1}. When comparing the carbon and nitrogen skeletal vibrations of $bipy^-$ with bipy it is expected that some vibrations will be shifted to higher energies and some to lower energies as the added electron is entering the π 7 orbital which has antibonding character. But it is difficult to see how the addition of an electron to the π-orbitals should cause changes in the C-H vibrations unless there is some sort of π-contribution to the C-H bonding. This might show up in a Normal Co-ordinate Analysis of $bipy^-$. However, for bipy, Normal Co-ordinate Analysis[117] shows that there is no contribution from the C-C modes to the C-H vibrations. Nevertheless, the experimental results

show that addition of an electron into the π 7-antibonding orbital of bipy, results in some antibonding character being conferred on to the C-H bonds of the compound.

The resonance Raman spectra of Libipy were obtained in deutero-dioxan and were found to be in excellent agreement with the literature spectrum[42] which was run in tetrahydrofuran. The use of a deuterated solvent has lead to the unambiguous assignment of bands in the 3000 cm^{-1} region of the spectrum to the C-H stretching vibrations of $bipy^-$. These bands had not previously been reported in the literature.[41,42] Literature Raman spectra were obtained using 350.7 nm[42] and 406.7 nm[41] laser excitations, whereas the resonance Raman spectra in this work were obtained using a variety of excitation lines (457.9 nm, 476.5 nm, 488.0 nm, 514.5 nm, 520.8 nm, 568.9 nm and 647.1 nm) of which the 647.1 nm and 514.5 nm excitations are shown in Figures 18 and 19.

When the 647.1 nm laser line is used (Figure 18), the Raman spectrum of Libipy is extremely weak with only the 1488 cm^{-1} line being visible along with the deutero-dioxan lines. As the energy of the laser excitation line is increased through 568.9 nm and 520.8 nm to 514.5 nm (Figure 19), the Raman bands of Libipy gain in intensity versus the deutero-dioxan lines. 514.5 nm is approximately in the centre of the π 7 $\rightarrow$ π 10 absorption of Libipy (Figure 14) and so at this energy resonance enhancement of the intensities of the $bipy^-$ Raman bands is at a maximum. As the energy of the laser line is further increased through 488.0 nm and 476.5 nm to 457.9 nm the intensities of the Raman lines of Libipy decrease again as the laser energy becomes greater in energy compared to the π 7 $\rightarrow$ π 10 absorption of $bipy^-$ and resonance enhancement decreases.

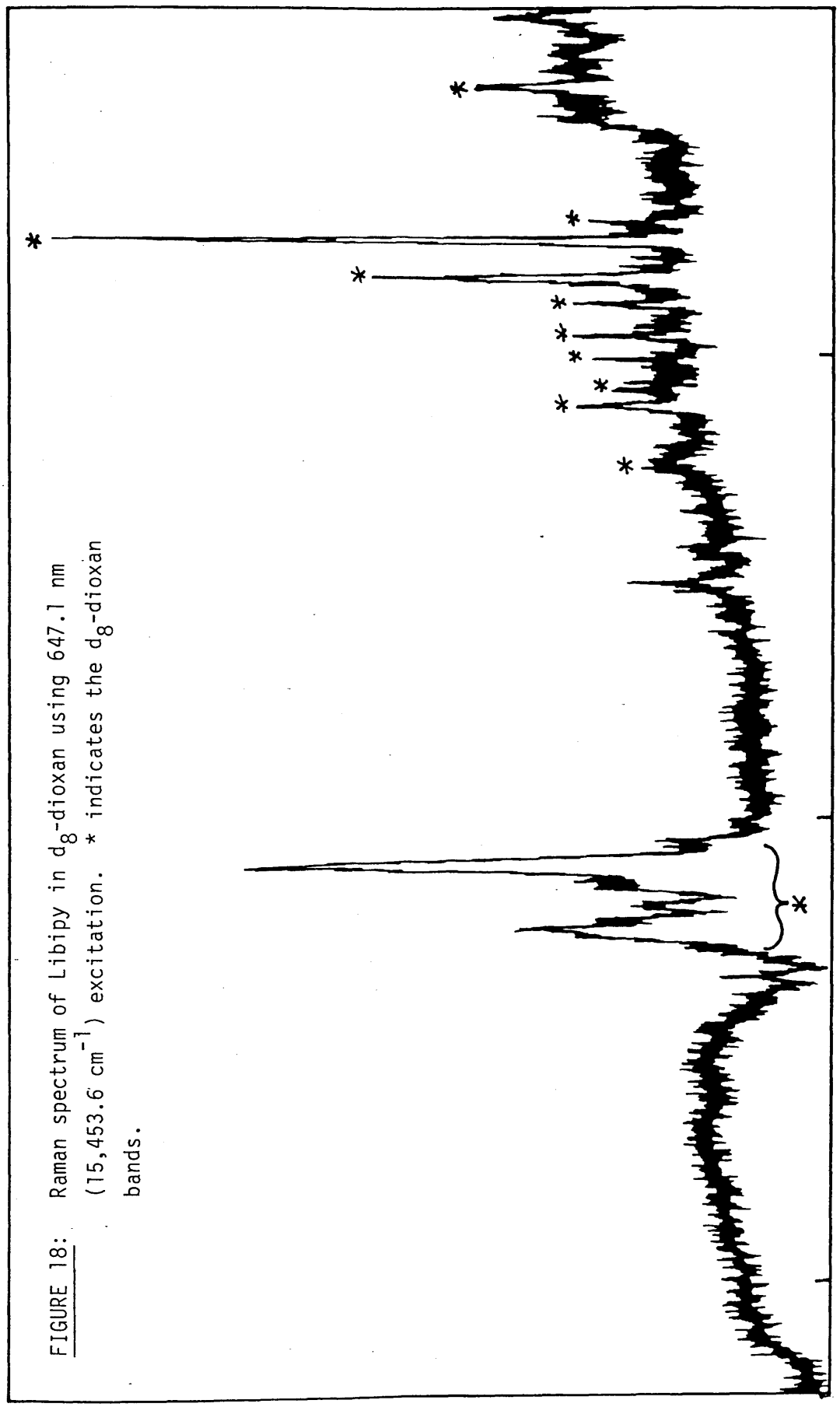

FIGURE 18: Raman spectrum of Libipy in d_8-dioxan using 647.1 nm (15,453.6 cm^{-1}) excitation. * indicates the d_8-dioxan bands.

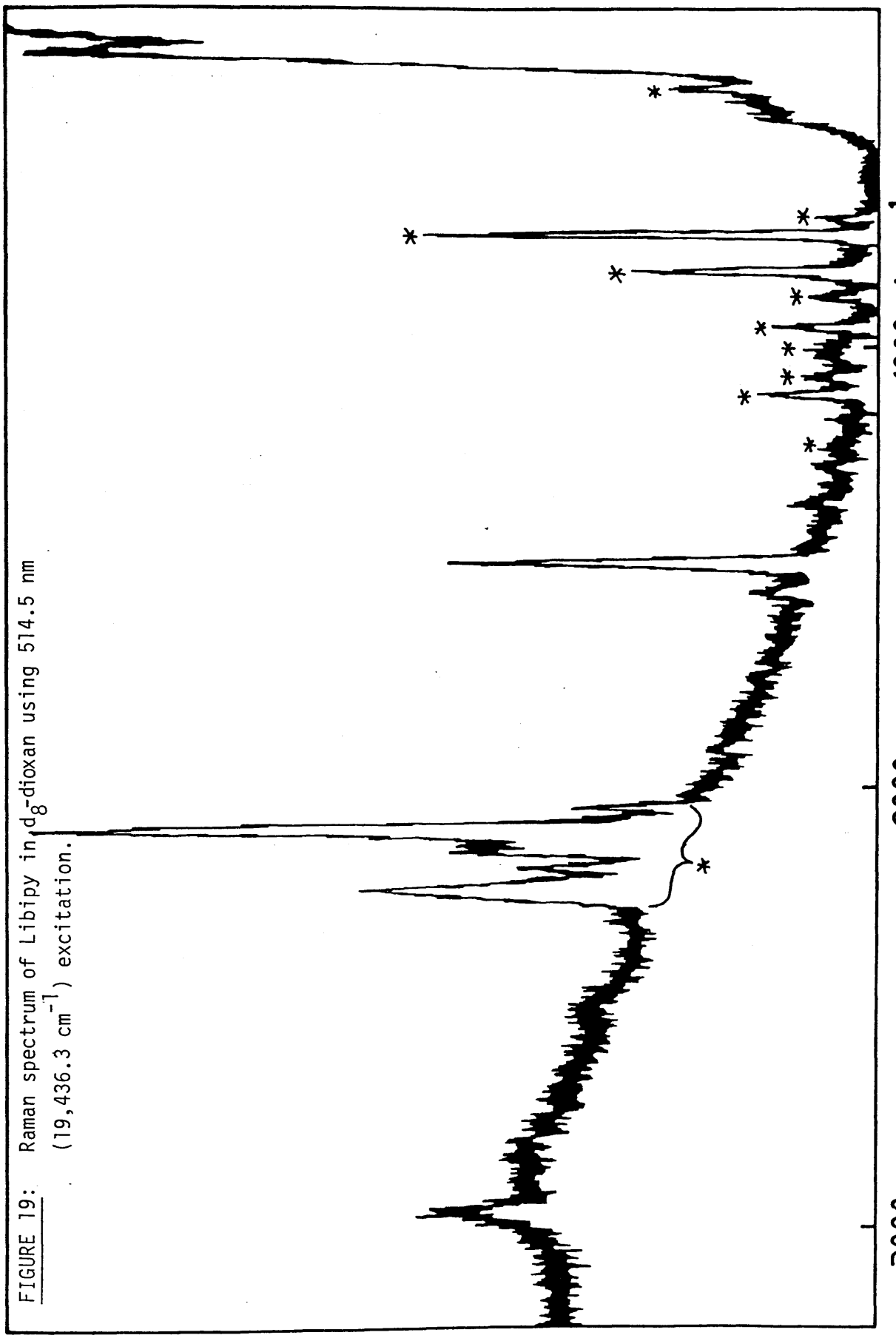

FIGURE 19: Raman spectrum of Libipy in d_8-dioxan using 514.5 nm (19,436.3 cm^{-1}) excitation.

As the resonance Raman intensities of bipy$^-$ increase to a maximum at 514.5 nm it is interesting to note that the intensity of the 1488 cm^{-1} band of bipy$^-$ is enhanced by an order of magnitude compared to the other lines of bipy$^-$. As the 1488 cm^{-1} line is enhanced so much it is concluded that this is the same vibrational mode as in the vibrational progression of 1245 cm^{-1} in the π 7 $\rightarrow$ π 10 absorption band. The difference in energy is because the Raman band is a ground-state vibration whilst the vibrational progression is due to the same vibration in the excited state of the compound.

The three C-H stretching bands below 3000 cm^{-1} in the resonance Raman spectra confirm that the bands in the infra-red spectrum of bipy$^-$ are more likely to be the C-H stretching modes of bipy$^-$ rather than solvent bands. Furthermore, this evidence from the resonance Raman spectra supports the theory that some antibonding character has been conferred on to the C-H bonds of bipy by adding an electron to the π-antibonding orbitals of the compound.

Luminescence

The luminescence of 2,2′-bipyridine has been well known since Gondo et al[118] measured its spectrum in 1965. In 2,2′-bipyridine a π 7 $\rightarrow$ π 6 type excited triplet state is believed to be responsible for the observed phosphorescence. There were no reports of the bipyridinyl anion having any luminescence in the literature and so investigations were carried out to see if luminescence could be detected from Libipy.

When a 10^{-3} mole l^{-1} solution of Libipy in either diethylether or deutero-dioxan was excited with the 514.5 nm laser line a very weak (approximately 2 orders of magnitude weaker than $[Ru(bipy)_3]^{2+}$

luminescence) luminescence was detected between approximately 12,000 and 18,000 cm^{-1}. The luminescence spectrum of Libipy in deutero-dioxan excited with the 514.5 nm laser line is shown in Figure 20. The high energy edge shows the resonance Raman spectrum of Libipy in which the resonance enhanced Raman band of $\Delta 1488\ cm^{-1}$ at approximately 18,000 cm^{-1} is clearly visible between the deutero-dioxan Raman bands.

The luminescence spectrum of Libipy is shown in relation to the absorption spectrum of Libipy in Figure 21. Now the laser excitation is at 514.5 nm which is in the centre of the π 7 $\rightarrow$ π 10 absorption band of $bipy^-$. It is extremely unlikely that higher energy transitions for example the π 6 $\rightarrow$ π 7 transition of $bipy^-$ at 380 nm could be excited and so the luminescence decay is unlikely to originate from these transitions. The lower energy π 7 $\rightarrow$ π 8 and 9 transitions could be excited by the laser line, however the luminescence band is at a higher energy than these transitions and so could not originate from them. Therefore it is concluded that the luminescence originates from the decay of the π 7 $\rightarrow$ π 10 transition of $bipy^-$.

Now since the luminescence spectrum originates from the decay of the π 7 $\rightarrow$ π 10 transition of $bipy^-$, both the ground and excited states must be doublet states (one unpaired electron in each state). In theory therefore neglecting any other interactions, the absorption and luminescence spectra should coincide, that is, be at the same energy. However, it is found that the absorption spectrum is approximately 2000 cm^{-1} higher in energy than the emission spectrum. This difference in energy has been attributed to a solvent shift as the maximum of luminescence occurs at 15,957 cm^{-1} in d_8-dioxan and is at 16,315 cm^{-1} in diethylether.

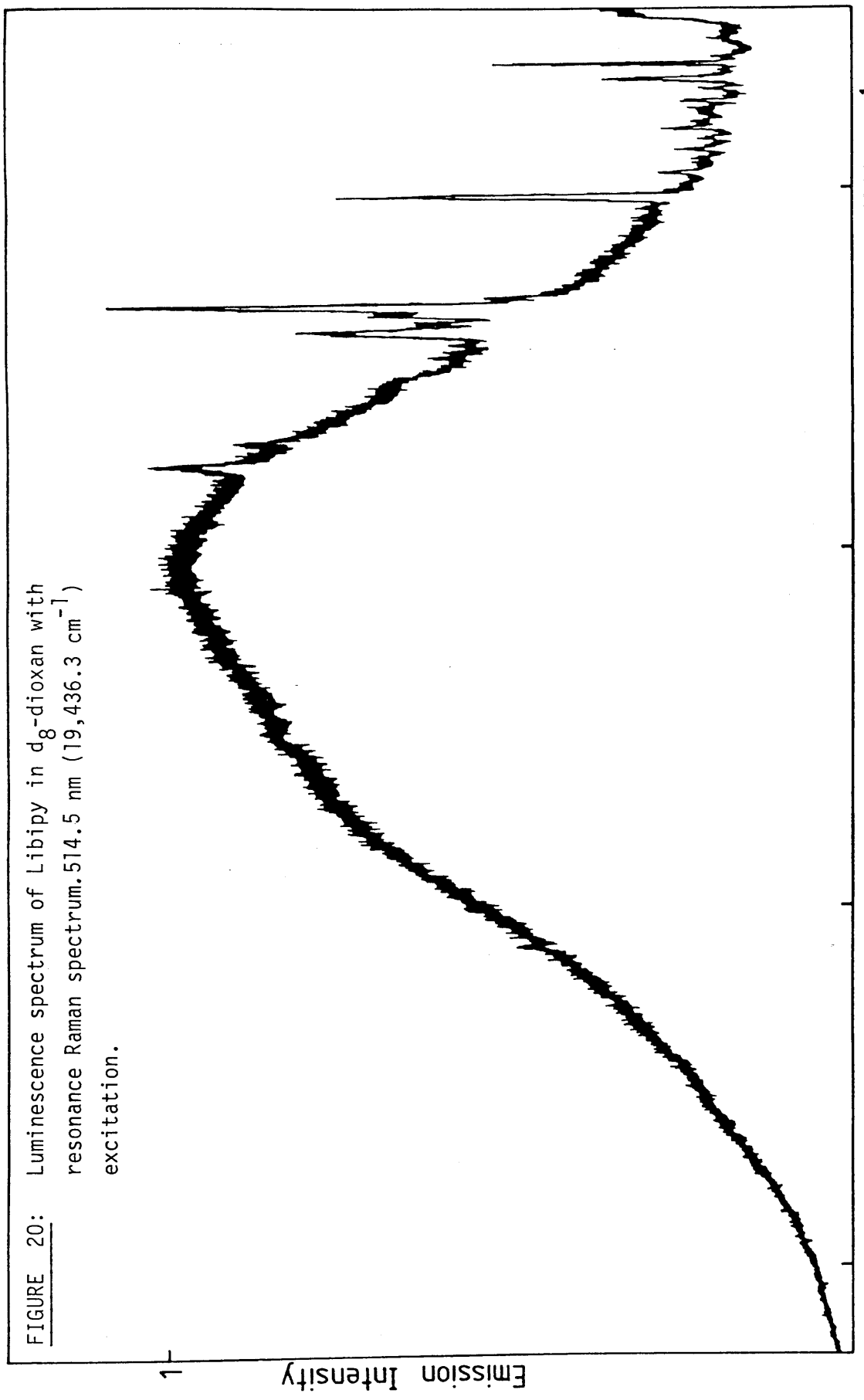

FIGURE 20: Luminescence spectrum of Libipy in d_8-dioxan with resonance Raman spectrum.514.5 nm (19,436.3 cm^{-1}) excitation.

FIGURE 21: Absorption and luminescence spectra of Libipy in ether.

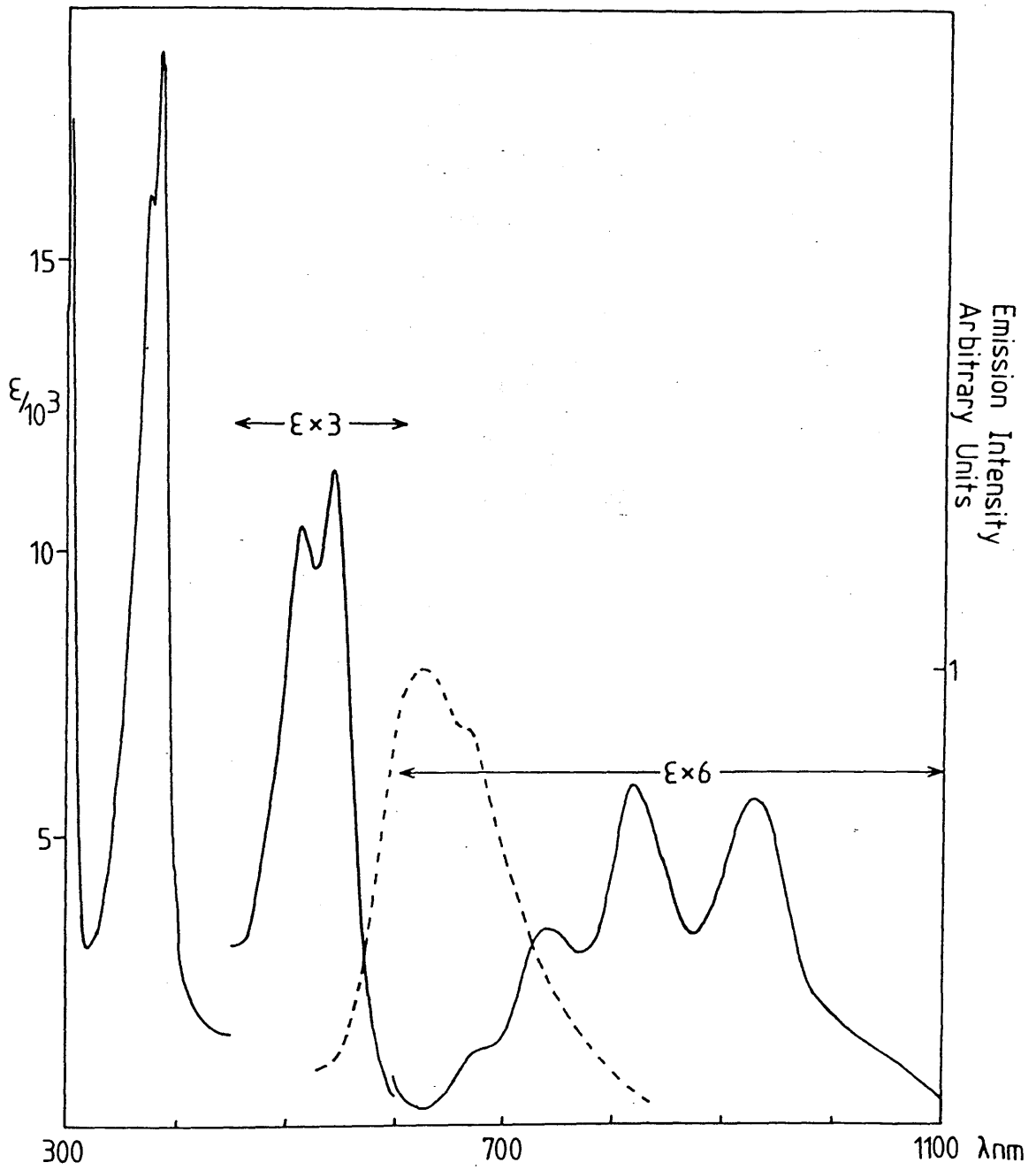

The luminescence band has a maximum at 15,957 cm^{-1} and a low energy shoulder at 14,465 cm^{-1}. The energy difference between these two bands should correspond to the energy of one of the Raman bands of $bipy^-$. The energy difference is 1492 cm^{-1} which is in excellent agreement with the Raman band of $bipy^-$ at 1488 cm^{-1}. Now it was postulated earlier that as the resonance Raman band at 1488 cm^{-1} is enhanced compared to the other bands, then this vibration is likely to be the same as the vibration in the progression of the π 7 $\rightarrow \pi$ 10 absorption band. Since the luminescence band originates from the decay of the π 7 $\rightarrow \pi$ 10 absorption any vibrational structure on the luminescence band should correspond to the same vibrational mode in the π 7 $\rightarrow \pi$ 10 absorption. As the ground-state vibration is given by the Raman band and since vibrations in luminescence spectra correspond to ground-state vibrations, the two should be the same. Since they have been shown to be equal to within experimental error the argument above confirms the assignment of both the luminescence and vibrational bands. Further, if the assignment of the vibrational mode in the π 7 $\rightarrow \pi$ 10 absorption is correct (namely that it is the symmetric inter-ring stretching mode of $bipy^-$) then the vibrational mode of 1488 cm^{-1} should also correspond to the symmetric inter-ring stretch of $bipy^-$. The difference in energy between the vibrations being due to in the 1245 cm^{-1} vibration there is only a single bond between the two rings of $bipy^-$ whilst the 1488 cm^{-1} vibration has double bond character between the rings and is therefore of higher energy.

Induced Circular Dichroism

2,2´-bipyridine, when in the planar configuration has C_{2v} symmetry for

the cis-conformation and C_{2h} symmetry for the trans-conformation. If one of the rings is rotated out of the plane at any angle with respect to the other ring then the molecule will have C_2 symmetry and hence will be chiral. In the solid state, 2,2′-bipyridine has been found to adopt the planar trans-configuration[119] and in solution it has a trans configuration with an angle of approximately 28° between the two rings.[120] Therefore in solution, 2,2′-bipyridine is chiral but of course a racemic mixture will be formed and no optical activity would be detected.

The 2,2′-bipyridinyl anion has the same symmetry properties as 2,2′-bipyridine, but unlike 2,2′-bipyridine it will adopt a planar configuration in solution. This is because the added electron to the π_7 orbital confers some double bond character across the central bond between the two pyridine type rings (in 2,2′-bipyridine the central bond has single-bond character) and the rings will orientate themselves to become planar with respect to each other in order to maximise the π-overlap across the bond. Furthermore when lithium 2,2′-bipyridinyl is synthesised, evidence from the e.s.r. spectra[73,74] of the compound indicates that the bipyridinyl anion co-ordinates to the lithium ion through both nitrogen atoms, hence the cis-conformation is formed in solution.

The lithium cation is normally four-co-ordinate, so in solution when Libipy is formed, two solvent molecules will occupy the vacant co-ordination sites round Li^+. If these solvent molecules could be replaced by a chiral bidentate ligand however, steric hindrance may force the two rings of the bipyridinyl anion to become non-planar with respect to each other (that is, the molecule would become twisted about the central bond) and it would then become chiral. Induced circular dichroism of this nature has recently been achieved using the chiral bidentate ligands, (-)-sparteine and

(+) and (-)-2,3-dimethoxy-1,4-bis(dimethylamino)butane with a variety of arylmethyllithium compounds.[121] In this work the induced circular dichroism of Libipy was achieved using the chiral bidentate ligands, (+) and (-)-tetra-N,N,N′,N′-methylpropane-1,2-diamine and the naturally occurring alkaloid (-)-sparteine (Figure 22).

FIGURE 22: (-)-sparteine

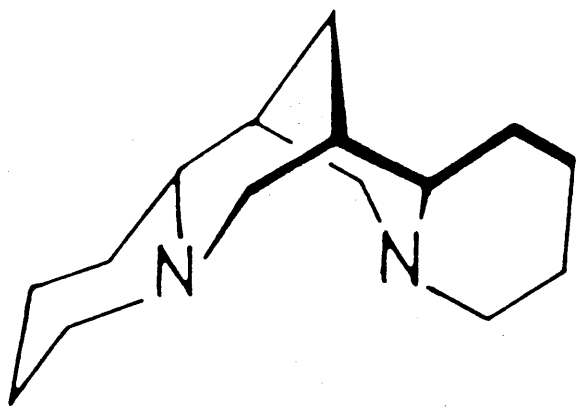

A typical circular dichroism spectrum of Libipy$^-$ using the chiral bidentate ligand (+)-tetra-N,N, N′,N′-methylpropane-1,2-diamine ((+)-Me_4pn) is shown in Figure 23. The circular dichroism spectrum shows two negative bands under the $\pi 6 \rightarrow \pi 7$ and $\pi 7 \rightarrow \pi 10$ transitions of bipy$^-$ with values of $\Delta\varepsilon$ of -6.3 and -0.7 $1mol^{-1}cm^{-1}$ respectively. The values of $\Delta\varepsilon$ are of the same magnitude as those for the induced circular dichroism of various carbanions reported by Okamota et al.[121] The circular dichroism spectrum could only be measured up to 900 nm which is approximately three quarters of the way under the $\pi 7 \rightarrow \pi 9$ band of bipy$^-$, up to this point no circular dichroism could be detected under this absorption.

FIGURE 23: Induced circular dichroism of lithium bipyridinyl in the presence of (+)-tetra-N,N,N′,N′-methylpropane-1,2-diamine

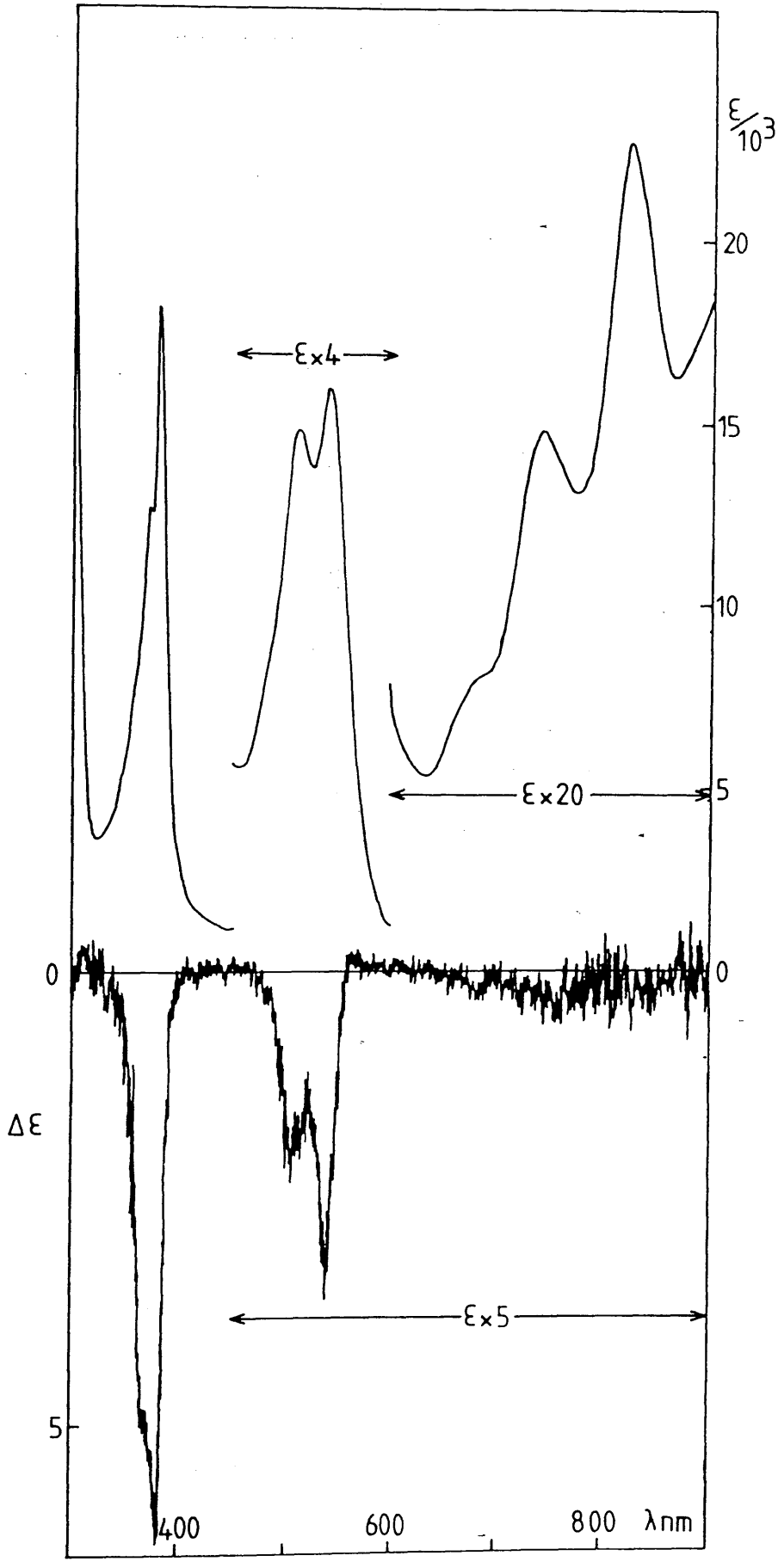

The 2,2′-bipyridinyl anion can be thought of in two ways:

i) as two symmetric groups (like two pyridine molecules) coupled together in a dissymmetric environment or

ii) as an inherently dissymmetric chromophore.

In the first case each of the two rings in the 2,2′-bipyridinyl anion have transitions which can be either long or short axis polarised (Figure 24). The transitions can be combined into various coupling modes and the resultant transition is optically active.

In Figure 24, the short-axis polarised transitions are represented by the a transitions and the long-axis polarised transitions as the b transitions. Considering the short-axis polarised transitions, if the molecule has the twisted structure according to Figure 24, for the (a,a) coupling mode, the charge will follow a right handed helix along and around the z-axis of the molecule. For the (a,-a) coupling mode, the charge will follow a left handed helix along and around the x-axis of the molecule. Therefore, if the two short-axis polarised coupling modes have different energies, then the circular dichroism spectrum would be expected to show two bands of equal area but opposite sign under the short-axis polarised absorption band of the molecule. Furthermore, the coupling would be strong and a large value of $\Delta\varepsilon$ would be expected for the c.d. bands. Considering the long-axis polarised transitions, the (b,b) transition has both a zero electric dipole moment and a zero rotatory strength. The (b,-b) transition has an electric dipole moment directed along the y-axis of the molecule and a small magnetic moment with the same orientation, arising from the rotatory displacement of charge across the twisted internuclear bond

FIGURE 24: Separate short-(a) and long-axis (b) polarised transition moments in twisted 2,2′-bipyridine

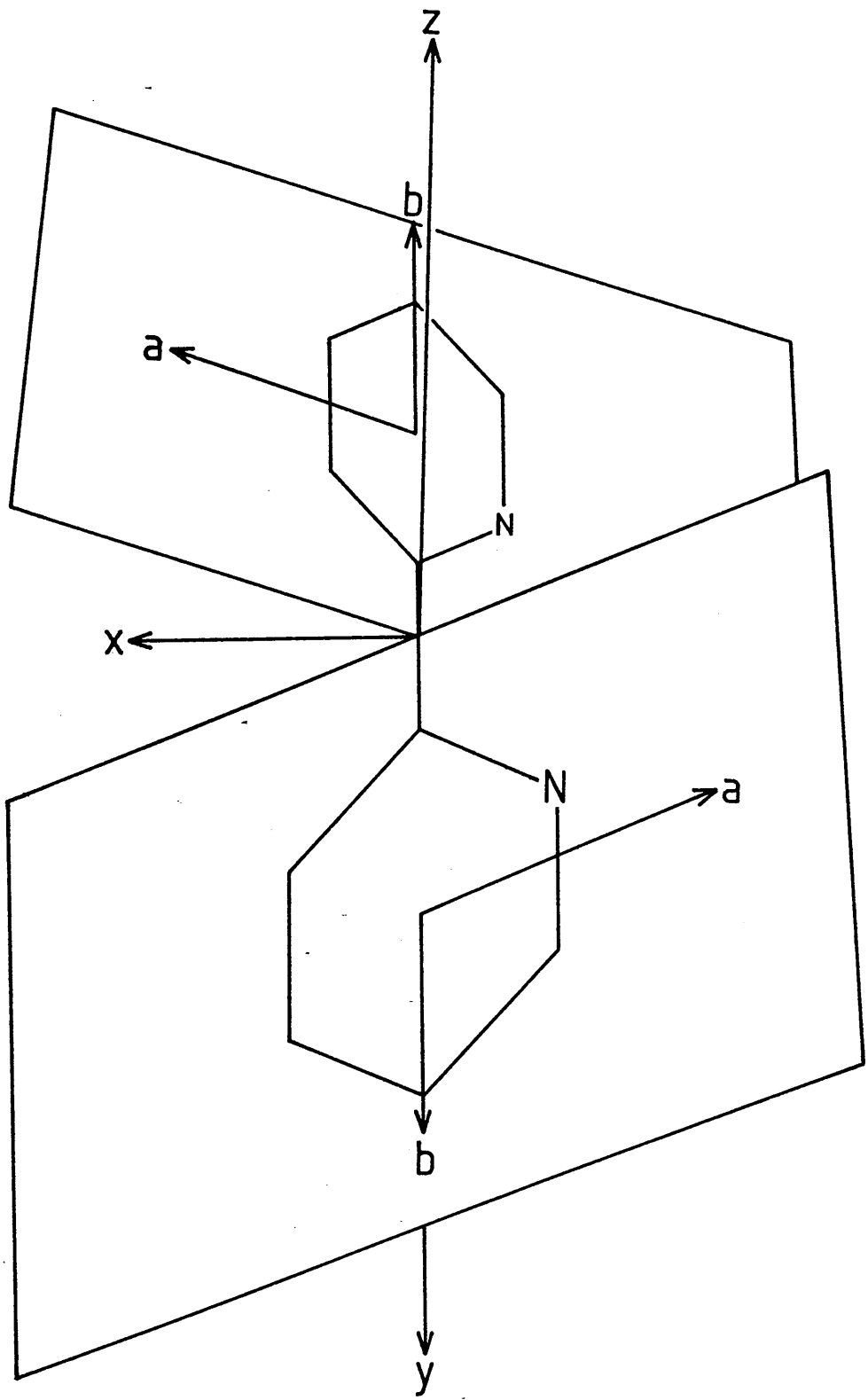

and so a very weak circular dichroism would be expected for this transition.

In the second case, that of the inherently dissymmetric chromophore, each electronic excitation has an intrinsic electric and magnetic dipole transition moment and each transition would be expected to have a very weak circular dichroism.

Both the $\pi 6 \rightarrow \pi 7$ and the $\pi 7 \rightarrow \pi 10$ transitions are long-axis polarised and on examination of the spectra both bands have a weak circular dichroism associated with these transitions, which fits both of the above cases. Now the $\pi 7 \rightarrow \pi 9$ transition which was assigned to the band between 600 and 1000 nm in the absorption spectrum (Figure 14) is short-axis polarised, so from the first case, that of the symmetric chromophores in a dissymmetric environment, there would be expected to be a strong exciton couplet in the region of this band similar to the 1,1 -bianthryls.[122] This is clearly not the case and hence the inherently dissymmetric chromophore model is the best description of the molecule.

This is not entirely unexpected as in the first case that of the coupled chromophore model, there is assumed to be no π-electron delocalisation between the two pyridine rings of the bipy$^-$ anion. But since the added electron enters the $\pi 7$ orbital and the central bond between the rings takes on double-bond character, this implies by its very nature that delocalisation of the electrons and π-overlap between the two rings will occur. The weak circular dichroism for bipy$^-$ is probably evidence that the central double-bond holds the molecule very nearly planar even in the proximity of chiral chelating agents.

This explains the intensities and the general form of the bands in the circular dichroism spectra of Libipy but it does not explain the signs

of the various bands. The experimental circular dichroism spectra obtained for Libipy were not as simple as the spectrum shown in Figure 23. The induced circular dichroism spectrum of Libipy using (-)-sparteine is shown in Figure 25 and additional spectra using (+) and (-)-Me_4pn are shown in Figure 26.

The form of all of the circular dichroism spectra are basically the same with two bands under the $\pi 6 \rightarrow \pi 7$ and $\pi 7 \rightarrow \pi 10$ long-axis polarised transitions of $bipy^-$. The only real difference is the signs of the circular dichroism bands and to a lesser degree in the magnitudes, both of which are given in Table 5.

TABLE 5

Ligand	Figure	($l\ mol^{-1} cm^{-1}$)	
		$\pi 6 \rightarrow \pi 7$	$\pi 7 \rightarrow \pi 10$
(+)-Me_4pn	23	-6.3	-0.7
	26c	-2.6	+0.3
	26a	+4.3	+0.3
(-)-Me_4pn	26b	-0.9	-0.1
(-)-sparteine	25	-1.1	+0.3

The circular dichroism spectrum of Libipy with (+)-Me_4pn generally started off as in Figure 26c, then would change to that of either Figure 23 or Figure 25a and so in effect three different circular dichroism spectra could be obtained. The time the spectra took to change varied from several hours in some cases to several days in other cases and changes in the spectra occurred in both diethylether and toluene. Possible reasons for the changes in the spectra could be that as the (+)-Me_4pn ligand is in excess, as well as having the

FIGURES 25: The induced circular dichroism spectrum of Libipy using (-)-sparteine

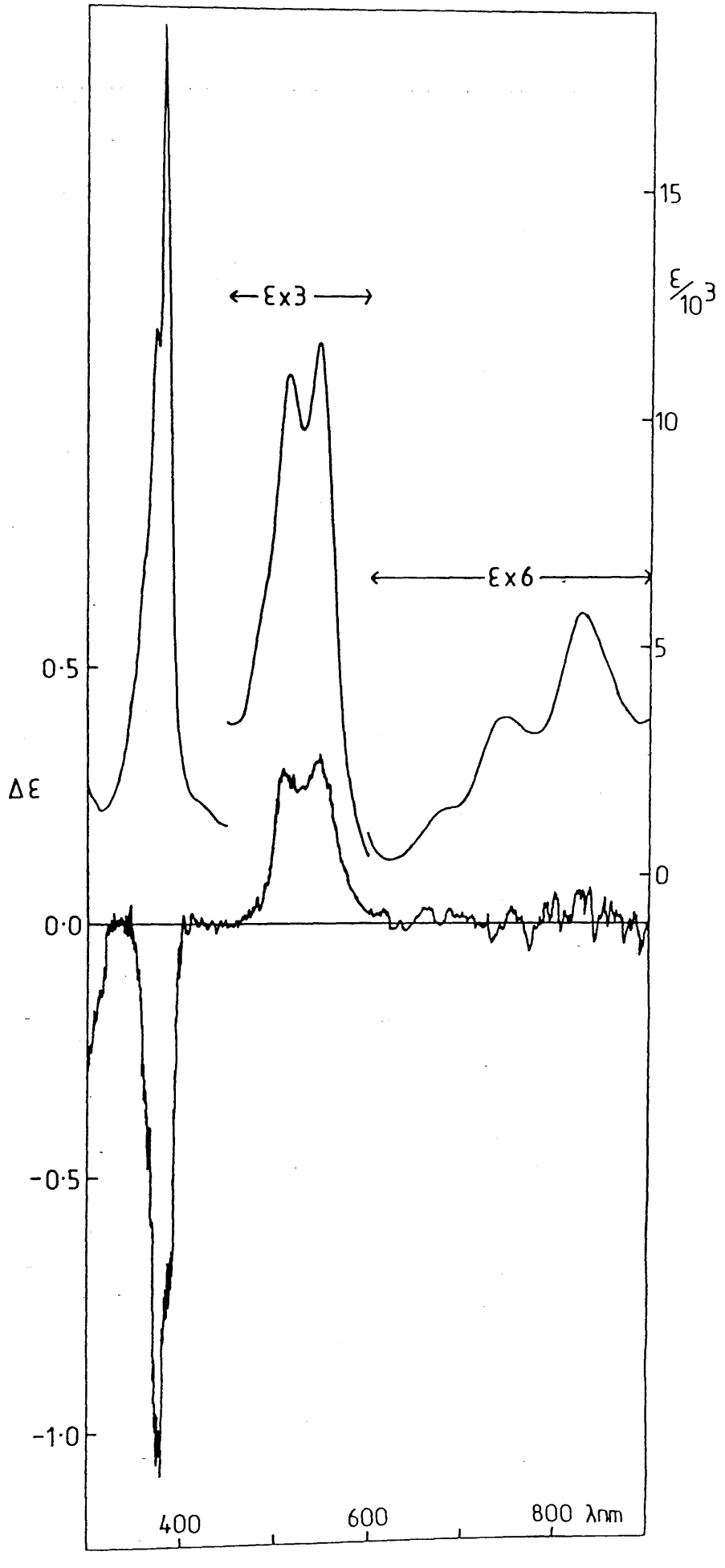

FIGURE 26: Induced circular dichroism specta of Libipy with a) (+)-Me_4pn, b) (-)-Me_4pn and c) (+)-Me_4pn

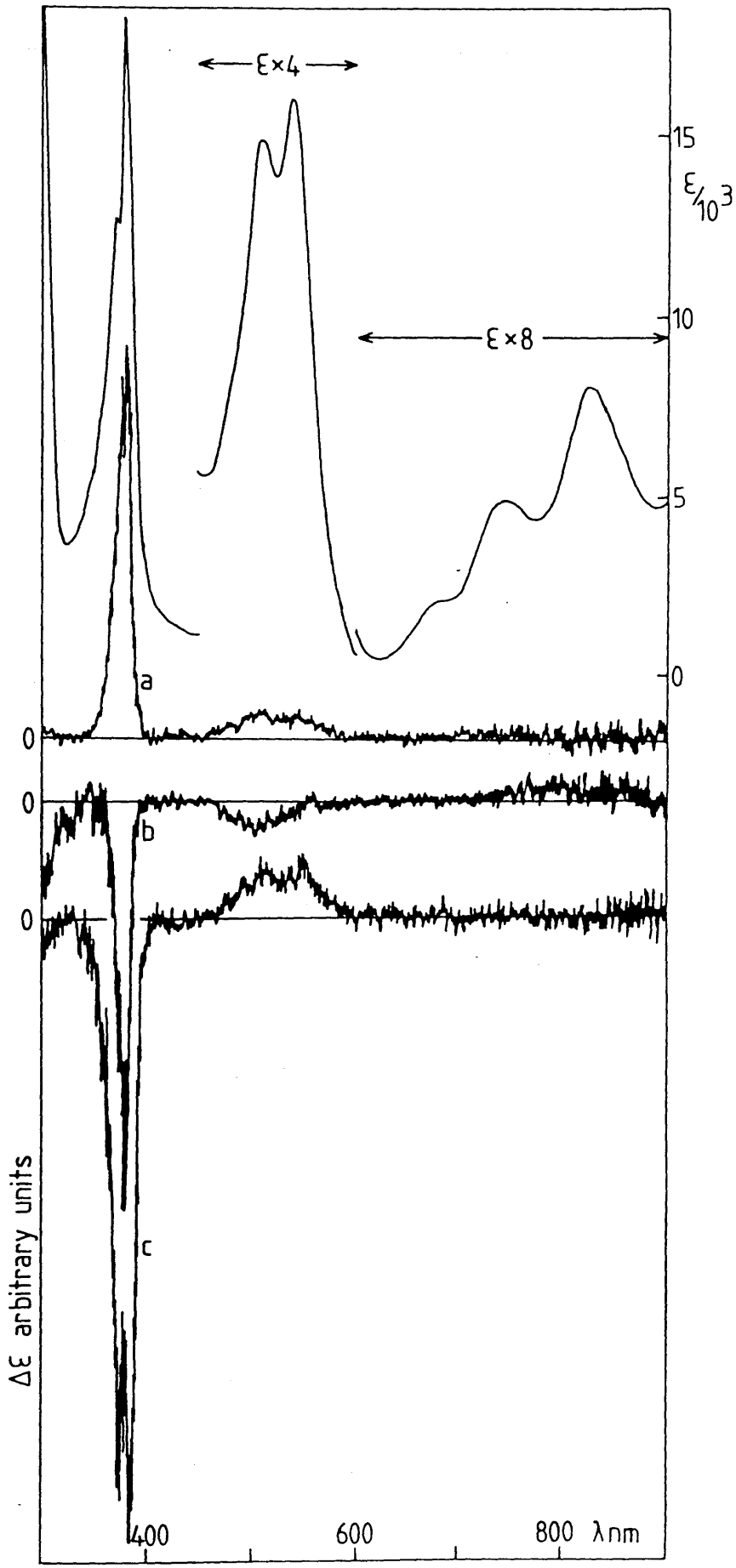

1:1 complex, it may be possible to have two (+)-Me_4pn ligands bound to one lithium ion. Or, it may be possible that some sort of lithium clusters are formed. As the structures of the various intermediates are not know it is difficult to give reasons for the changes in the circular dichroism spectra and will not therefore be attempted.

Only one circular dichroism spectrum was obtained when (-)-sparteine was used and this may be because the molecule is too bulky to allow other groups near the complex. It certainly seems unlikely that two sparteine molecules could bind to one lithium ion.

When (-)-Me_4pn was used, again only one circular dichroism spectrum was obtained. However, this was probably due to the fact that the ligand was only approximately 75% resolved and all spectra were extremely weak so intermediate spectra were probably too weak to be seen.

CHAPTER 4

THE ABSORPTION AND CIRCULAR DICHROISM SPECTRA OF Δ-$[Ru(bipy)_3]^{2+}$, Δ-$[Os(bipy)_3]^{2+}$ AND THEIR REDUCED ANALOGUES

It is now generally accepted[69] that the one, two and three-electron reduction products of $[Ru(bipy)_3]^{2+}$, I, are complexes in which the ruthenium is in the formal +II oxidation state and the electrons are localised on the bipy ligands. Electrochemical measurements,[59] e.s.r,[60] absorption,[63] and Raman spectroscopy[64] all suggest that the reduced compounds contain both bipy and $bipy^-$ ligands so that, for example, $[Ru(bipy)_3]^+$ must be formulated $[Ru(bipy)_2(bipy^-)]^+$ (I^-). In this work evidence for localisation in the reduced complexes I^-, I^{2-} and I^{3-} has been obtained independently by examination of the circular dichroism spectra of the series of complexes I to I^{3-} and by application of the exciton theory of optical activity to the experimental results in the near ultraviolet region of the spectra. Theroetical calculations[77,78] have been performed for the exciton couplet of I in the near ultraviolet region of the spectrum and the results have been extended to include I^-, I^{2-}, I^{3-} and $[Os(bipy)_3]^{2+}$ (II) and its reduced analogues, II^-, II^{2-} and II^{3-}.

Δ-$[Ru(bipy)_3]^{2+}$(I)

Before the spectroelectrochemistry of any compound can be measured, the potentials at which the new species are electrogenerated must first be found. This is achieved by using the technique of cyclic voltammetry.

The thermodynamic understanding of electrochemical processes derives from the application of Nernst's well-known equation;[123,124]

$$E = E^\circ - \frac{RT}{nF} \ln \frac{a_{ox}}{a_{red}} \qquad (47)$$

where E is the applied cell voltage, E° is the standard electrode

potential, R is the gas constant, n is the number of electrons and F is the Faraday constant. For a balanced cell where E° is the standard electromotive force (e.m.f.) of a reaction, a_{ox} and a_{red} are the equilibrated activities of the reactants and products adopted at E under a given set of conditions.

In cyclic voltammetry the characteristic features of the d.c. voltage curve are derived as a result of the potential dependent changes of the redox system, controlled by diffusion processes. Measurement of E_{p_a} and E_{p_c} (the anodic and cathodic peak potentials) permits the calculation of the half-wave potential $E_{\frac{1}{2}}$, where;

$$E_{\frac{1}{2}} = \frac{E_{p_a} + E_{p_c}}{2} \qquad (48)$$

and $E_{\frac{1}{2}}$ is related to the theromodynamic standard redox potential E° by;

$$E_{\frac{1}{2}} = E° + \frac{RT}{nF} \ln\left(\frac{Dr}{Do}\right)^{\frac{1}{2}} \qquad (49)$$

where Do and Dr are the diffusion coefficients of the oxidised and reduced species. Under the assumption that Do and Dr are approximately equal, equation 49 is reduced to;

$$E_{\frac{1}{2}} = E° \qquad (50)$$

For a reversible electrode process, the magnitude of the theoretical separation between E_{p_a} and E_{p_c} is calculated to be 57 mV at 25°C and is independent of the scan rate.[99,125]

The cyclic voltammogram of I is shown in Figure 27 and the results of the experiment are listed in Table 6.

FIGURE 27: Cyclic Voltammogram of Δ-[Ru(bipy)$_3$](BF$_4$)$_2$ in acetonitrile

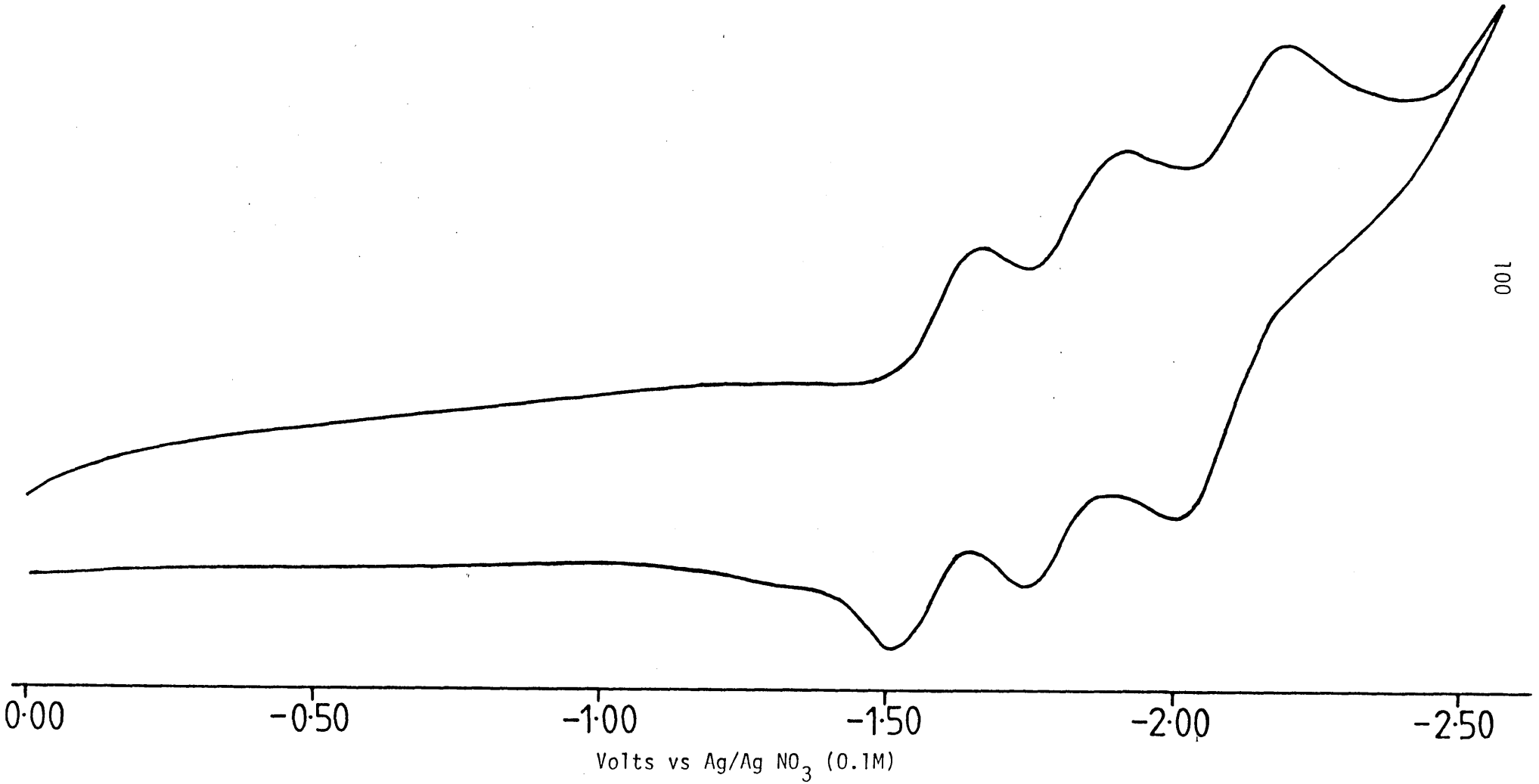

TABLE 6: Cyclic Voltammetry Results for Δ-$[Ru(bipy)_3](BF_4)_2$

Couple	$E_{\frac{1}{2}}$(V)[a]	ΔE_p(mV)[b]
I/I^-	- 1.58	150
I^-/I^{2-}	- 1.83	170
I^{2-}/I^{3-}	- 2.09	190

a Volts versus $Ag/AgNO_3$ (0.1M)

b $\Delta E_p = |E_{p_c} - E_{p_a}|$

All the electrode potentials obtained in this work are given with respect to the $Ag/AgNO_3$ (0.1M) reference electrode. Table 7 shows the relationship between the above reference electrode and other common reference systems.

TABLE 7: The relationship between the $Ag/AgNO_3$ (0.1M) reference electrode and other common reference systems at 298K

Potential (V)	Electrode System
+ 0.06	Hg/Hg_2SO_4, sat'd K_2SO_4
0.00	$Ag/AgNO_3$ (0.1M)
- 0.24	0.1M KCl calomel
- 0.30	1.0M KCl calomel
- 0.34	S.C.E. (saturated calomel)
- 0.38	Ag/AgCl(sat'd)
- 0.48	Hg/HgO, 1.0M NaOH
- 0.58	N.H.E. (normal hydrogen electrode)
- 1.16	Tl/TlCl 40 wt % in Hg (Thalamid)

The values of $E_{\frac{1}{2}}$ for complex $\underline{I}$ (Table 6) are in good agreement with those obtained by earlier workers.[58,126] The values of ΔEp given in Table 6 are larger than the theoretical value of 57mV. This is because I.R. compensation was not available at the time the cyclic voltammogram was recorded. I.R. compensation is needed to allow for the internal resistance of the cell which causes a voltage lag when the potential across the cell is swept with time. This is most noticeable at high sweep rates and causes an increase in the voltage separation between the anodic and cathodic peak potentials. However, the value of $E_{\frac{1}{2}}$ is not affected to any great degree and the results are in good agreement with those of earlier workers.[58,126] Yellowlees[126] found values of ΔE_p of 65mV for each of the three reduction couples of $\underline{I}$ showing the system to be completely reversible and hence $E_{\frac{1}{2}}$ values give good estimates of E° values for this system.

From the results of the cyclic voltammetry experiment, the potentials used to electrogenerate the reduced species $\underline{I}^-$, $\underline{I}^{2-}$ and $\underline{I}^{3-}$ were -1.78V, -2.00V and -2.30V respectively. The potentials used were as high as possible before the next reduced species would be formed or before the solvent limit was reached in the case of $\underline{I}^{3-}$ and so were necessarily a compromise. It has been assumed in each case that 100% of the desired product was formed in the spectroelectrochemical experiments. The actual amount of $\underline{I}$ present when $\underline{I}^-$, $\underline{I}^{2-}$ and $\underline{I}^{3-}$ are electrogenerated can be calculated easily using equation 47 (Appendix 3). It is found for an average solution concentration of 5×10^{-4} mol/ℓ that the concentration of $\underline{I}$, when $\underline{I}^-$, $\underline{I}^{2-}$ and $\underline{I}^{3-}$ are electrogenerated, is 1.8×10^{-7}, 3.0×10^{-11} and 2.1×10^{-16} mol/ℓ respectively. So even when $\underline{I}^-$ is electrogenerated, the concentration of $\underline{I}$ will be negligible.

As new species were generated, isosbestic points were produced implying

a simple one-to-one conversion of $\underline{I}$ to $\underline{I}^{-}$, $\underline{I}^{-}$ to $\underline{I}^{2-}$ and $\underline{I}^{2-}$ to $\underline{I}^{3-}$ and for each species the steady state spectrum was recorded after approximately twenty minutes, which also corresponded to a minimum in the current monitored at each potential.

As the complex was reduced, the original orange colour of $\underline{I}$ was replaced by a progressively deeper blood red colour of the species $\underline{I}^{-}$, $\underline{I}^{2-}$ and $\underline{I}^{3-}$. The reduced species were all very air-sensitive and quickly reverted back to $\underline{I}$ in the presence of oxygen or mositure.

The absorption and c.d. spectra of the four complexes are shown in Figures 28 and 29. They are presented in pairs for comparison; Figure 28 shows the spectra of the two complexes with equivalent ligands, Δ-$[Ru(bipy)_3]^{2+}$ and Δ-$[Ru(bipy^{-})_3]^{-}$ and Figure 29 shows those of the mixed ligand complexes. The spectra were run at -40°C as the triply reduced species $\underline{I}^{3-}$ was found to racemise spontaneously at room temperature (this will be discussed later). There was virtually no change in the redox potentials when the cyclic voltammetry was carried out at -40°C and so the species were electrogenerated with the above potentials.

The absorption[20,21] and c.d.[21] spectra of $\underline{I}$ (Figure 28) are well-known and have been frequently discussed in the past. The strong c.d. couplet centred at 300 nm is due to the exciton coupling of the long-axis polarised $\pi 6 \rightarrow \pi 7$ transitions of the three bipy molecules into A_2 and E combinations which should, neglecting other perturbations, have equal and opposite rotational strengths. The absorption and c.d. spectra in the visible region is due to Ru $\rightarrow$ bipy charge transfer; the origin of the c.d. in particular has been uncertain[127] until recently.[25]

The absorption spectra of the reduced species $\underline{I}^{-}$, $\underline{I}^{2-}$ and $\underline{I}^{3-}$ have

FIGURE 28:

Absorption and c.d. spectra of Δ-$[Ru(bipy)_3]^{2+}$ (full line) and Δ-$[Ru(bipy^-)_3]^-$ (dashed line) in acetonitrile. Note the scale change in the c.d. spectra between the ligand and charge-transfer regions.

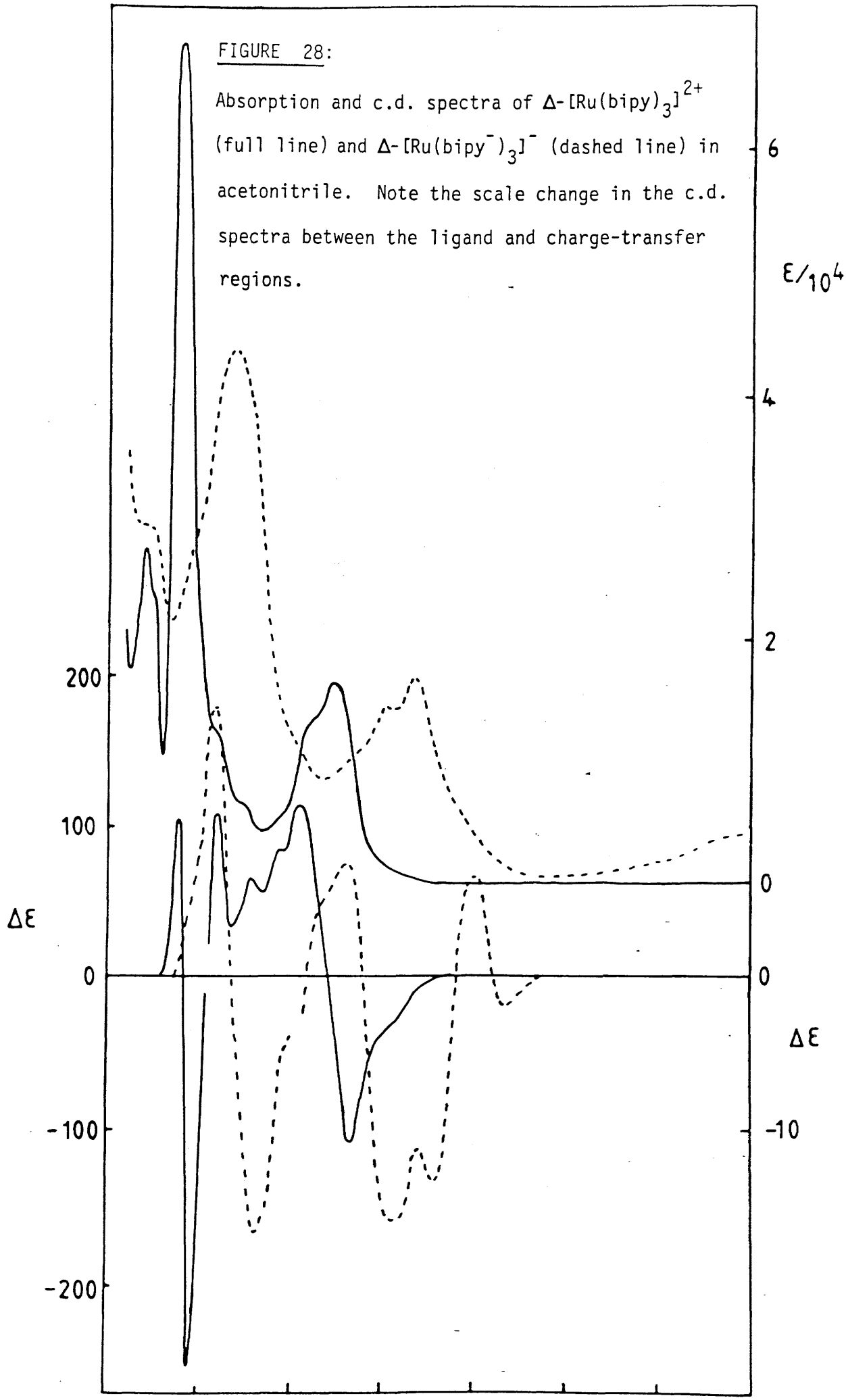

FIGURE 29: Absorption and c.d. spectra of Δ-$[Ru(bipy)_2(bipy^-)]^+$ (full line) and Δ-$[Ru(bipy)(bipy^-)_2]$ (dashed line) in acetonitrile. Note the scale change in the c.d. spectra. The insets show the calculated c.d. spectra for the singly and doubly reduced species (upper and lower diagrams respectively).

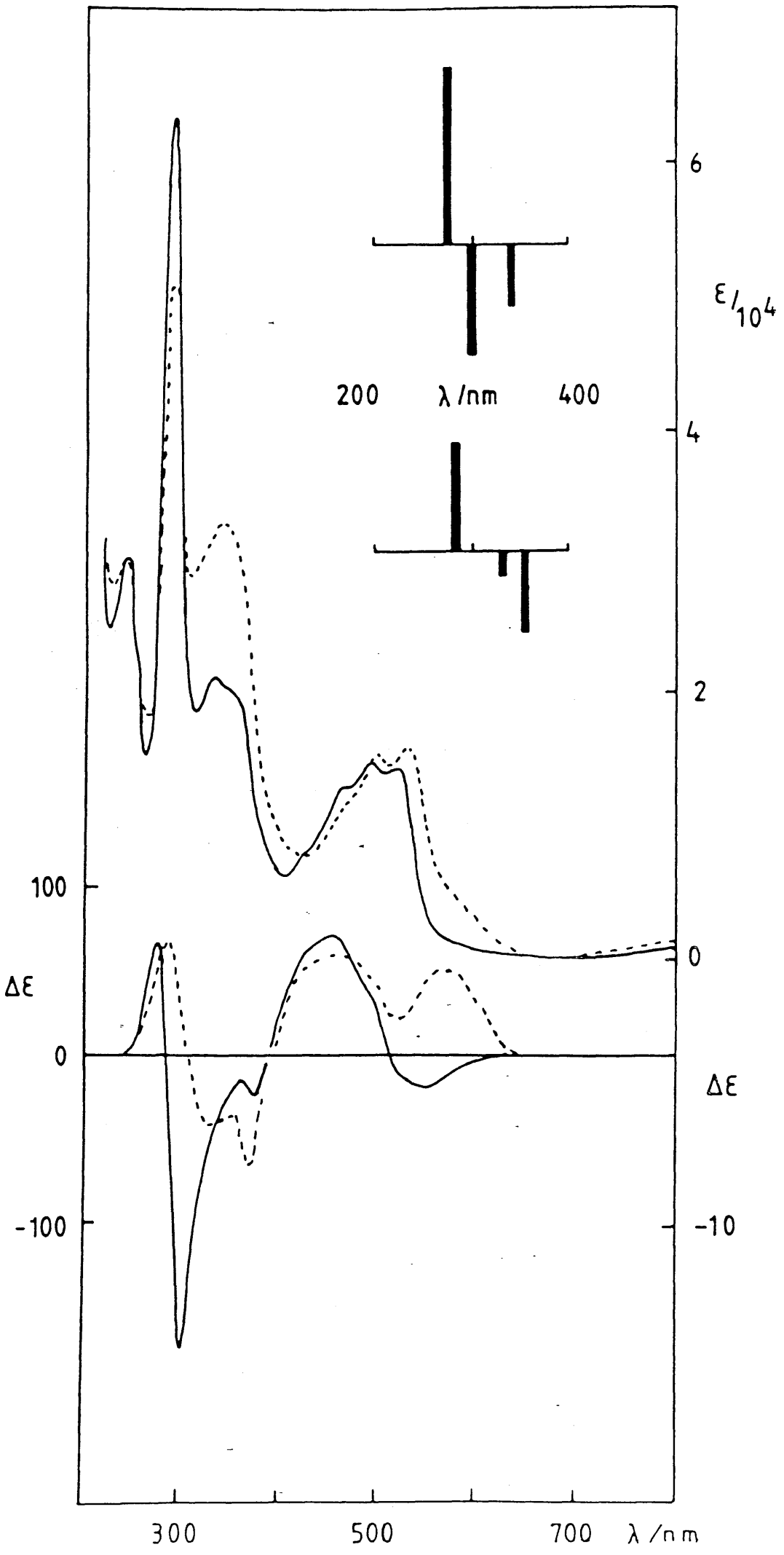
6
ε/10⁴
200
λ/nm
400
4
2
100
ΔE
0
0
ΔE
-100
-10
300
500
700
λ/nm

been measured previously.[63,126] Only the region between 270 and 400 nm containing the main long-axis polarised ligand $\pi 6 \rightarrow \pi 7$ absorptions will be considered at this stage.

The absorption spectra of $\underline{I}$ to $\underline{I}^{3-}$ (Figures 28 and 29) show the progressive collapse of the absorption band at 284 nm in $\underline{I}$ and the growth of the broad absorption band at 335 nm for $\underline{I}^{3-}$.

Comparison[63] of the absorption spectrum of $\underline{I}^{3-}$ with those of $[Mo(CO)_4(bipy)]^-$, formulated as $[Mo(CO)_4(bipy^-)]^-$ and $bipy^-$ have led to the assignment of the absorption band at 335 nm in $\underline{I}^{3-}$ to be primarily the $\pi 6 \rightarrow \pi 7$ transition of $bipy^-$, with perhaps some underlying metal-to-ligand charge-transfer (MLCT)[126] to account for its greater breadth compared to $bipy^-$. The absorption spectra of species $\underline{I}^-$ and $\underline{I}^{2-}$ have been assigned[63,126] as a mixture of $\pi 6 \rightarrow \pi 7$ transitions for discrete bipy and $bipy^-$ ligands in the same complex ion. If this assignment is correct then the presence of separate absorption bands for the $\pi 6 \rightarrow \pi 7$ transitions of bipy and $bipy^-$ indicates the presence of distinct bipy and $bipy^-$ ligands, hence the electrons must be localised on the individual ligands.

The circular dichroism spectra of $\underline{I}^-$ to $\underline{I}^{3-}$ is more complicated but can be interpreted using the exciton theory of optical activity. The case of $\underline{I}^{3-}$ will be discussed first; two extreme descriptions of the molecular orbitals are possible;

(i) the added electrons enter an acceptor orbital or orbitals which are completely delocalised over the entire complex. In this case the coupled-chromophore model merges with that of the inherently dissymmetric chromophore model as in the benzo [c] phenanthrenes[97] and the complex cannot be described using

degenerate exciton theory. With this model the circular dichroism would be expected to be less intense than that of $\underline{I}$ and there would not be expected to be an exciton couplet in the region of the ligand long axis polarised transitions, or,

(ii) the added electrons are completely localised on the individual $bipy^-$ ligands and there is no π-electron exchange between the individual ligands in the complex. In this case the compound would have D_3 symmetry and could be described as a homo-trischelated complex as in $\underline{I}$ and hence degenerate exciton theory would be applicable to $\underline{I}^{3-}$. Then two transitions of equal magnitude but opposite rotational strengths are predicted corresponding to the A_2 and E coupling modes. The non-degenerate A_2 coupling mode is predicted to be at a higher energy than the degenerate E coupling mode and for the Δ-enantiomer the A_2 mode is predicted to have a positive rotational strength and the E mode negative rotational strength.

On examination of the spectrum of $\underline{I}^{3-}$ (Figure 28) an exciton couplet is observed and as predicted the high energy band at 335 nm corresponding to the A_2 coupling mode has a positive rotational strength and the low energy band at 370 nm corresponding to the E coupling mode has a negative rotational strength of approximately the same magnitude as the A_2 band. Correlation of theoretical and experimental results in this case would appear to justify the triply reduced complex $\underline{I}^{3-}$ to be described using a localised model.

This would appear to be the first complex containing anionic ligands with an open shell configuration in which the stereochemistry of the complex could be reliably predicted using the exciton theory of

optical activity. Other transition metal complexes with anionic ligands such as oxalate[128] or pentane-2,4-dionate,[129] lack the characteristic exciton form owing to the probable greater importance of metal-to-ligand charge-transfer π-bonding.

The spectra of the partially reduced species are shown in Figure 29. The c.d. spectra in particular are quite distinct for each complex and illustrate graphically the individuality of the two species.

Under the delocalised theory, the ligands of the singly and doubly reduced complexes, $\underline{I}^-$ and $\underline{I}^{2-}$ respectively, could be thought of as having one third of an electron, that is one electron delocalised over all three bipy ligands in the former case and two thirds of an electron in the latter case. Each bipy ligand would be identical and the molecule could be described as a homo-trischelated complex with D_3 symmetry, formulated as $[Ru(bipy^{\frac{1}{3}-})_3]^+$ and $[Ru(bipy^{\frac{2}{3}-})_3]$. The degeneracy would be expected to lead to strong exciton coupling between the individual ligands and a strong exciton couplet would be expected to move steadily to lower energies for $\underline{I} \rightarrow \underline{I}^- \rightarrow \underline{I}^{2-} \rightarrow \underline{I}^{3-}$ as the transition energy becomes less with each successive reduction. This is clearly not the case for the singly and doubly reduced species as the circular dichroism spectra are more complicated than predicted for a simple delocalised model.

In a localised model the complexes would be formulated as $[Ru(bipy)_2(bipy^-)]^+$, $\underline{I}^-$ and $[Ru(bipy)(bipy^-)_2]$, $\underline{I}^{2-}$, where the added electrons are localised on one bipy ligand. Now the bipy and $bipy^-$ ligands are non-degenerate, the $\pi 6 \rightarrow \pi 7$ transition of $bipy^-$ is of a lower energy than that of bipy and hence the complex could be described as a hetero-trischelated complex similar to the mixed bipy/phen (where phen is 1,10-phenanthroline) complexes of ruthenium,[78*] $[Ru(bipy)(phen)_2]^{2+}$

* NB Spectra of mixed bipy/phen ruthenium complexes are of the Λ enantiomers in reference 78.

and $[Ru(bipy)_2(phen)]^{2+}$, in which the symmetry of the complex would be reduced to C_2. In a hetero-trischelated complex with C_2 symmetry the exciton coupling modes which are doubly degenerate (E modes in Figure 5) in the analogous D_3 complex are split and give rise in principle to distinct circular dichroism bands. Thus if the energy difference between the long-axis polarised excitations of dissimilar ligands is not too great, coupling should occur to produce in principle three circular dichroism bands and theory predicts the sum of the three rotational strengths of the three bands to be equal to zero.

The absorption and circular dichroism spectra of $\underline{I}^-$ and $\underline{I}^{2-}$ are shown in Figure 29. The circular dichroism spectra in particular are quite distinct for each complex and illustrate graphically the individuality of the two species, this is further confirmation that the complexes contain both bipy and $bipy^-$. Recently Heath et al[66] observed a weak absorption band near 4000 cm^{-1} for the species $\underline{I}^-$ and $\underline{I}^{2-}$ which they attributed to a ligand $\rightarrow$ ligand inter-valence charge transfer transition (IVCT). This implies the simultaneous presence of discrete bipy and $bipy^-$ groups and as the IVCT band was weak in intensity, there cannot be much interaction between the different ligands in the complex. The assumption that there is no π-overlap between the ligands is therefore a good approximation and the exciton theory of optical activity should provide a good method to predict the c.d. of the ligand transitions. Since there can be very little π-overlap in the singly and doubly reduced species it is likely that this assumption is also valid for the triply reduced species which is further evidence for localisation in $\underline{I}^{3-}$.

The exciton coupling of the ligand transitions in mixed tris-chelate complexes such as $[Ru(bipy)_2(phen)]^{2+}$ and $[Ru(bipy)(phen)_2]^{2+}$ have

been treated in some detail by Bosnich[78]. There is considerable similarity between the c.d. spectra of the mixed $(bipy)_n(bipy^-)_{3-n}$ species and the mixed $(bipy)_n(phen)_{3-n}$ complexes which suggests that the exciton patterns of $\underline{I}^-$ and $\underline{I}^{2-}$ should be able to be calculated in the same way. Taking average energies for the bipy and $bipy^-$ transitions from the absorption spectra of the respective tris-chelates and using exciton interaction energies of 970 cm^{-1} [21] for bipy with bipy, 1400 cm^{-1} for $bipy^-$ and $bipy^-$ and 1200 cm^{-1} for bipy with $bipy^-$, the exciton splitting patterns shown in the insets to Figure 29 were calculated. The parameters used in the calculation of the exciton splitting patterns of $\underline{I}^-$ and $\underline{I}^{-2}$ are given in Table 8. The results of the calculations are shown in Table 9 and these were used to give an energy level diagram (Figure 30) of the ligand orbitals before and after exciton exchange. The energies and relative signs and intensities are quite well reproduced and completely confirm the localised electron model for the complexes.

Δ-$[Os(bipy)_3]^{2+}$(II)

The complex ion Δ-$[Os(bipy)_3]^{2+}$, II, (Figure 31), shows a redox chemistry which is almost identical to that of the ruthenium analogue I. The cyclic voltammogram (Figure 32) shows a sequence of reversible reductions at narrowly spaced potentials corresponding, as before, to successive reduction of each of the bipy ligands. The results of the electro-chemistry are listed in Table 10 and are in good agreement with Yellowlees.[126]

From the results of the cyclic voltammetry experiments the potentials used to electrogenerate the reduced species $\underline{II}^-$, $\underline{II}^{2-}$ and $\underline{II}^{3-}$ were - 1.74, - 2.00 and - 2.29V respectively. The reduced osmium complexes were very similar in colour to those of the analogous ruthenium species,

TABLE 8: Parameters used to calculate the exciton splitting patterns of $\underline{I}^-$ and $\underline{I}^{2-}$.

Parameter	$\underline{I}^-$	$\underline{I}^{2-}$
ΔE_1	34,480 cm^{-1}	29,410 cm^{-1}
ΔE_3	29,850 cm^{-1}	34,360 cm^{-1}
V_{12}	970 cm^{-1}	1,400 cm^{-1}
V_{13}	1,200 cm^{-1}	1,200 cm^{-1}
$r_1 = r_3$	2.63×10^{-8} cm	2.63×10^{-8} cm^{-1}
p_1	3.74×10^{-18} c.g.s.	3.58×10^{-18} c.g.s.
p_3	3.58×10^{-18} c.g.s.	3.74×10^{-18} c.g.s.
$\bar{\nu}_1$ [a]	35,150 cm^{-1}	28,370 cm^{-1}
$\bar{\nu}_3$ [a]	28,370 cm^{-1}	35,150 cm^{-1}

a $\bar{\nu}_1$ and $\bar{\nu}_3$ were taken to be the energy at the midpoint of the exciton couplet for complexes $\underline{I}$ and $\underline{I}^{3-}$ respectively.

TABLE 9: Results of the calculations of the exciton splitting parameters of $\underline{I}^-$ and $\underline{I}^{2-}$.

Δ-$[Ru(bipy)_2(bipy^-)]^+$		Δ-$[Ru(bipy)(bipy^-)_2]$	
E_B^+	35,925 cm^{-1}	E_B^+	35,044 cm^{-1}
E_A	33,510 cm^{-1}	E_B^-	30,132 cm^{-1}
E_B^-	29,376 cm^{-1}	E_A	28,012 cm^{-1}
D_B^+	25.3×10^{-36} c.g.s.	D_B^+	21.2×10^{-36} c.g.s.
D_A	7.0×10^{-36} c.g.s.	D_B^-	11.9×10^{-36} c.g.s.
D_B^-	8.5×10^{-36} c.g.s.	D_A	6.4×10^{-36} c.g.s.
R_B^+	4.49×10^{-38} c.g.s.	R_B^+	2.72×10^{-38} c.g.s.
R_A	-2.88×10^{-38} c.g.s.	R_B^-	-0.59×10^{-38} c.g.s.
R_B^-	-1.61×10^{-38} c.g.s.	R_A	-2.12×10^{-38} c.g.s.

FIGURE 30: Schematic energy level diagram for wave functions Ψ_0, Φ_1, Φ_2 and Φ_3 before exciton interaction and for wave functions Ψ_0, Ψ_B^+, Ψ_A and Ψ_B^- after exciton exchange.

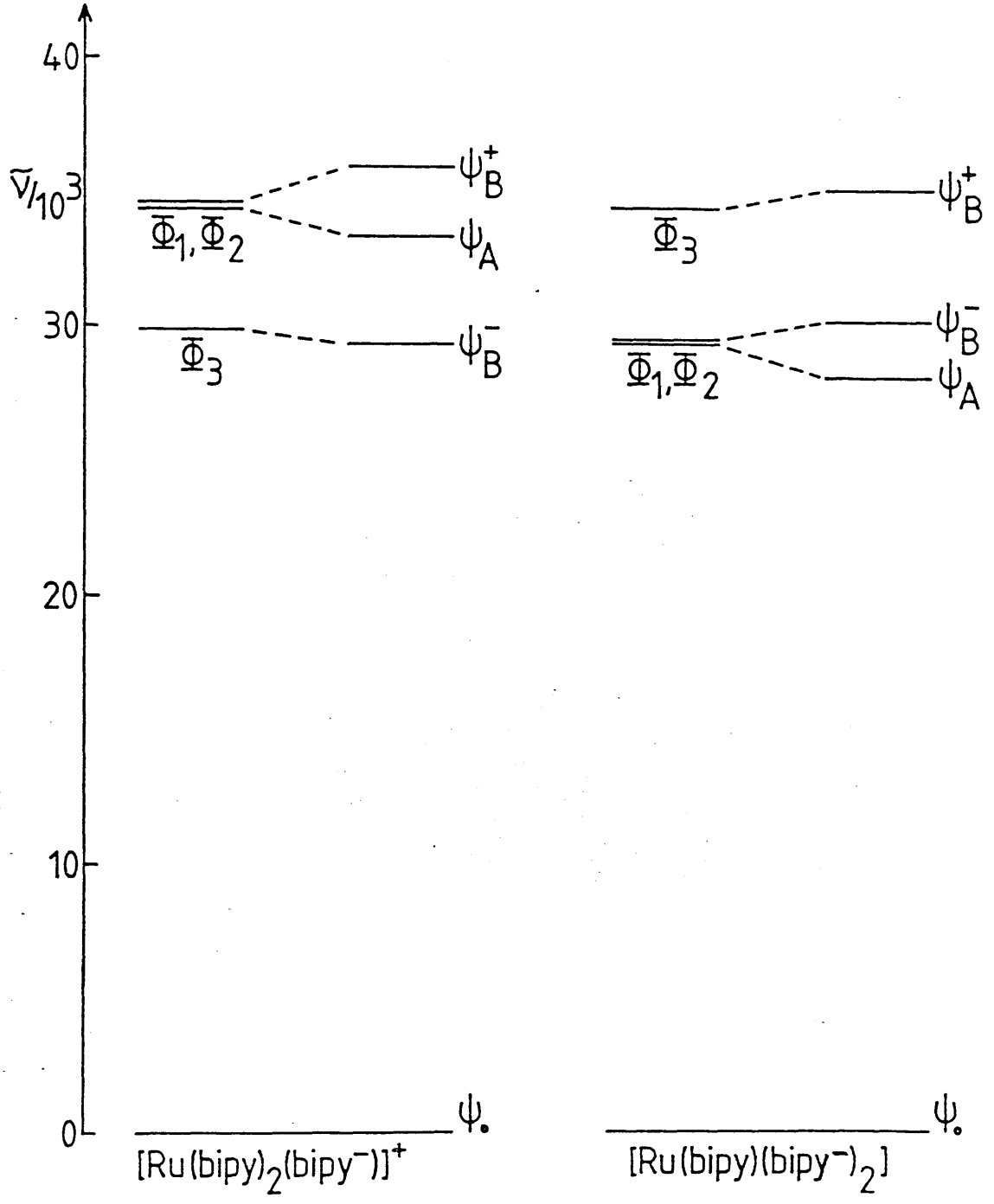

FIGURE 31: The structure of Δ-$[Os(bipy)_3]^{2+}$

Δ-$[Os(bipy)_3]^{2+}$

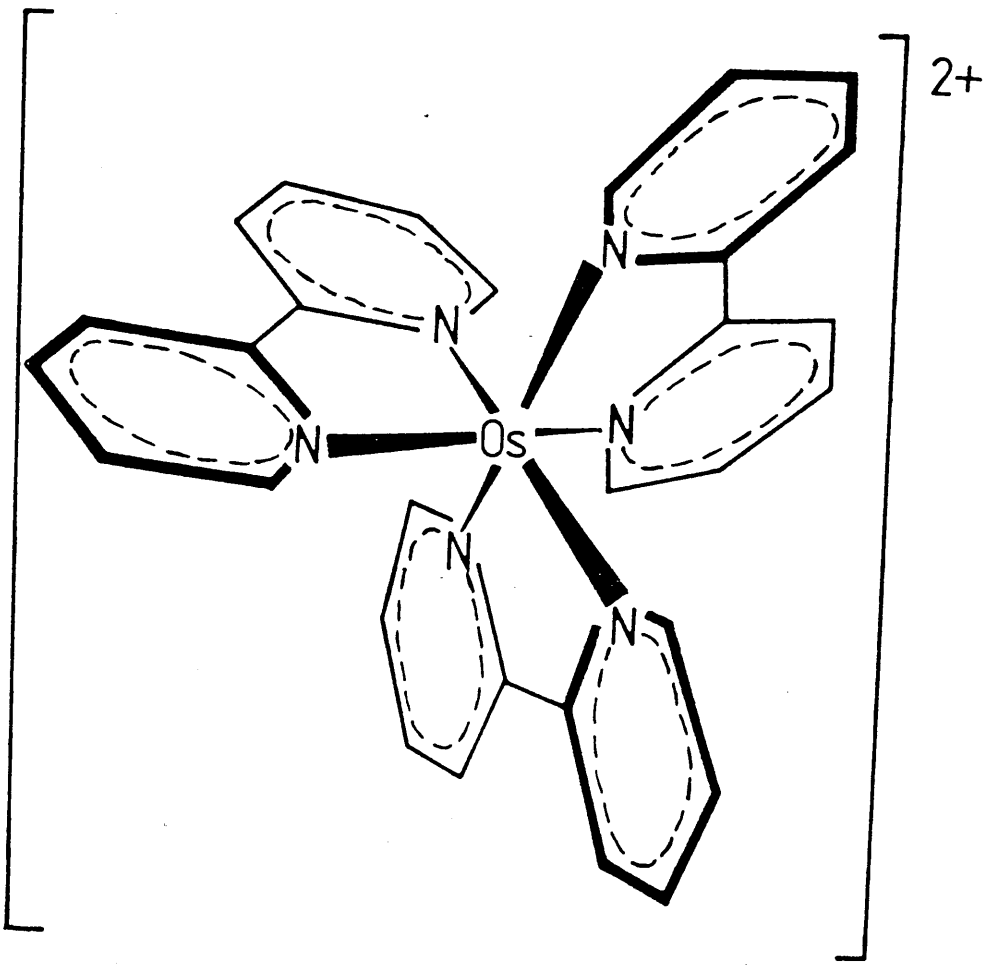

FIGURE 32: The cyclic voltammogram of Δ-[Os(bipy)$_3$](BF$_4$)$_2$ in acetonitrile

TABLE 10: Cyclic voltammetry results for Δ-[Os(bipy)$_3$](BF$_4$)$_2$, (II)

Couple	$E_{\frac{1}{2}}$ (V)	E_p (mV)
II/II$^-$	-1.62	69
II$^-$/II^{2-}	-1.81	83
II^{2-}/II^{3-}	-2.10	116

a dark blood red colour and again like the ruthenium species, the reduced osmium complexes were very air and moisture sensitive.

The absorption and c.d. spectra of the four complexes are shown in Figures 33 and 34. They are presented in pairs for comparison; Figure 33 shows the spectra of the two complexes with equivalent ligands, Δ-[Os(bipy)$_3$]$^{2+}$ and Δ-[Os(bipy$^-$)$_3$]$^-$ and Figure 34 shows those of the mixed ligand complexes. The absorption and c.d. spectra of the reduced complexes have not been previously recorded.

The discussion of the absorption and circular dichroism spectra of the four complexes will at this stage be limited to the region of the spectrum between 200 and 400 nm, corresponding to the ligand $\pi \rightarrow \pi^*$ transitions.

The absorption and circular dichroism spectra of II^{21} are well known and have been frequently discussed in the past. The strong c.d. couplet centred on 288 nm is due to the exciton coupling of the long-axis polarised $\pi 6 \rightarrow \pi 7$ transitions of the three bipy molecules into A_2 and E modes which should as before, neglecting other perturbations, have equal and opposite rotational strengths. As predicted the A_2 mode has a positive rotational strength and the E mode has a negative rotational strength for the Δ-enantiomer.

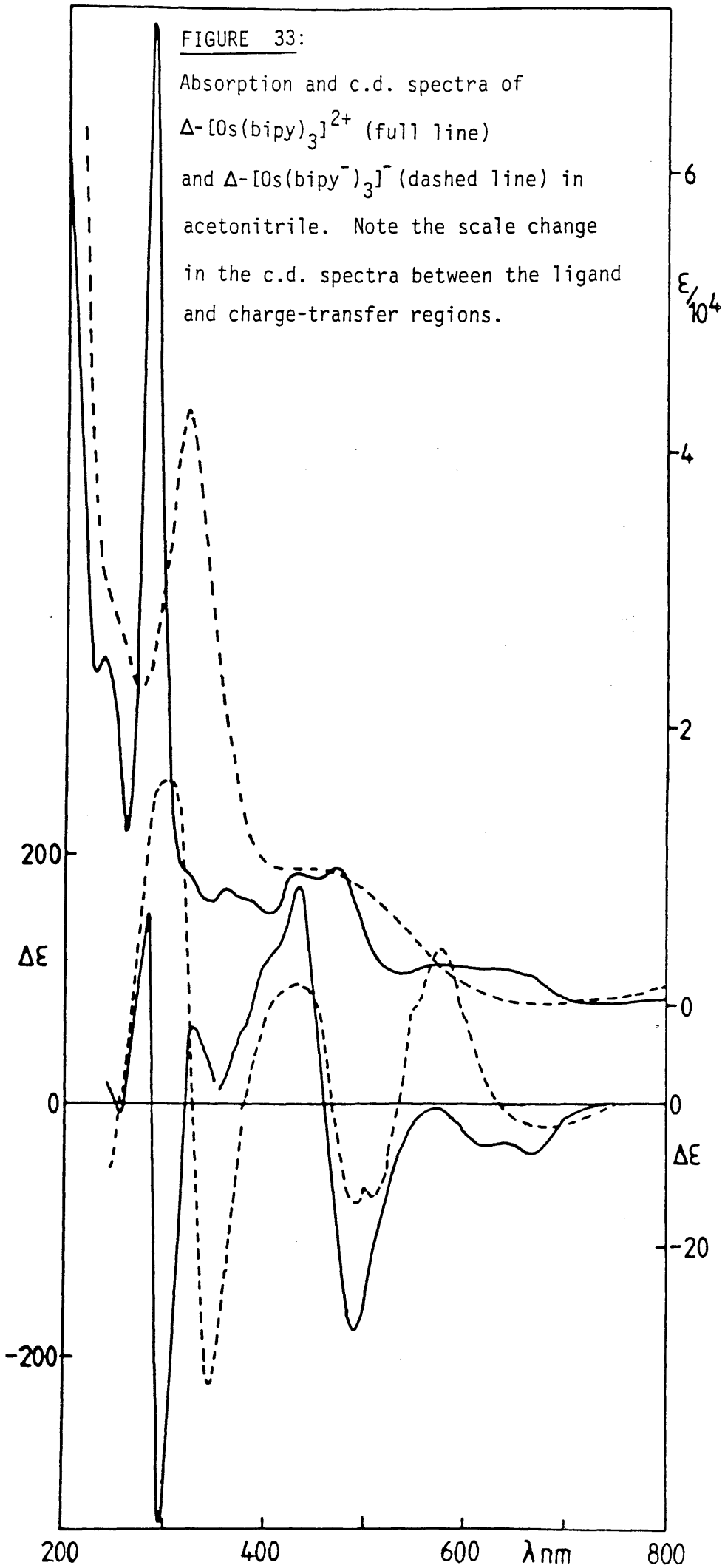

FIGURE 33:

Absorption and c.d. spectra of Δ-$[Os(bipy)_3]^{2+}$ (full line) and Δ-$[Os(bipy^{-})_3]^{-}$ (dashed line) in acetonitrile. Note the scale change in the c.d. spectra between the ligand and charge-transfer regions.

FIGURE 34: Absorption and c.d. spectra of Δ-$[Os(bipy)_2(bipy^-)]^+$ (full line) and Δ-$[Os(bipy)(bipy^-)_2]$ (dashed line) in acetonitrile. Note the scale change in the c.d. spectra. The insets show the calculated c.d. spectra for the doubly and singly reduced species (upper and lower diagrams respectively).

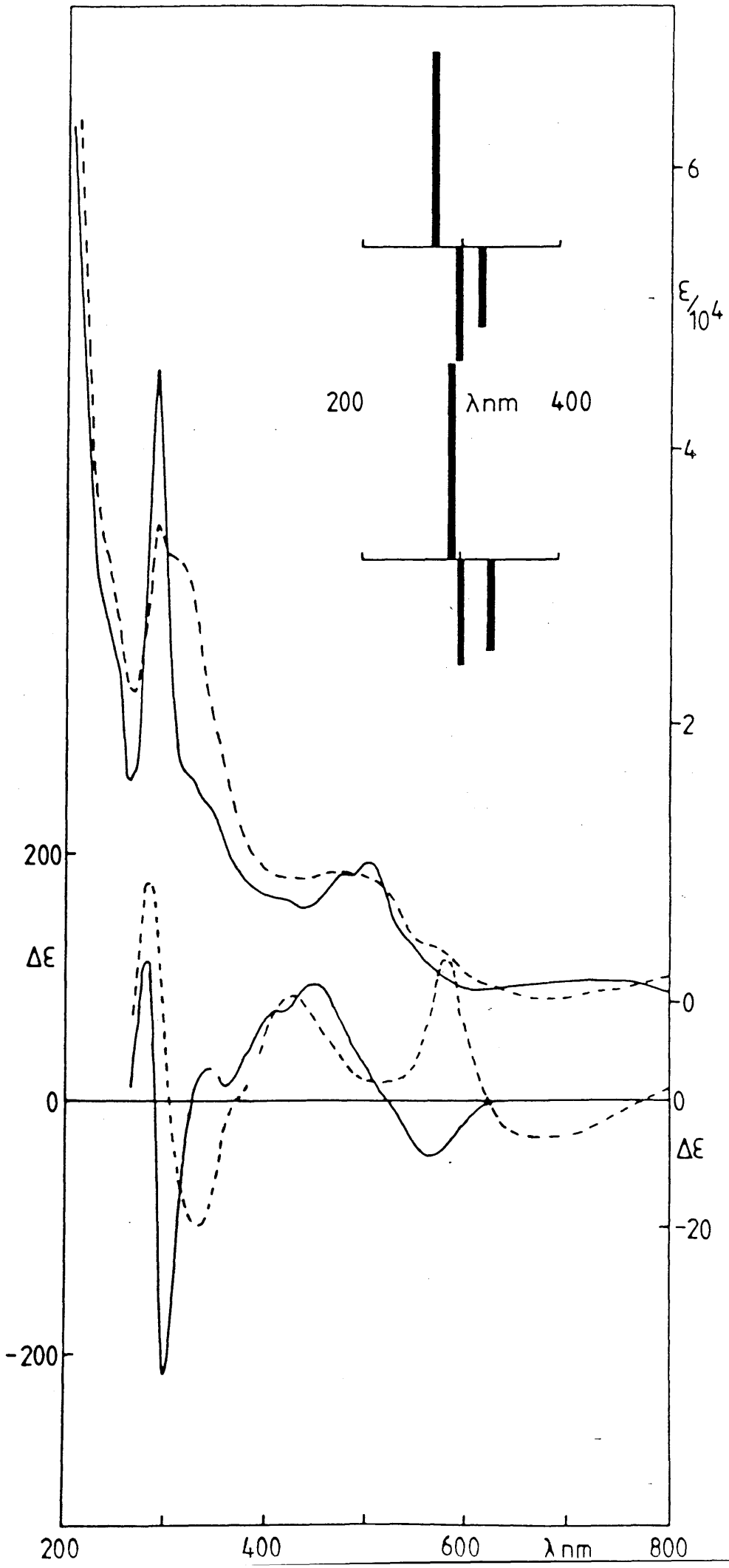
200
λnm
400
6
ε/10⁴
4
2
0
200
Δε
0
-200
0
Δε
-20
200
400
600
λnm
800

The absorption spectra of II to II^{3-} again show the progressive collapse of the $\pi 6 \rightarrow \pi 7$ absorption band of bipy at 278 nm and the growth of the broad absorption band at 321 nm of the $\pi 6 \rightarrow \pi 7$ transition of $bipy^{-}$. In the osmium case however, the new absorption band is closer in energy to the absorption band of bipy and so the new band appears as a low energy shoulder in II^{-} and II^{2-} until it is fully resolved in II^{3-}. The absorption spectra are however distinct enough to distinguish between the $\pi 6 \rightarrow \pi 7$ transitions of bipy and those of $bipy^{-}$. The two spearate absorption bands are taken as evidence that distinct bipy and $bipy^{-}$ ligands exist in the singly and doubly reduced complexes, hence the electrons must be localised. If the electrons were delocalised, all three bipy ligands would be identical and a single absorption band which moved steadily to lower energy as the different reduced species were formed would be expected.

In the interpretation of the c.d. spectra of the reduced complexes, the same arguments as before hold. The exciton couplet for II^{3-} implies that the electrons are localised on the individual $bipy^{-}$ ligands and the complex can be thought of as a homo-trischelated complex with D_3 symmetry. As predicted by the degenerate exciton theory, the high energy A_2 coupling mode at 300 nm has a positive rotational strength and the low energy E coupling mode at 343 nm has a negative rotational strength for the Δ-enantiomer. The c.d. spectrum of II^{3-} is strikingly similar to that of I^{3-} and both have quite broad exciton bands compared to those in complexes II and I. It is thought[21] that in I and II the energy separation between the A_2 and E modes is quite small which leads to overlap and hence mutual cancellation of the rotational strengths of the two bands. There is a greater energy difference between the A_2 and E modes in the triply reduced complexes which accounts for the broadness of the bands and V_{12} for $bipy^{-}$ has been estimated as 1400 cm^{-1}

(compared to 970 cm^{-1} for bipy).

The spectra of the partially reduced species are shown in Figure 34. The c.d. spectra for the two species are quite similar, both having a positive and a negative band under the ligand $\pi 6 \rightarrow \pi 7$ absorptions. Now as has been stated earlier, if the electrons are delocalised over all three ligands, the complex could be described as a homo-trischelate with D_3 symmetry. In this case there would be strong exciton interactions between the ligands and the c.d. spectra would be expected to show an exciton couplet which moves to lower energy from $\underline{II}^-$ to $\underline{II}^{2-}$. On examination of the spectra, the c.d. does resemble an exciton couplet which moves to lower energy from $\underline{II}^-$ to $\underline{II}^{2-}$ so at first sight this would appear to support the delocalised model.

There is the possibility that the electrons are localised on the individual ligands but no exciton exchange takes place between non-identical ligands. In this case for $\underline{II}^-$ the compound would be expected to have a spectrum similar to that of a cis-bis (bipy) complex in which there would be an exciton couplet of approximately half the intensity of that of $\underline{II}$ due to coupling of the two bipy ligands and a very weak circular dichroism due to the $bipy^-$ ligand. This model fits the description of the c.d. for $\underline{II}^-$ but can be ruled out for $\underline{II}^{2-}$ as in the latter case there would be an exciton couplet due to the interaction of two $bipy^-$ ligands but on examination of the spectrum the exciton band with positive rotational strength is at an energy which is too high for it to be associated with the absorption of $bipy^-$. This theory is unlikely to be correct for $\underline{II}^-$ because in the analogous ruthenium complexes there is strong exciton interactions even although there is a fairly large difference in energy between the bipy and $bipy^-$ transitions and in the osmium complexes the difference in energy between the bipy and

$bipy^-$ transitions is much less and so there should be a much greater exciton interaction in the osmium complexes.

The theoretical circular dichroism spectra (shown in the insets in Figure 34) were calculated as before using the parameters given in Table 11. The results of the calculations are shown in Table 12 and these were used to construct the schematic energy level diagram shown in Figure 35.

TABLE 11: Parameters used to calculate the exciton splitting patterns of $\underline{II}^-$ and $\underline{II}^{2-}$.

Parameter	$\underline{II}^-$	$\underline{II}^{2-}$
ΔE_1	34,600 cm^{-1}	31,746 cm^{-1}
ΔE_3	31,750 cm^{-1}	34,483 cm^{-1}
$^bV_{12}$	970 cm^{-1}	1,400 cm^{-1}
$^bV_{13}$	1,200 cm^{-1}	1,200 cm^{-1}
$^ar_1 = r_3$	2.63 x 10^{-8} cm	2.63 x 10^{-8} cm
p_1	3.74 x 10^{-18} c.g.s.	3.58 x 10^{-18} c.g.s.
p_3	3.58 x 10^{-18} c.g.s.	3.74 x 10^{-18} c.g.s.
$\bar{\nu}_1$	34,722 cm^{-1}	31,104 cm^{-1}
$\bar{\nu}_3$	31,104 cm^{-1}	34,722 cm^{-1}

a The distance between the "centre" of the transition dipole moment of the bipy molecule and the centre of the metal atom was assumed to be equal in ruthenium and osmium.

b V_{12} and V_{13} were assumed to have the same value in the corresponding ruthenium and osmium complexes.

TABLE 12: Results of the calculations of the exciton splitting parameters of $\underline{II}^{-}$ and $\underline{II}^{2-}$

Δ-[Os(bipy)$_2$(bipy$^-$)]$^+$		Δ-[Os(bipy)(bipy$^-$)$_2$]	
E_B^+	36,215 cm^{-1}	E_B^+	34,463 cm^{-1}
E_A	33,632 cm^{-1}	E_B^-	33,166 cm^{-1}
E_B^-	31,105 cm^{-1}	E_A	30,346 cm^{-1}
D_B^+	26.3 x 10^{-36} c.g.s.	D_B^+	26.4 x 10^{-36} c.g.s.
D_A	7.0 x 10^{-36} c.g.s.	D_B^-	6.7 x 10^{-36} c.g.s.
D_B^-	7.6 x 10^{-36} c.g.s.	D_A	6.4 x 10^{-36} c.g.s.
R_B^+	4.90 x 10^{-38} c.g.s.	R_B^+	5.00 x 10^{-38} c.g.s
R_A	-2.84 x 10^{-38} c.g.s.	R_B^-	-2.65 x 10^{-38} c.g.s.
R_B^-	-2.06 x 10^{-38} c.g.s.	R_A	-2.33 x 10^{-38} c.g.s.

On examination of the theoretical circular dichroism spectra of the species $\underline{II}^{-}$ and $\underline{II}^{2-}$ it is immediately apparent that they differ considerably from the c.d. spectra calculated for $\underline{I}^{-}$ and $\underline{I}^{2-}$ and so it is no surprise that the experimental c.d. spectra of $\underline{II}^{-}$ and $\underline{II}^{2-}$ are different from those of $\underline{I}^{-}$ and $\underline{I}^{2-}$. For the case of $\underline{II}^{-}$ it is easy to fit the calculated c.d. spectrum with the experimental spectrum especially if the value of R_A was increased and the value of R_B^- was decreased. The calculated c.d. spectrum for $\underline{II}^{2-}$ is in excellent agreement with the experimental c.d. as both have a high energy positive band and the two negative bands in the calculated c.d. spectrum would form a broad band as is shown in the experimental c.d. spectrum. The c.d. spectrum of $\underline{II}^{2-}$ is also very similar to that of the hetero-trischelated complex[77] [Os(bipy)$_2$(phen)]$^{2+}$ in which it is assumed that there is no π-electron exchange between the individual ligands in the complex.

FIGURE 35: Schematic energy level diagram for wave functions Ψ_0, Φ_1, Φ_2 and Φ_3 before exciton interaction and for wave functions Ψ_0, Ψ_B^+, Ψ_A and Ψ_B^- after exciton exchange.

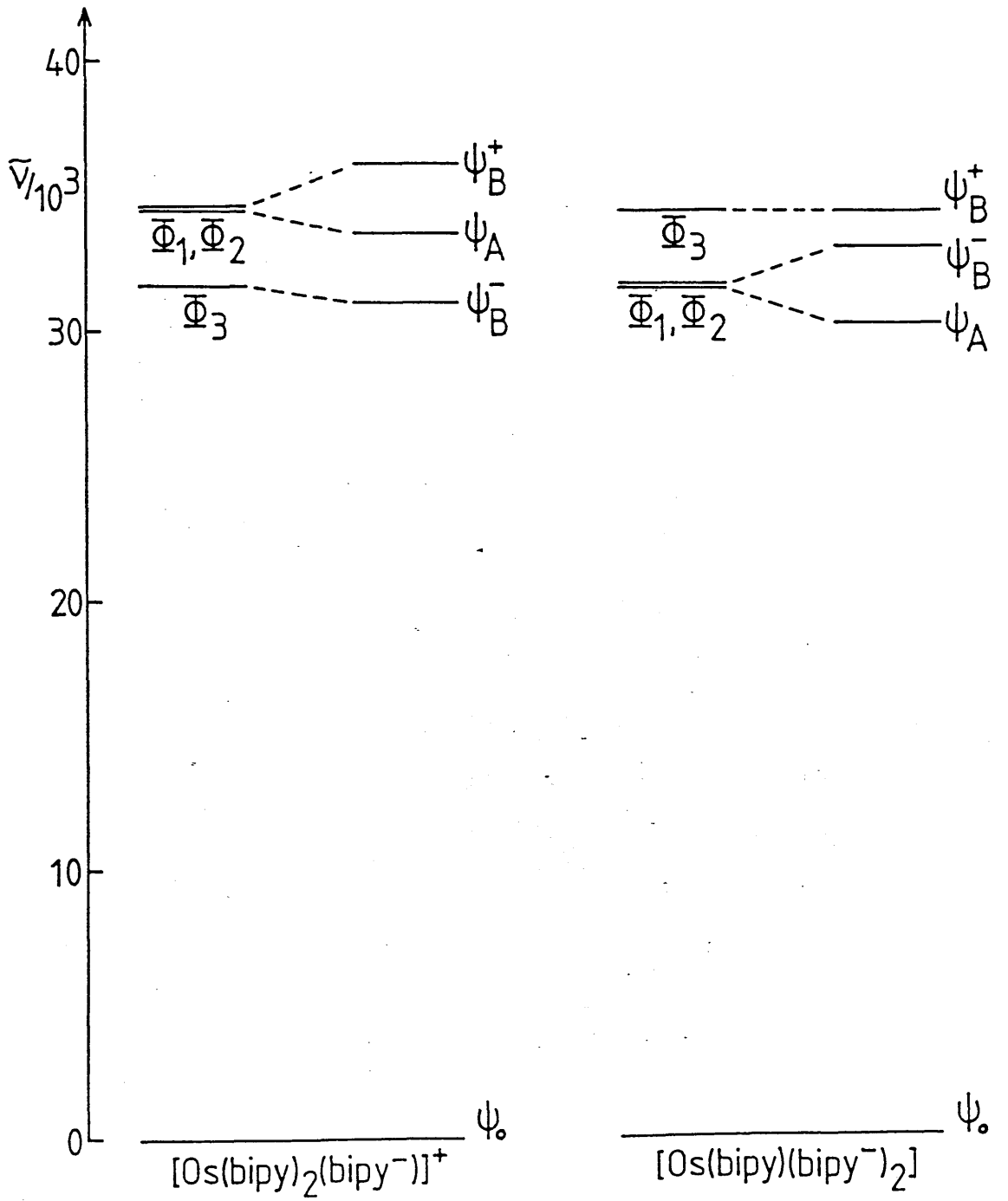

This strongly suggests that $\underline{II}^{2-}$ can be formulated using the localised theory with exciton exchange occuring between distinct bipy and bipy$^-$ ligands and it is therefore very likely that $\underline{II}^-$ behaves in a similar fashion. The calculated c.d. spectra have again reproduced quite well the energies, intensities and relative signs found in the measured spectra and so based on this evidence and that of the absorption spectra it is proposed that osmium complexes behave like the analogous ruthenium complexes. The added electrons are localised on the bipy ligands and exciton coupling takes place between the individual bipy and bipy$^-$ ligands.

Chemical Reduction

All previous syntheses of the reduced complexes of I and II were done electrochemically. This method makes it extremely difficult to isolate samples of the compounds produced and so a chemical method of reducing the complexes was sought. This was achieved by reacting complexes I and II with lithium metal in N, N-dimethylformamide. The reaction proceeds exothermically right through until the triply reduced complexes $\underline{I}^{3-}$ and $\underline{II}^{3-}$ are formed. These were identified by their absorption and circular dichroism spectra which are shown in Figures 36 and 37 for $\underline{I}^{3-}$ and $\underline{II}^{3-}$ respectively. Similar chemical reductions using lithium and other alkali and alkaline earth metals have been used to synthesise reduced first row transition metal tris (2,2′-bipyridine) complexes in the past and these have been reviewed by McWhinnie et al.[130]

It was mentioned earlier that the c.d. spectra of the reduced ruthenium complexes had to be run at low temperature because the triply reduced complex was found to racemise in the acetonitrile solution. When the triply reduced species $\underline{I}^{3-}$ is prepared by chemical reduction it is

FIGURE 36: The absorption and circular dichroism spectra of lithium Δ-tris(2,2′-bipyridinyl)ruthenate(II).

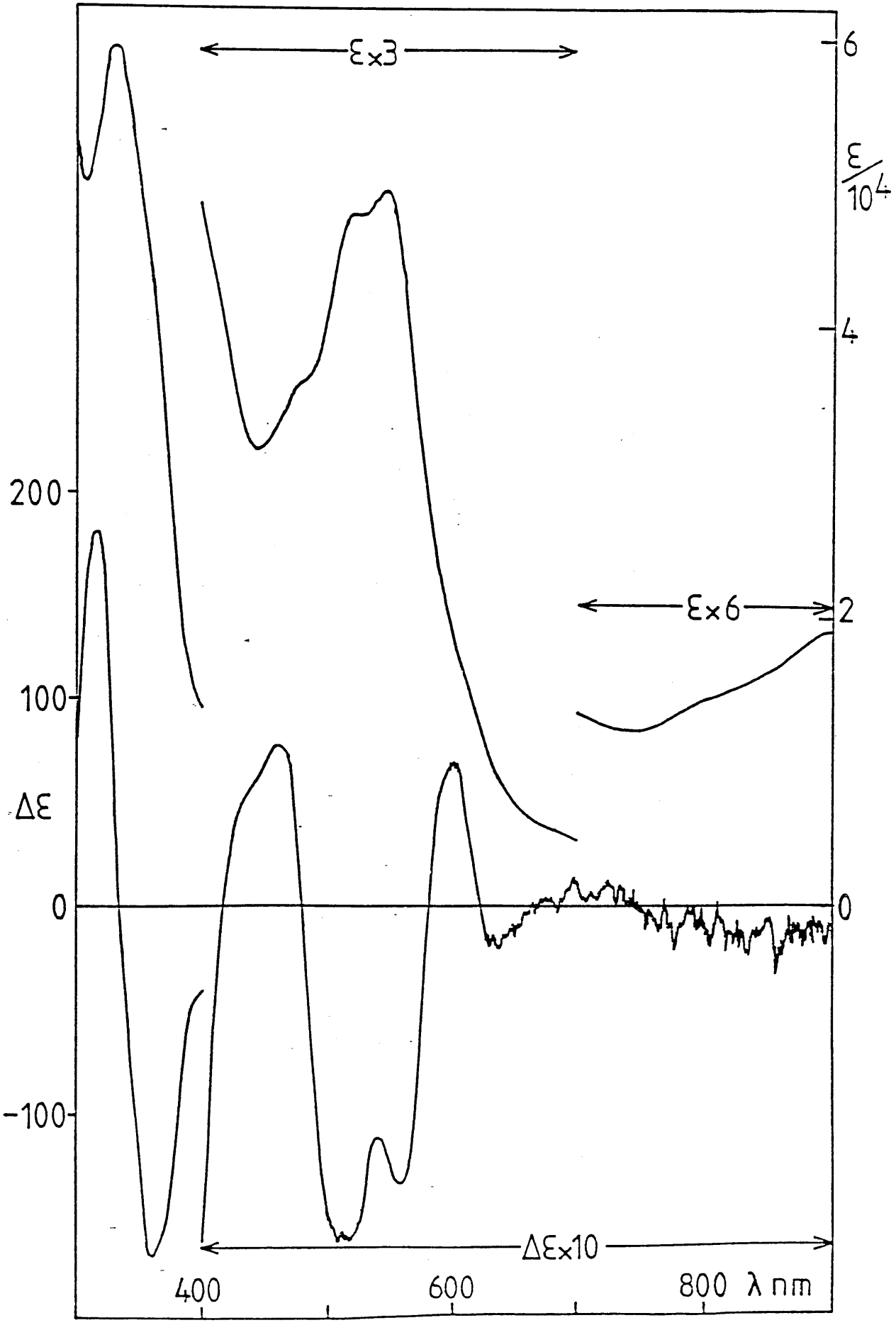

FIGURE 37: The absorption and circular dichroism spectra of lithium Δ-tris(2,2′-bipyridinyl)osmate(II).

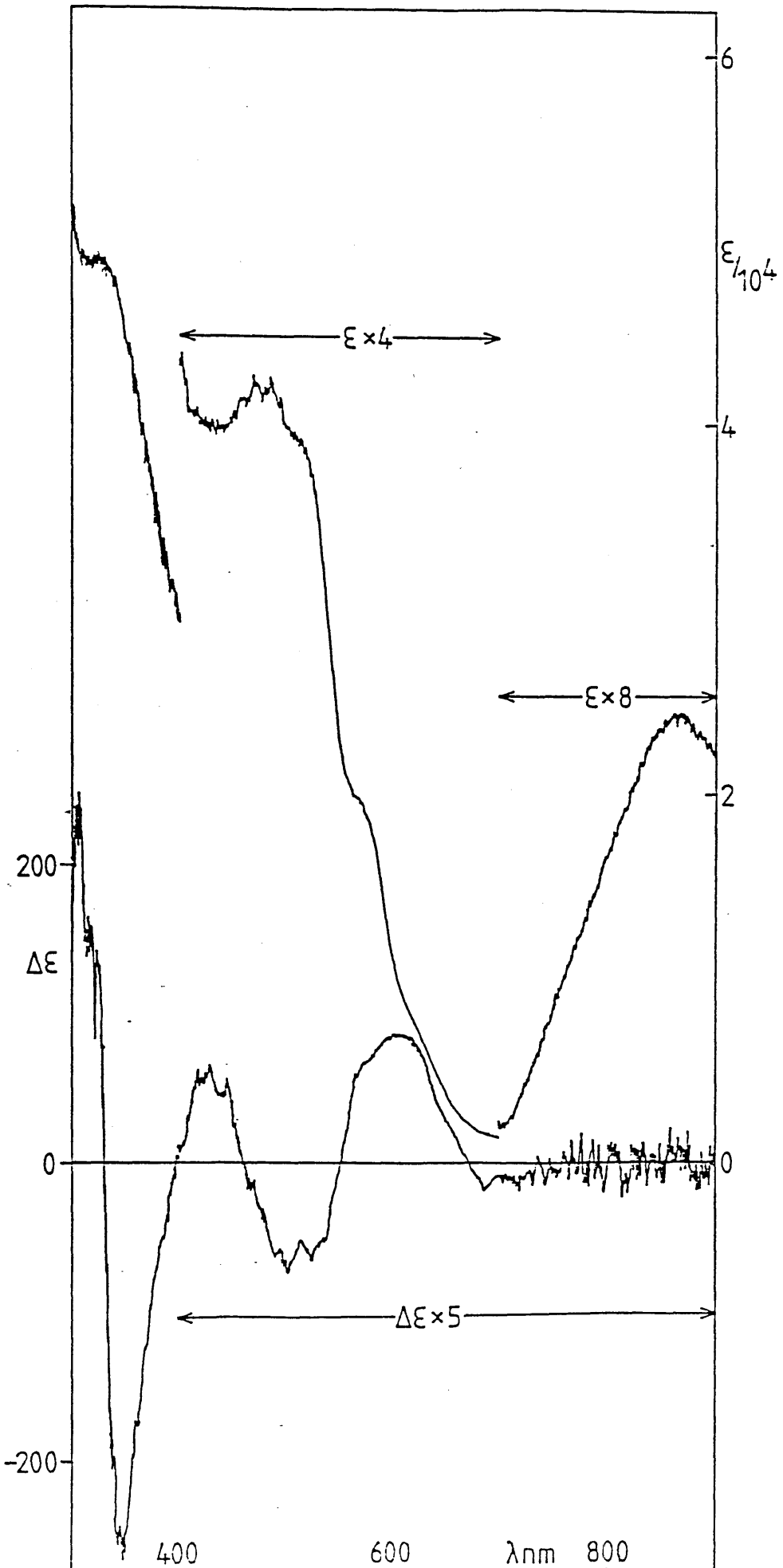

optically stable in both the solid state and in N, N-dimethylformamide but racemises (with a half-life of approximately one hour) in acetonitrile. There are three possibilities why the triply reduced complex is more labile than Δ-$[Ru(bipy)_3]^{2+}$ itself: there is substantial electron delocalisation from ligand to metal producing a partial d^7 configuration, the ligand field of $bipy^-$ is considerably less than that of bipy, or repulsion between the negatively charged bulky $bipy^-$ ligands leads to much easier dissociation.

The first possibility, that of electron delocalisation from ligand to metal is the most unlikely reason for the racemisation of $\underline{I}^{3-}$ as bipy is known to be a very good electron acceptor taking up to two extra electrons within the molecule and also this mechanism would be expected to occur in the analogous osmium complexes which have been found to be completely optically stable. Also the circular dichroism spectra of the ligand transitions have been modelled successfully by the exciton theory of optical activity in which it is assumed that no delocalisation of electrons takes place between the ligands and the metal ion. If electron delocalisation between the metal and ligands did take place to any great extent then the assumptions of the exciton theory would be invalid and the spectra would be expected to be different from that predicted by the theory. This has been found to be the case with other transition metal complexes with anionic ligands such as oxalate[128] or pentane-2,4-dionate[129] in which metal-to-ligand charge-transfer π-bonding is thought to occur to a large extent and these complexes lack the characteristic exciton form in their c.d. spectra.

The last possibility, that of electronic replusion between the ligands, may have a small effect in the labilisation of the $bipy^-$ ligands but on its own this effect should be fairly minor. The ionic radius of

Os^{4+} (0.067 nm) is larger than that of Ru^{4+} (0.065 nm) but the difference is negligible,[131] similarly the ionic radius of Os^{2+} should be virtually the same as that of Ru^{2+}. If this was the sole reason for racemisation then $\underline{II}^{3-}$ would be expected to racemise also (perhaps a little slower than $\underline{I}^{3-}$) but in practice $\underline{II}^{3-}$ appears to be completely optically stable.

The most likely reason for the labilisation in $\underline{I}^{3-}$ is the second reason, that is, bipy$^-$ has a weaker ligand field than bipy. Bipy is known to be a π-electron acceptor ligand and stabilises many transition metal low-oxidation states.[130] Therefore some metal-to-ligand π-back-bonding will take place in tris(2,2′-bipyridine) complexes. This is born-out by the finding that the Ru(II)-N bond length in $\underline{I}$ was found to be shorter than that of Ru(III) bond lengths in similar complexes,[36] contrary to the expected longer bond length due to the larger ionic radius of Ru(II) compared with Ru(III). Bipy$^-$ however has an electron in the π7 antibonding orbital and so π-back donation from the metal into the ligand antibonding orbitals should be reduced. This should be accompanied by an increase in the Ru-N bond length (i.e. a weakening of the metal-ligand bond) in the reduced complexes and thus the triply reduced complex would be expected to be more labile. The singly and doubly reduced complexes would not be expected to racemise as in these cases there are two and one respectively, non-labile bipy ligands preventing the complex from racemising. Racemisation in the osmium complex, $\underline{II}^{3-}$, presumably does not occur because osmium is a third-row transition metal and so its ligand field stabilisation energy is greater than that of Ru, counteracting the reduced ligand stabilisation energy of bipy$^-$. Note, this effect is well known for example the tris (bipy) complexes of Fe(II) and Ni(II) lose nearly all of their optical activity after approximately two hours in aqueous media[8]

whereas I and II are optically stable due to their greater ligand field stabilisation energy. Another example is of course the tris (bipy) complexes of Ru(III) and Os(III); $[Ru(bipy)_3]^{3+}$ loses approximately half its optical activity in one day whereas $[Os(bipy)_3]^{3+}$ is completely optically stable[9] as Os(III) has a larger ligand field stabilisation energy than Ru(III).

CHAPTER 5

THE LUMINESCENCE AND INFRARED SPECTRA OF $[Ru(bipy)_3]^{2+}$, $[Os(bipy)_3]^{2+}$ AND THEIR REDUCED ANALOGUES

Luminescence

The luminescence spectrum of $[Ru(bipy)_3]^{2+}$ is well known and has recently been reviewed by Kalyanasundaram[20]. The origin of the emission is from the decay of the MLCT excited state, the emitting state being formulated as $[Ru^{III}(bipy)_2(bipy^-)]^{2+}$,[126] in which the transferred electron has been localised on one bipy ligand; this has been treated in more detail in a recent discussion.[68] Since the emission is essentially of $\pi^* \rightarrow d$ in nature it would be interesting to see how the luminescence of the complex would be affected when it is reduced. Accordingly the room temperature emission spectra of $\underline{I}$ to $\underline{I}^{3-}$ have been measured spectroelectrochemically and are shown in pairs for comparison in Figures 38 and 39.

The emission spectra of $\underline{I}$ and $\underline{I}^{3-}$ are shown in Figure 38. The original band of $\underline{I}$ is centred on 16,498 cm^{-1} and is approximately sixty times as intense as the new emission band of $\underline{I}^{3-}$ which has a higher energy and is centred on 17,650 cm^{-1}. The emission spectra of $\underline{I}^-$ and $\underline{I}^{2-}$ are shown in Figure 39. The original emission band of $\underline{I}$ has been reduced more than ten times in $\underline{I}^-$ but the energy of the emission has remained the same and the band shape is more asymmetric compared to that of $\underline{I}$. There is another decrease in intensity by a factor of approximately six when $\underline{I}^{2-}$ is produced from $\underline{I}^-$ and jump to higher energy of the band maximum. The main points to note about the emission spectra of the series of complexes $\underline{I}$ to $\underline{I}^{3-}$ are:

(i) The intensity decreases rapidly from $\underline{I}$ to $\underline{I}^-$ to $\underline{I}^{2-}$ and then increases again (by a small amount) from $\underline{I}^{2-}$ to $\underline{I}^{3-}$.

(ii) The energy maximum of the bands are approximately constant from $\underline{I}$ to $\underline{I}^-$, there is a jump to higher energy from $\underline{I}^-$ to $\underline{I}^{2-}$ and then

FIGURE 38: Emission spectra of $[Ru(bipy)_3]^{2+}$ (solid line) and $[Ru(bipy^-)_3]^-$ (broken line) in acetonitrile using 20,481.5 cm^{-1} (488.0 nm) excitation. Emission intensity is in arbitrary units, note that the intensity of I is x 1/60

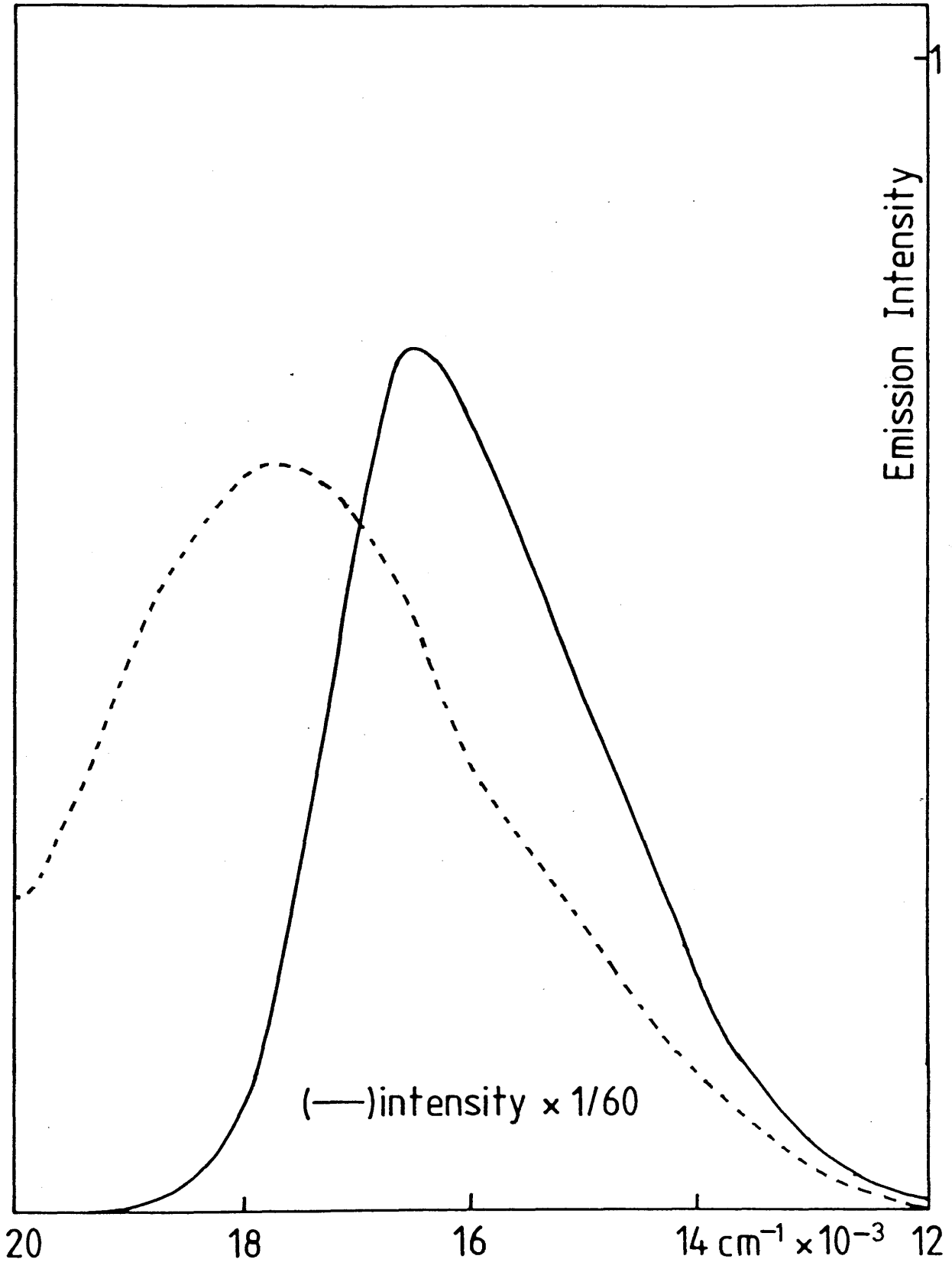

FIGURE 39: Emission spectra of $[Ru(bipy)_2(bipy^-)]^+$ (solid line) and $[Ru(bipy)(bipy^-)_2]$ (broken line) in acetonitrile using 20,481.5 cm^{-1} (488.0 nm) excitation. Emission intensity is in arbitrary units, note that the intensity of I^- is x 1/6

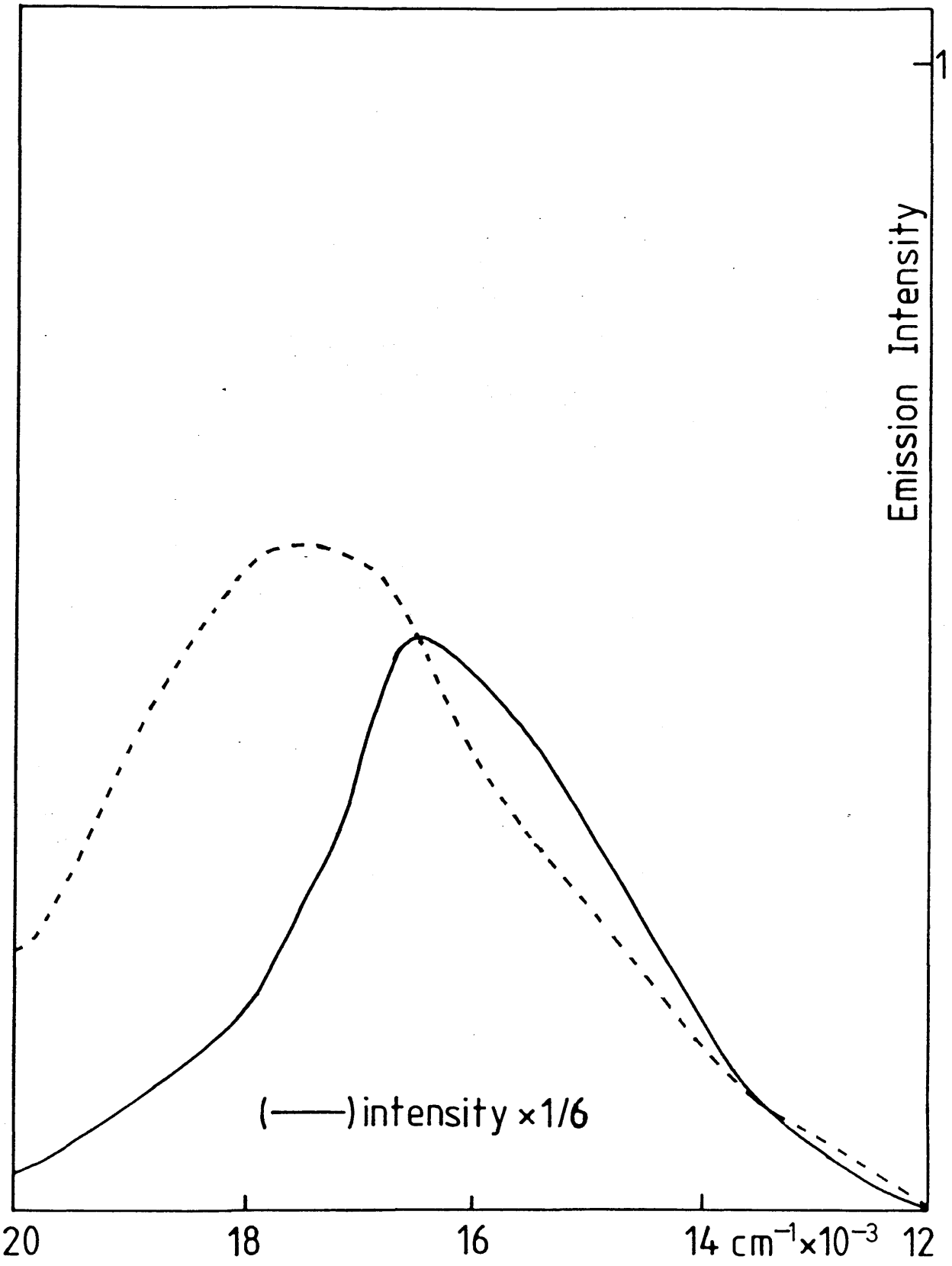

from $\underline{I}^{2-}$ to $\underline{I}^{3-}$ the energy is approximately the same again.

(iii) Bands $\underline{I}$ and $\underline{I}^{3-}$ are reasonably symmetrical, whereas bands $\underline{I}^{-}$ and $\underline{I}^{2-}$ are asymmetric with high and low energy shoulders respectively

It is obvious from these points that the emission spectra are not simply showing a gradual decrease in intensity and a gradual shift to higher energy of the emission band, but something more complicated is occurring as the complex is reduced in successive stages. Also the emission in $\underline{I}$ is from the decay of the metal to bipy charge transfer state. However, as the complex is reduced the number of bipy ligands decreases until $\underline{I}^{3-}$ is formed in which there are only bipy^{-} ligands, so the question arises, what is the emitting state in $\underline{I}^{3-}$?

In an attempt to clarify these results, the emission spectra of the series of osmium complexes $\underline{II}$ to $\underline{II}^{3-}$ were measured, and these are shown in Figures 40 and 41. Figure 40 shows the emission spectra of $\underline{II}$ and $\underline{II}^{3-}$ which are very similar to those of $\underline{I}$ and $\underline{I}^{3-}$, the only main difference is that the energy of the emission in $\underline{II}$ is at a lower energy than the corresponding emission of $\underline{I}$. Again the intensity of the new band of $\underline{II}^{3-}$ is much weaker and at a higher energy than the band of $\underline{II}$. The emission spectra of $\underline{II}^{-}$ and $\underline{II}^{2-}$ are shown in Figure 41 and it is immediately obvious that two emission bands are present in the emission spectra of $\underline{II}^{-}$ and $\underline{II}^{2-}$. The intensities of the emission bands follow the same pattern as in the ruthenium cases, with large drops in the intensity from $\underline{II}$ to $\underline{II}^{-}$ to $\underline{II}^{2-}$ and then a slight increase in intensity from $\underline{II}^{2-}$ to $\underline{II}^{3-}$ which suggests that the same process is occurring in both series of compounds. Table 13 gives the energies in wave-numbers of the emission band of both series of compounds, the new

FIGURE 40: Emission spectra of $[Os(bipy)_3]^{2+}$ (solid line) and $[Os(bipy^-)_3]^-$ (broken line) in acetonitrile using 20,149.5 cm^{-1} (496.5 nm) excitation. Emission intensity is in arbitrary units, note that the intensity of II is x 10^{-2}.

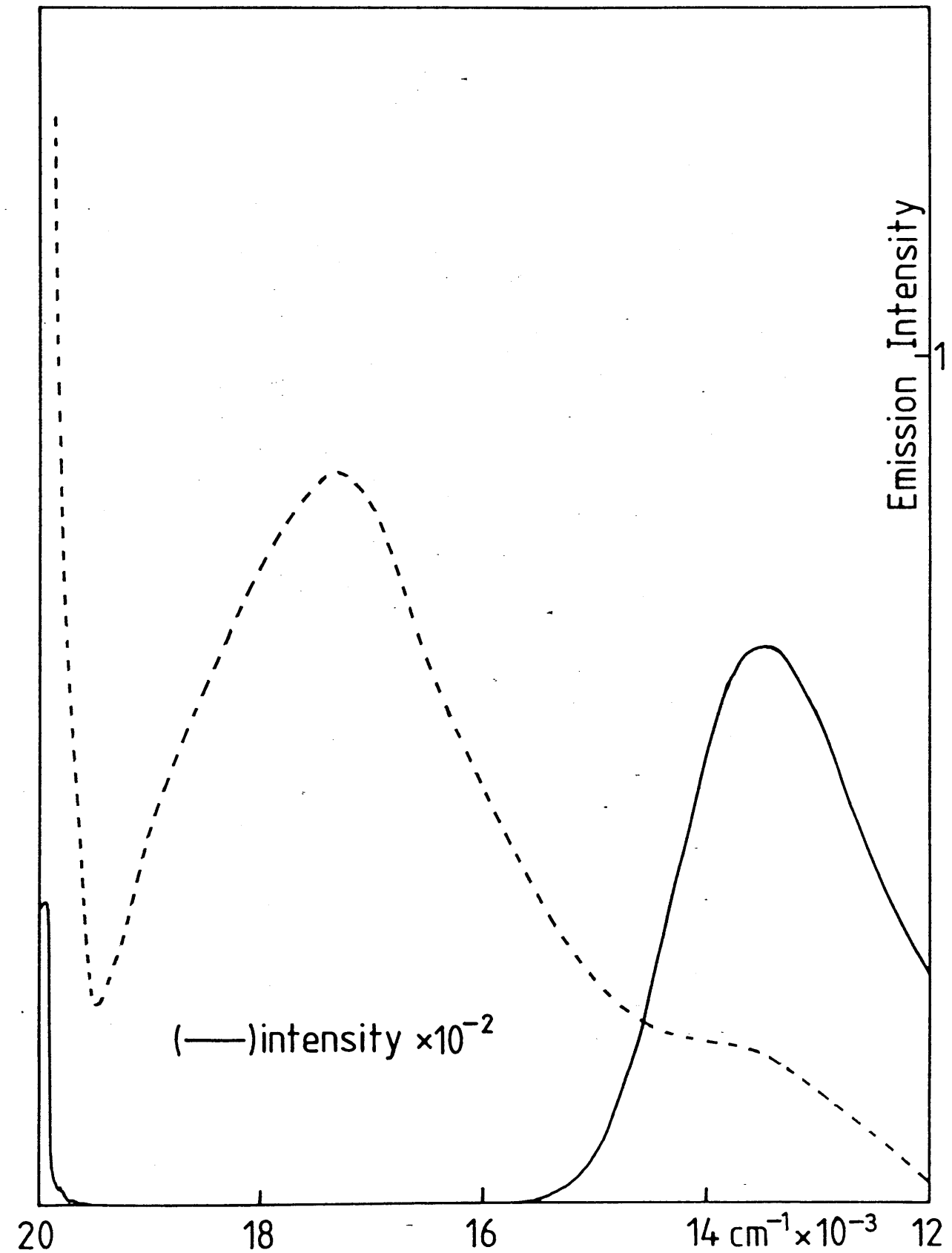

FIGURE 41: Emission spectra of $[Os(bipy)_2(bipy^-)]^+$ (solid line) and $[Os(bipy)(bipy^-)_2]$ (broken line) in acetonitrile using 20,149.5 cm^{-1} (496.5 nm) excitation. Emission intensity is in aribitary units, note that the intensity of II$^-$ is 2 x 10^{-1}.

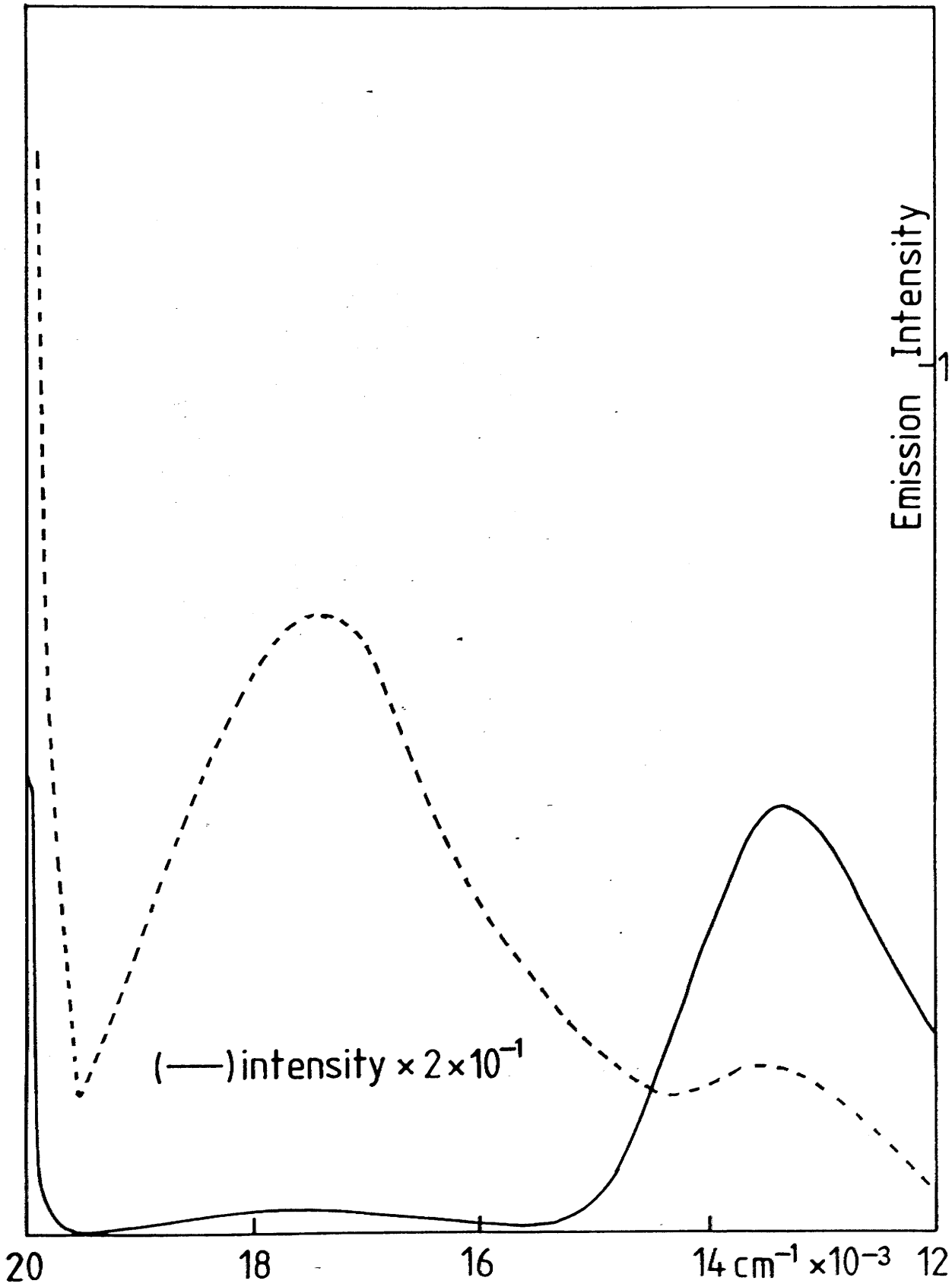

emission bands in the reduced complexes are under the heading $bipy^-$, the original bands are under the heading bipy.

TABLE 13: The energies of the emission bands of I to I^{3-} and II to II^{3-} in wavenumbers (cm^{-1})

	bipy	$bipy^-$		bipy	$bipy^-$
I	16,498	-	II	13,458	-
I^-	16,500	-	II^-	13,352	17,649
I^{2-}	15,243	17,604	II^{2-}	13,514	17,468
I^{3-}	-	17,650	II^{3-}	13,427*	17,314

* see text for explanation

In the emission spectra of II^- and II^{2-} there is the possibility that residual II is causing the emission band at 13,352 and 13,514 cm^{-1} respectively. However, as has been shown already, the concentration of II should be reduced by three orders of magnitude when II^- is electrogenerated and since the emission at that energy is only reduced by five times, it is unlikely to be due to the small amount of II which would be present. Similarly, when II^{2-} is electrogenerated the concentration of II will be reduced by more than seven orders of magnitude, therefore it is extremely unlikely that some residual II is causing the low energy emission in the spectrum of II^{2-}. It is therefore concluded that the two emission bands present in the mixed osmium species are real and it is likely that the mixed ruthenium species also have two emission bands, which would also be an explanation for the asymmetry of the bands in I^- and I^{2-}. So what the emission spectra appear to show in both the ruthenium and osmium complexes is the progressive reduction in the intensity of the charge transfer emitting state from the starting complexes

to the doubly-reduced complexes until it has been completely removed in $\underline{I}^{3-}$ and $\underline{II}^{3-}$ and the replacement of this band with a new higher energy emission which increases in intensity until it is at a maximum in the triply-reduced complexes. Now the emission spectrum of $\underline{II}^{3-}$ appears to have two bands which is contrary to the statement above. The production of the triply-reduced complex is at a voltage where the solvent is just beginning to be reduced (especially if impurities are present) and the explanation of why there is a low energy band in $\underline{II}^{3-}$ is probably because of incomplete reduction resulting in some $\underline{II}^{2-}$ present in the solution. This is the most likely explanation as in some absorption and c.d. experiments incomplete reduction occurred. If complete reduction to produce pure $\underline{II}^{3-}$ was achieved it would be expected on this basis to have only one weak emission band like the spectrum of $\underline{I}^{3-}$.

The origin of the new emission band has still to be decided. If the absorption spectrum of $\underline{II}^{-}$ is re-examined in relation to its luminescence spectrum and the 496.5 nm (20,149.5 cm^{-1}) laser excitation (Figure 42) the picture soon becomes clear. The laser excitation is at an energy where only the MLCT transitions can be excited in the starting complex. Now as the complex is reduced, the MLCT bands are steadily replaced by what is thought to be the $\pi 7 \rightarrow \pi 10$ transition of $bipy^{-}$. It was shown earlier in Chapter 3 that "free" $bipy^{-}$ has an emitting state which was thought to be a $\pi 10 \rightarrow \pi 7$ ligand centred decay at approximately the same energy. Also the new emission is at a much higher energy than the $\pi 7 \rightarrow \pi 8$ and $\pi 9$ absorptions of the complexed $bipy^{-}$ (these occur between 700 and 1600 nm) and so it is concluded that the new emission band in the reduced complexes are due to the ligand centred $\pi 10 \rightarrow \pi 7$ decay of the complexed $bipy^{-}$. The same conclusion is reached for the reduced complexes of the analogous ruthenium complex.

FIGURE 42: The absorption (solid line) and luminescence (broken line) of $[Os(bipy)_2(bipy^-)]^+$, II$^-$ in relation to the 496.5 nm (20,149.5 cm^{-1}) laser excitation. Note, the luminescence intensity is an arbitrary scale and the intensity of the high energy luminescence band has been increased 18 times compared to that of the low energy band.

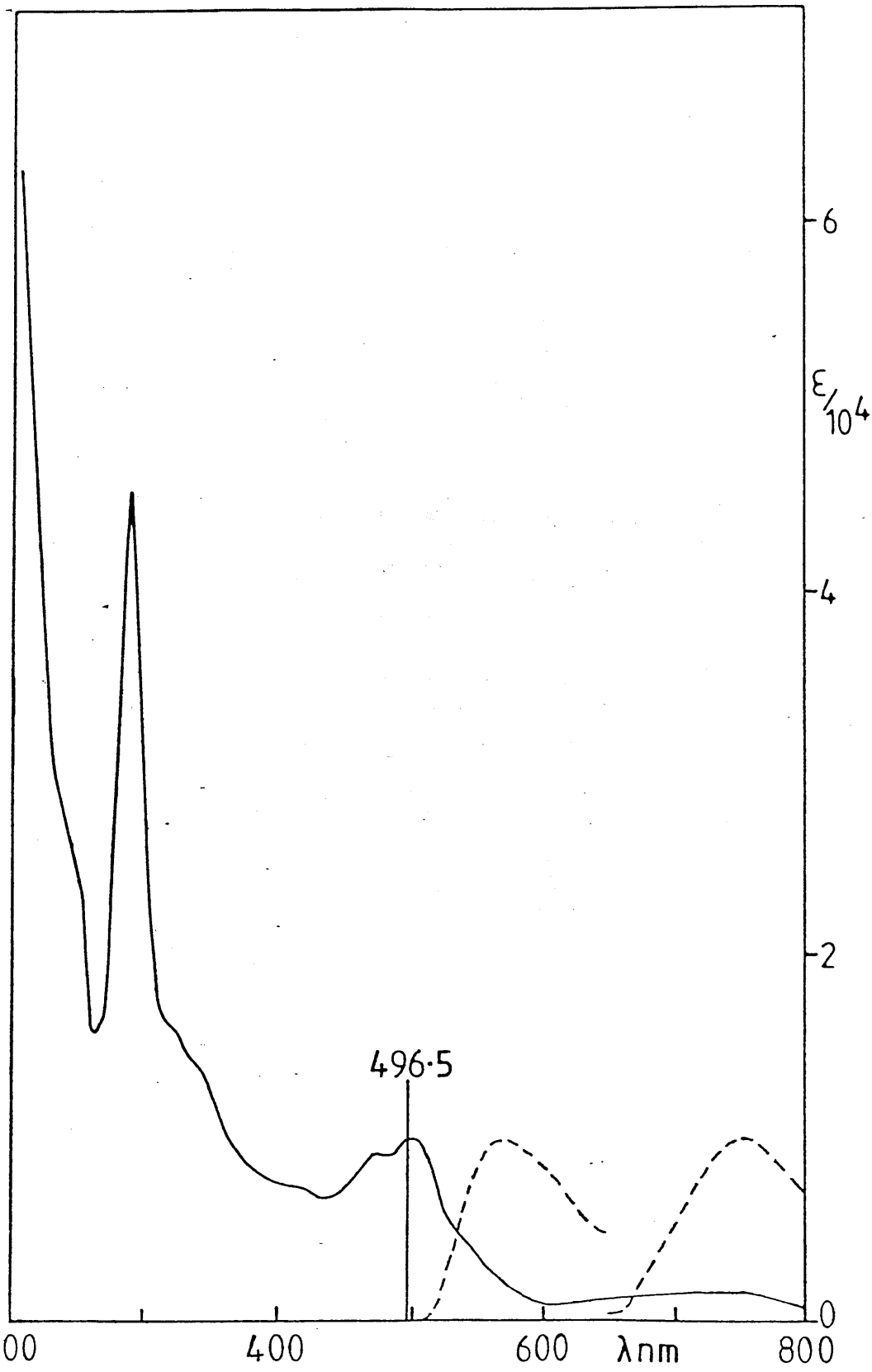

Support for the ligand centred emission also comes from comparison of the energies of the emitting states in the ruthenium and osmium complexes. The energies of the emitting states in I and II are quite different as would be expected for MLCT transitions with two different metal centres. However the energies of the emitting states in I^{3-} and II^{3-} are very similar as would be expected for the same transition in the same molecule in slightly different chemical environments.

The intensities of the luminescence spectra of the complexes and their reduced analogues do not increase and decrease steadily by a third as each successive electron is added like the absorption spectra intensities. The variation in the intensities is considerably more complex than that.

For the MLCT luminescence when the singly and doubly reduced complexes I^{-} and II^{-} and I^{2-} and II^{2-} respectively are formed the intensity of their luminescence decreases by approximately an order of magnitude on each reduction. The $bipy^{-}$ luminescence on the other hand appears to increase by approximately one third on each successive reduction similar to the absorption intensities for $bipy^{-}$.

Simplified energy level diagrams for the reduced complexes I^{-} and II^{-} are shown in Figure 43. On consultation of this energy level diagram, it can be seen that it is extremely difficult to derive any information concerning the intensities of any of the luminescing states. This is because none of the quantum yields Ø are known for any of the decay processes, be they radiative or non-radiative. The fact that there are two emitting states complicates matters because now there could also be non-radiative decay ($Ø_2$) between the two luminescing levels in the complex. All that can be said is that the non-radiative decay $Ø_3$ is presumably more efficient than the non-radiative decay $Ø_1$ as in

FIGURE 43: Experimental energy level diagram of the emitting states of the singly reduced complexes $\underline{I}^-$ and $\underline{II}^-$. [radiative decay (⟶), non-radiative decay (⇝)].

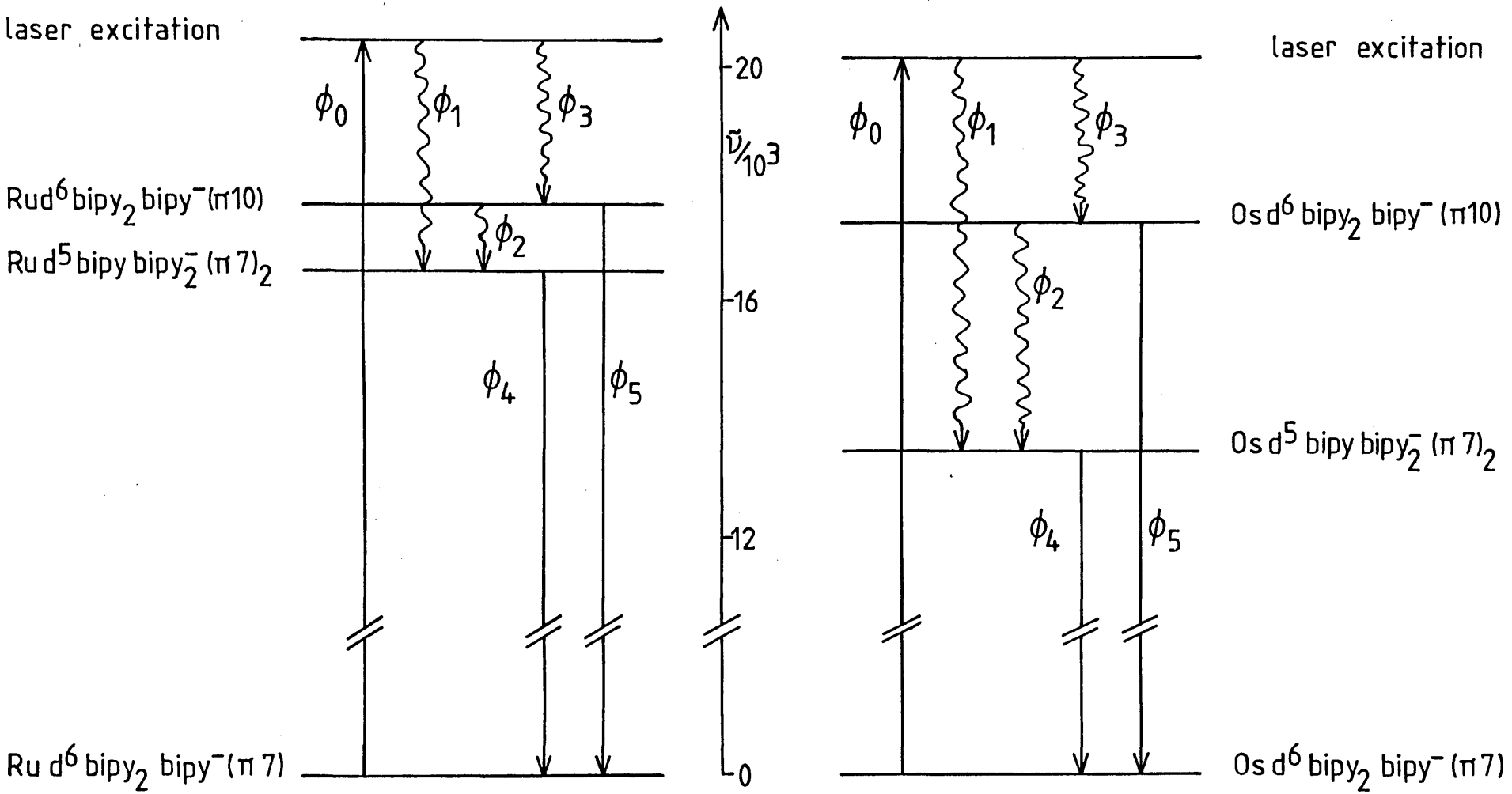

the singly and doubly reduced species the intensity of the MLCT luminescence $\emptyset_4$ falls dramatically. However, there must be considerable non-radiative decay from the $\pi 10$ level as its luminescence intensity is very low, that is the quantum yield $\emptyset_5$ for this decay is very low.

If these emission assignments are correct, namely the lower energy emission in each complex is a charge transfer emission and the higher energy emission is an intra-ligand $\pi 10 \rightarrow \pi 7$ transition then the two emission processes must occur on electronically distinct $bipy^-$ ligands. Furthermore, since the charge transfer emission is a property of bipy and the $\pi 10 \rightarrow \pi 7$ emission is a property of $bipy^-$ and since the two processes occur together in the hetero-trischelated complexes, then there must be distinct bipy and $bipy^-$ ligands present together in the hetero-trischelates. Hence charge localisation must occur in the mixed bipy and $bipy^-$ complexes which supports the results of the circular dichroism spectra.

Infrared Spectra

The infrared spectra of bipy and its complexes have been measured on numerous occasions in the past and have been well documented.[113,117,130] The infrared spectrum of Libipy has been measured by Konig and Lindner[113] in solution and more recently (Chapter 3, this work) in the solid-state and compared with that of bipy. It would therefore be of interest to see how the infrared spectrum of I and II compare with those of the analogous reduced complexes I^{3-} and II^{3-} and with the spectra of both bipy and $bipy^-$.

Conventional electrochemical preparations of the reduced complexes of I and II have made it extremely difficult for their infrared spectra to be measured and this has not hitherto been accomplished.

Chemical reduction of I and II has however provided a relatively simple method for isolating the species I^{3-} and II^{3-} and the use of vacuum line and dry-box techniques has enabled the solid-state infrared spectra of these complexes to be measured.

The infrared spectra of I, I^{3-}, II and II^{3-} are shown in Figures 44, 45, 46 and 47 respectively and the band energies in wavenumbers for the four complexes are listed in Table 14 together with their empirical assignments.

The infrared spectra of various first row transition metal tris(2,2′-bipyridine) complexes have been examined in some depth by Konig and Lindner.[113] The empirical assignments in Table 14 are based on their findings.

One of the main things to note about the infrared spectra of I, I^{3-}, II and II^{3-} is that the pairs of complexes I and II and I^{-3} and II^{3-} have extremely similar spectra, both in the number of bands and in the band energies. A further point to note is that in the spectra of the triply reduced complexes I^{3-} and II^{3-}, bands characteristic of dimethylformamide (DMF) are present. These are probably due to co-ordinated solvent rather than residual solvent from the preparation of the complexes. The solvent bands are quite weak compared to the bands of the complex so there is probably only one solvent molecule present and this is possibly co-ordinated to the lithium counter ion.

The infrared spectra are essentially those of the ligand molecules as the metal-nitrogen vibrations occur at energies lower than 400 cm^{-1}. The spectra can be divided up simplistically into two regions, the C-H stretching vibrations above 2600 cm^{-1} and the ring stretching and bending modes together with the C-H bending modes below 2600 cm^{-1}.

FIGURE 44: Infrared spectra of $[Ru(bipy)_3]Cl_2$, I, in flurorlube and nujol mulls

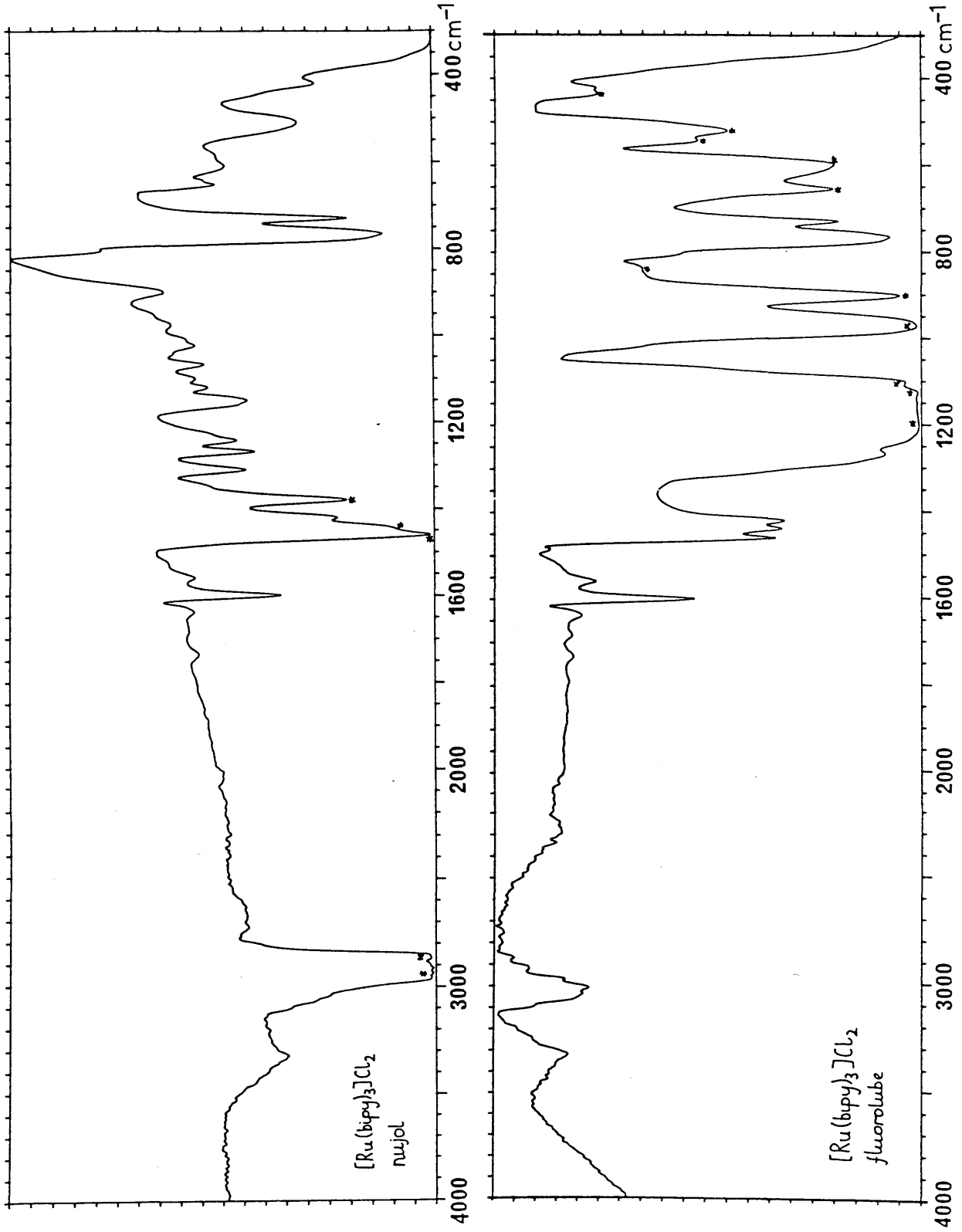

FIGURE 45: Infrared spectra of $[Ru(bipy^{-})_3]Li$, $\underline{I}^{3-}$, in fluorolube and nujol mulls

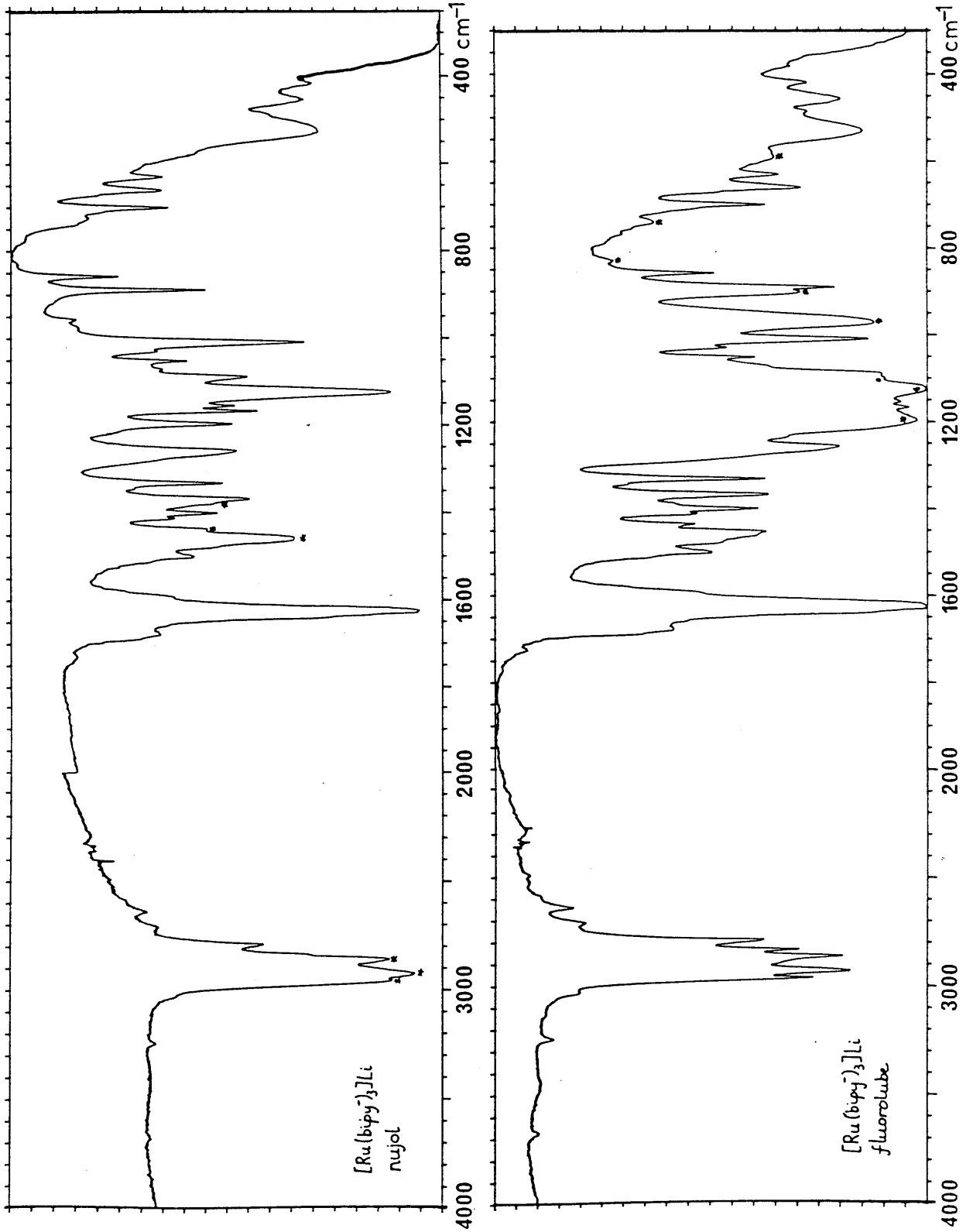

FIGURE 46: Infrared spectra of $[Os(bipy)_3]Cl_2$, II, in fluorolube and nujol mulls

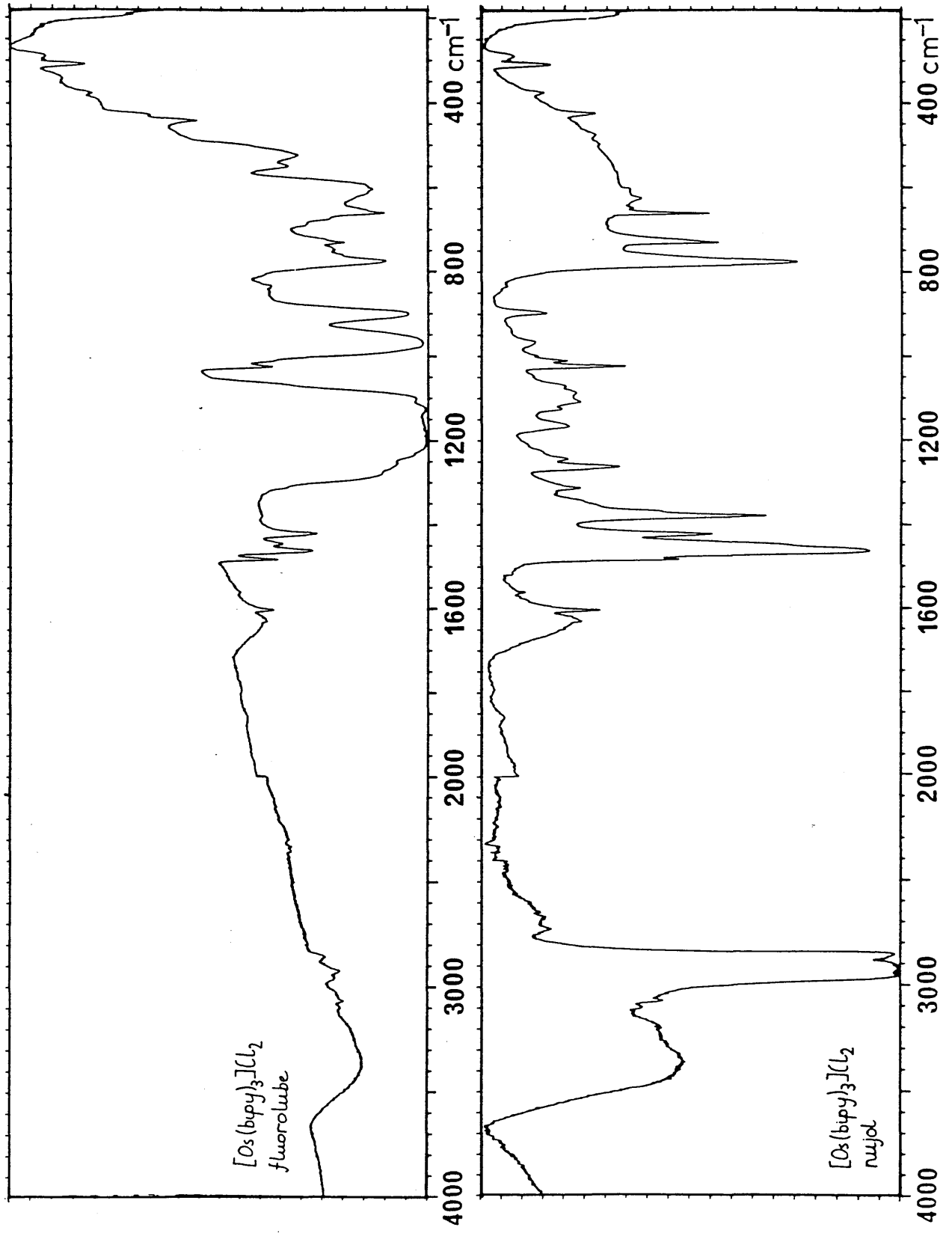

FIGURE 47: Infrared spectra of $[Os(bipy^{-})_3]Li$, $\underline{II}^{3-}$, in fluorolube and nujol mulls

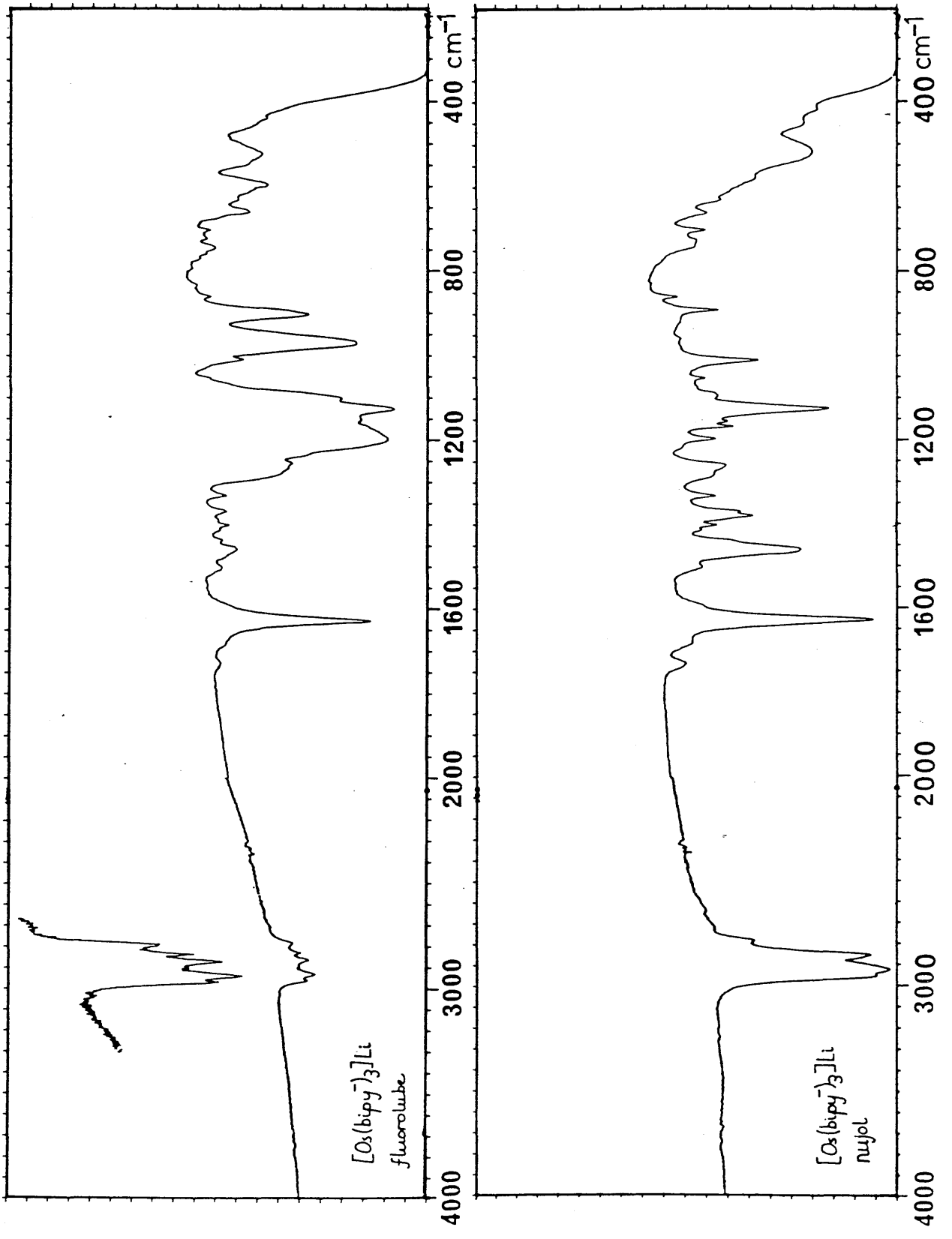

TABLE 14: Infrared band energies, wavenumbers and empirical assignments[113] of I, I^{3-}, II and II^{3-}

I	I^{3-}	II	II^{3-}	Empirical Assignments
3100	3025	3100		
3060	2960	3065	2960	
3040	2930	3025	2930	
3010	2860		2863	
2970	2828	2960	2829	C-H stretch
2920	2785	2920	2785	
2870	2705	2855		
	2635			
	1730		1730	
	1675		1680	DMF
1637	1625	1625	1629	
1599	1590	1601	1590	ring stretch
1560		1560		(C = C and C = N)
	1500		1500	DMF
1530	1475			ring stretch
1486	1460	1481	1460	(C = C and C = N)
1460	1452	1461		ring stretch
1438	1434	1444	1435	(C = C and C = N)
1420	1410	1420	1410	+ C-H bend
	1400		1400	DMF
	1368		1368	
1310	1330	1311	1330	ring stretch
1268	1280	1261	1280	(C = C and C = N)
1241	1257	1242	1256	ring stretch +
1230	1295		1195	inter-ring stretch
1160	1165	1165	1165	
1150	1152	1124	1153	ring-H in-plane
1120	1123	1106	1124	bend
	1088		1090	DMF
1068	1070	1070		ring stretch
	1050		1050	ring-H out-of-plane
1024	1030	1022		bend
975	1009	1010	1009	ring stretch (breathing)
806	890	897	890	
775	859	775	859	ring-H out-of-plane
766	700		700	bend
730		730		
	660		660	DMF
651	630	660	630	
611	525		520	ring bend
	484			
	455		450	inter-ring deformation
421	419	422	418	ring torsion

Theory predicts that when the ligands are reduced the main differences in the infrared spectra will occur in the C-N skeletal bands, with some bands moving to higher energies and some moving to lower energies. When the spectra of the reduced complexes are compared with those of the starting complexes it is found that this appears to be the case. For example the strong skeletal band at approximately 1600 cm^{-1} in I and II is shifted some 25 cm^{-1} to higher energy in the reduced complexes I^{3-} and II^{3-} whereas many of the other bands in the reduced complexes are at lower energies than in the non-reduced complexes.

The most surprising feature about the reduced spectra however is the effect that reduction has had on the hydrogen bending and stretching modes. In particular the hydrogen stretching modes are very different in the reduced complexes compared to the non-reduced complexes. They appear to be more intense in the reduced complexes and are shifted by approximately 120 cm^{-1} to lower energy leaving only one band in I^{3-} above 3000 cm^{-1}.

The infrared spectra of the reduced complexes have very similar band energies to those of Libipy (Table 4), although the complexes have more vibrational modes than Libipy. This is most noticeable in the C-H stretching region where the C_{2v} symmetry of Libipy is expected to produce eight infrared active C-H stretching modes.[113] Whereas in the complexes each bipy ligand contributes eight C-H stretches. The resulting twenty-four frequencies transform within the overall D_3 symmetry of the complex according to $4A_1 + 4A_2 + 8E$. Of these only the A_2 and E modes are infrared active and thus twelve C-H stretching vibrations are expected. In practice only five bands are distinguished in Libipy and only eight bands are visible in I^{3-} due to low intensity and poor resolution of the spectra.

The fact that the band energies in the osmium and ruthenium complexes and the band energies in Libipy are so similar to those of the reduced complexes reinforces the assumption that the central metal ion confers only minor perturbations to the co-ordinated ligands in the complexes.

CHAPTER 6

SPECTROSCOPY OF $[Ir(bipy)_3]^{3+}$, III, AND ITS REDUCED ANALOGUES

The tris(2,2′-bipyridine)iridium(III) ion was first prepared in 1973 by Flynn and Demas.[14] Since then various workers have characterised its absorption,[14] luminescence[14,132] and n.m.r.[14,132] spectra and its electrochemistry[126,133,134] and spectroelectrochemistry[126,134] have recently been reported. Prior to this work, however, the complex had not been optically resolved. This has now been achieved and the circular dichroism spectrum of Λ-$[Ir(bipy)_3]^{3+}$, III, and its chemically reduced analogues have been obtained.

Circular Dichroism

The absorption and circular dichroism spectra of III are shown in Figure 48. The near-infrared and visible regions of the absorption spectrum are entirely featureless and the first major absorption band at 318 nm is thought to be the intraligand $\pi 6 \rightarrow \pi 7$ transition[38] of bipy. The circular dichroism spectrum of III is almost certainly of reduced intensity due to the small amount of sample available for resolution. The spectrum is similar to those of the analogous cobalt and rhodium complexes[12,13,22] and the bands are similarly assigned. The first two positive circular dichroism bands have the characteristic pattern of similar 3+ metal complexes and this confirms that the complex is the Λ-enantiomer. The energy of the first positive band at 320.5 nm (31,201 cm^{-1}) is also very similar to those of the corresponding cobalt and rhodium complexes[13,22] (31.2×10^3 and 31.3×10^3 cm^{-1} respectively). However, in other metal 3+ complexes the two positive (E mode) circular dichroism bands are followed by a higher energy (A_2 mode) negative circular dichroism band. This is absent from the spectrum of $[Ir(bipy)_3]^{3+}$ so there is possibly some other transition like a charge-transfer band present which has cancelled with the A_2 mode of III in this region of the spectrum.

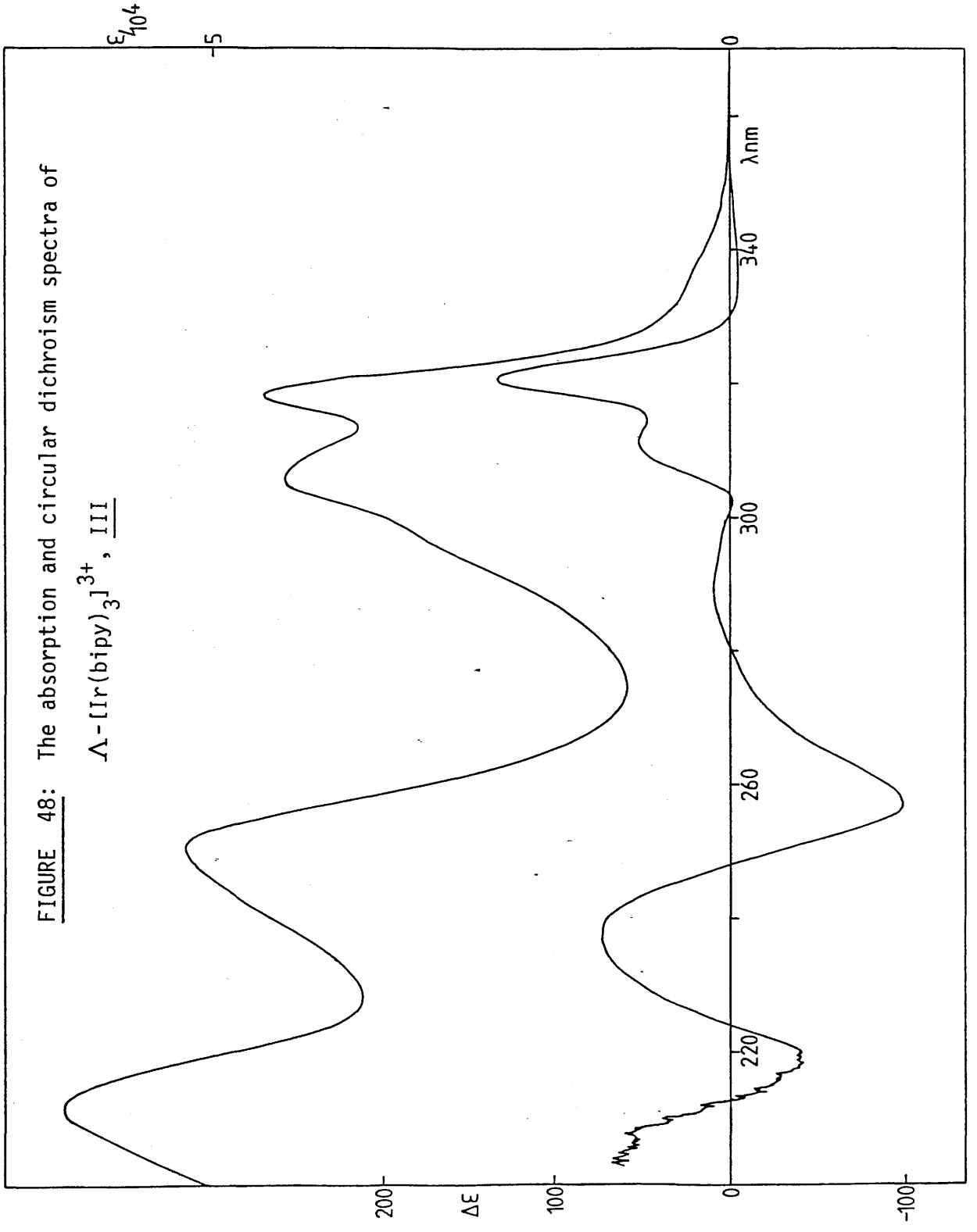

FIGURE 48: The absorption and circular dichroism spectra of Λ-$[Ir(bipy)_3]^{3+}$, III

Unfortunately, not enough $[Ir(bipy)_3]^{3+}$ was synthesised to be able to run any spectroelectrochemical experiments, however, the complex was successfully reduced chemically with lithium, the absorption and circular dichroism spectra of which are shown in Figure 49.

The absorption spectrum of the reduced complex is identical with that of the triply reduced species reported previously by Yellowlees[126,134] and confirms that it is the triply reduced complex $\underline{III}^{3-}$. The absorption spectrum in this work has been extended to below 300 nm to reveal the intense band at approximately 285 nm with a low energy shoulder at approximately 315 nm. Yellowlees[126,134] assigned the bands centred on 500 nm to the $\pi 7 \rightarrow \pi 10$ transition of $bipy^-$ and the bands centred on 380 nm to the $\pi 6 \rightarrow \pi 7$ transition of $bipy^-$. It is intersting to note that the profiles of these two groups of bands are virtually the same, the only difference being that one set are less intense and are situated at lower energies. Also the intensity of this $\pi 6 \rightarrow \pi 7$ transition of $bipy^-$ ($\varepsilon = 2.6 \times 10^4$) is less than half of those found for the corresponding ruthenium and osmium complexes (Chapter 4).

On examination of the circular dichroism spectrum, it is found unexpectedly that there is no exciton couplet centred around 380 nm for the $\pi 6 \rightarrow \pi 7$ transition of $bipy^-$. Like the absorption bands, the profile of the two circular dichroism bands centred on 380 and 500 nm are virtually the same with again the only major difference being that one is lower in intensity and at a lower energy.

When the high energy absorption band centred on 300 nm is considered, it is found this band has a comparable intensity to those of the $\pi 6 \rightarrow \pi 7$ transitions of $bipy^-$ in the triply reduced complexes $\underline{I}^{3-}$ and $\underline{II}^{3-}$. Furthermore there is what appears to be an exciton couplet under

FIGURE 49: The absorption and circular dichroism spectra of Λ-[Ir(bipy$^-$)$_3$], III^{3-}

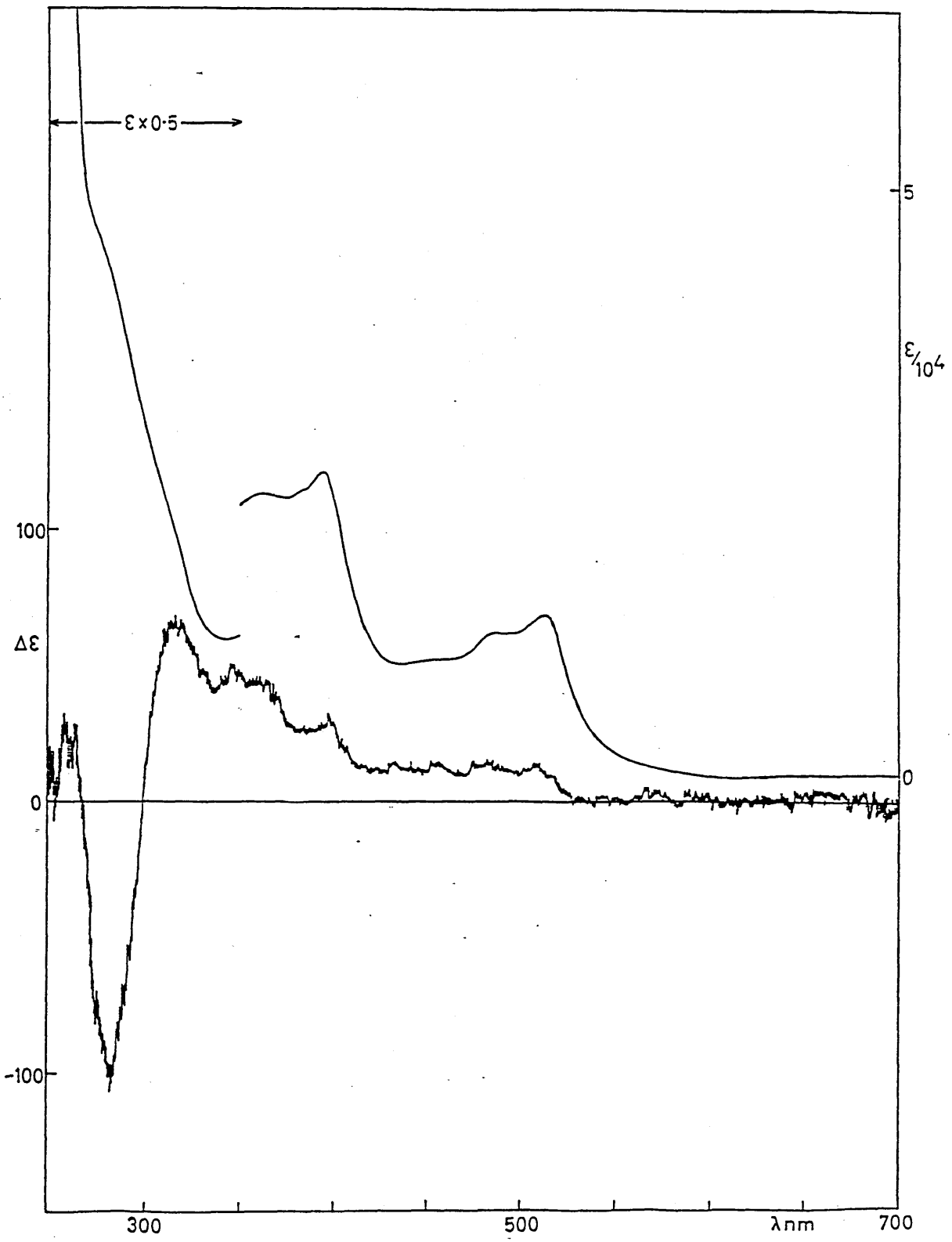

this absorption band which has the correct energy ordering of the bands (positive band at low energy, negative band at high energy) for the Λ enantiomer.

It is therefore concluded that the absorption band centred on approximately 300 nm is in fact the $\pi 6 \rightarrow \pi 7$ transition of $bipy^-$ and that the band centred on approximately 380 nm is the $\pi 7 \rightarrow \pi 10$ transition of $bipy^-$.

This assignment leads to speculation of what the lowest energy visible absorption band is. One possibility is that this is some sort of charge-transfer band, however as the bands in both the absorption and circular dichroism spectra are so similar it is perhaps more likely that this is a spin-forbidden $\pi 7 \rightarrow \pi 10$ transition of $bipy^-$. Presumably the ground-state for the triply reduced complex $\underline{III}^{3-}$ is a quartet state, therefore the spin-forbidden transition would have to be from a quartet ground-state to a doublet excited-state. The intensity of this band is very large for a spin-forbidden band, however, spin-forbidden ligand transitions of a similar intensity have been noted in the past for $\underline{III}$[14]. Their unusually high intensity was attributed to arise from a large internal heavy-atom effect (z = 77 for Ir) and possibly to some mixing with upper charge-transfer states.[14]

When chemically reducing $\underline{III}$ to $\underline{III}^{3-}$ with lithium, if the lithium was allowed to remain in the solution of $\underline{III}^{3-}$ then further changes to the spectra were observed. This is likely to be due to the formation of the quadruply reduced species $\underline{III}^{4-}$ as according to Yellowlees[126], $\underline{III}^{4-}$ is produced at a voltage of only -2.22V vs Ag/Ag^+ and this reduction was also reversible suggesting that $\underline{III}^{4-}$ is stable. It is thought that the fourth electron also enters the ligand orbitals, this would give the electronic configuration Ir d^6 $bipy^-_2$ $(\pi 7^1)_2 bipy^{2-}(\pi 7^2)$ for $\underline{III}^{4-}$. Now one of the bipy ligands has its $\pi 7$ orbitals completely filled and

so it cannot have a $\pi 6 \rightarrow \pi 7$ transition. This means that the complex $\underline{III}^{4-}$ should behave like a bis-complex for exciton coupled long-axis polarised transitions. Hence the absorption and circular dichroism spectra of $\underline{III}^{4-}$ have been compared with the absorption and circular dichroism spectra of the doubly reduced carbon-bonded species, (2,2′-bipyridinyl-C^3,N′)bis(2,2′-bipyridinyl-N,N′)iridium(III) (Figure 50).[135,136] Both the absorption and circular dichroism spectra are very similar. The exciton couplet of each species has the characteristic profile of other complexes where the central metal has a 3+ charge and the energy ordering of the bands is again consistent with the complex being the Λ enantiomer. The existence of exciton couplets in both $\underline{III}^{3-}$ and $\underline{III}^{4-}$ confirms that both complexes have the added electrons localised on the bipy ligands consistent with the results for the osmium and ruthenium complexes.

FIGURE 50: The absorption and circular dichroism spectra of Λ-[Ir(bipy^{-})$_2$(bipy^{2-})]$^{-}$, III^{4-} (solid line) and Λ-[Ir(bipy^{-})$_2$(bipy′)] (broken line).

NB The intensities of the latter spectra are not to scale.

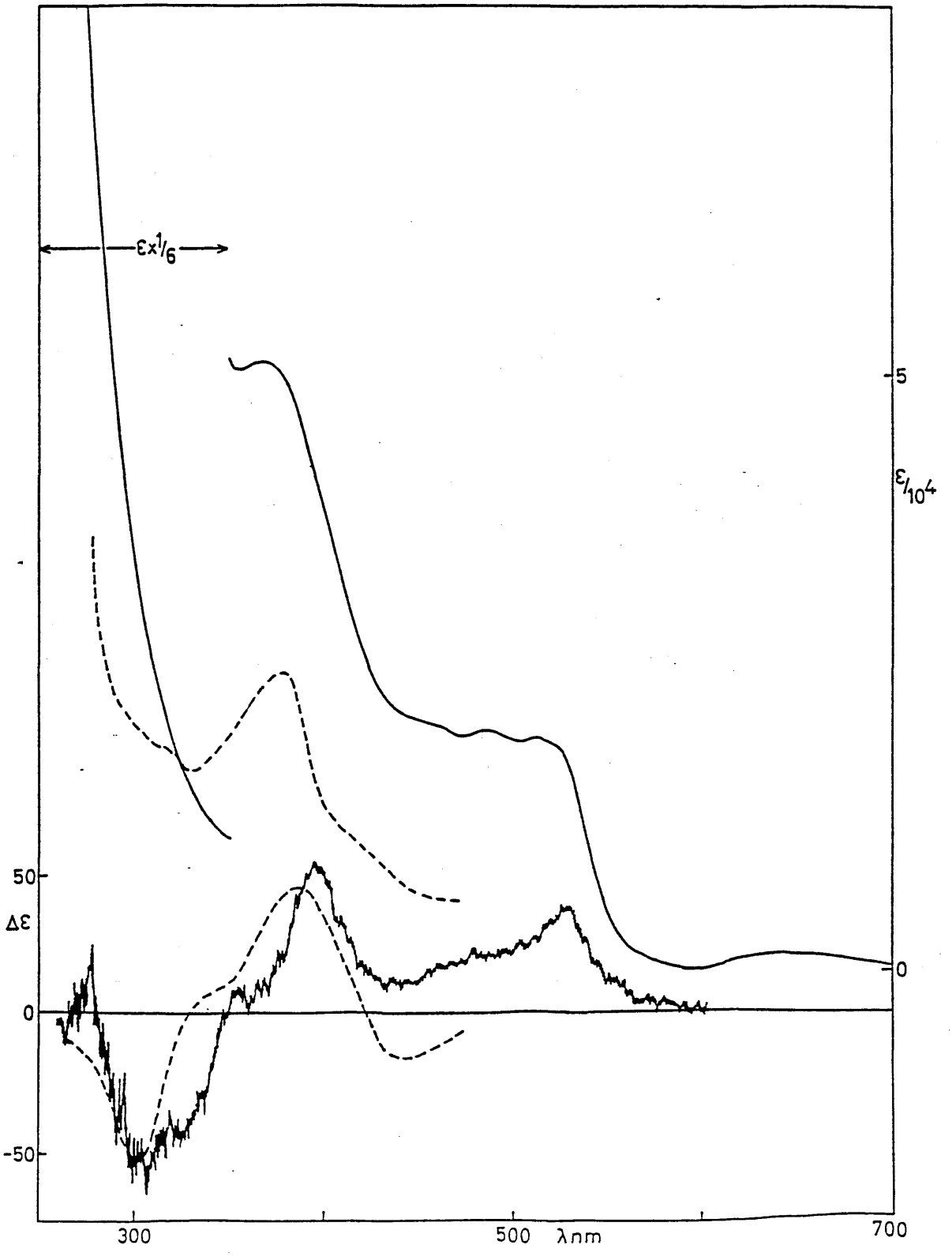

APPENDIX 1

The variation theorem states that the energy of an approximate wave function will always be greater than the lowest eigenvalue of the Hamiltonian. Thus, for a chosen wavefunction which contains variable parameters, if the energy of the function is evaluated in terms of the parameters and then minimised with respect to the parameters, the best approximation to the ground and excited state energies will be obtained.[137] So, if the total wave function, Ψ_j, corresponding to the jth excited state of the assembly, is expressed as a linear combination of the unperturbed singly excited-state wave functions, Φ_i, with mixing coefficients, C_{ij}, (the variation parameters) referring to the ith function of the jth level,

$$\Psi_j = C_{1j}\Phi_1 + C_{2j}\Phi_2 + ... + C_{ij}\Phi_i + ... C_{nj}\Phi_j \qquad (6a)$$

$$\text{or } \Psi = \sum_{i=1}^{n} C_i\Phi_i \qquad (6b)$$

$$\text{then, } E = \frac{\langle\Psi|H|\Psi\rangle}{\langle\Psi|\Psi\rangle} \qquad (6c)$$

and substituting 6b into this gives,

$$\sum_{i=1}^{n}\sum_{j=1}^{n} C_iC_j(H_{ij} - ES_{ij}) = 0 \qquad (6d)$$

$$\text{where } H_{ij} = \langle\Phi_i|H|\Phi_j\rangle \text{ and } S_{ij} = \langle\Phi_i|\Phi_j\rangle \qquad (6e)$$

Differentiating 6d with respect to C_j, keeping the other coefficients constant (remembering that H_{ij} and S_{ij} are constants) gives,

$$2\sum_{i=1}^{n} C_i(H_{ij} - ES_{ij}) - \sum_{i=1}^{n}\sum_{j=1}^{n} C_iC_jS_{ij}\frac{\partial E}{\partial C_j} = 0 \qquad (6f)$$

For an energy minimum, $(\partial E/\partial C_j) = 0$, we have,

$$\sum_{i=1}^{n} C_i(H_{ij} - ES_{ij}) = 0 \qquad (7)$$

There is one equation of this type for every coefficient C_j that can be varied; n equations in all. Now n linear equations in n unknown coefficients of the type in equation 7 are consistent only if the determinant of the factors multiplying the coefficients is zero; that is,

$$|H_{ij} - ES_{ij}| = 0 \qquad (8)$$

The determinant, equation 7, which is called the secular determinant, gives on expansion a polynomial of the nth degree in E. The n values of E obtained by solving the resulting equation all correspond to turning points of the function (6c). The lowest value of E gives the best value for the ground state energy that can be obtained from a function of the type (6b). The coefficients of this function are obtained by substituting this energy back into the set of simultaneous equations (7), and solving in the usual way; this will give the ratio of the coefficients and their absolute value will be obtained by normalising the function.

It can be shown[137] that the solutions of (7) give not only the best ground state function but also the best excited state functions that can be obtained from the limited expansion set (6b) (subject to the restriction that an excited state function is orthogonal to all states

of lower energy).

Expanding equation 8 gives the secular determinant which, for non-trivial solutions to the simultaneous equations, is set to zero.

$$\begin{vmatrix} H_{11} - ES_{11} & H_{12} - ES_{12} & H_{13} - ES_{13} \\ H_{21} - ES_{21} & H_{22} - ES_{22} & H_{23} - ES_{23} \\ H_{31} - ES_{31} & H_{32} - ES_{32} & H_{33} - ES_{33} \end{vmatrix} = 0 \qquad (8a)$$

now $S_{ij} = 1$ when $i = j$, and $S_{ij} = 0$ when $i \neq j$, and for three identical ligands, $H_{11} = H_{22} = H_{33}$ and $H_{12} = H_{13} = H_{23} = H_{31} = H_{21} = H_{32}$, so the secular determinant can be simplified to,

$$\begin{vmatrix} H_{11} - E & H_{12} & H_{12} \\ H_{12} & H_{11} - E & H_{12} \\ H_{12} & H_{12} & H_{11} - E \end{vmatrix} = 0 \qquad (8b)$$

In order that the ground-state interactions may be considered and so that the energies may be expressed as transition energies, the term $H_{00} = \langle \Psi_0 | H | \Psi_0 \rangle$ is subtracted off the diagonal terms in equation 8b,

$$\begin{vmatrix} H_{11} - H_{00} - E & H_{12} & H_{12} \\ H_{12} & H_{11} - H_{00} - E & H_{12} \\ H_{12} & H_{12} & H_{11} - H_{00} - E \end{vmatrix} = 0 \qquad (9)$$

(subraction in this way off the diagonal terms, does not affect the solutions to the secular determinant.) Dividing through by H_{12} and substituting $x = \dfrac{H_{11} - H_{00} - E}{H_{12}}$ gives,

$$\begin{vmatrix} x & 1 & 1 \\ 1 & x & 1 \\ 1 & 1 & x \end{vmatrix} = 0 \qquad (9a)$$

the secular determinant can be solved using,

$$\begin{vmatrix} a & b & c \\ d & e & f \\ g & h & i \end{vmatrix} = a \begin{vmatrix} e & f \\ h & i \end{vmatrix} - b \begin{vmatrix} d & f \\ g & i \end{vmatrix} + c \begin{vmatrix} d & e \\ g & h \end{vmatrix}$$

thus equation 9a can now be written,

$$x \begin{vmatrix} x & 1 \\ 1 & x \end{vmatrix} - 1 \begin{vmatrix} 1 & 1 \\ 1 & x \end{vmatrix} + 1 \begin{vmatrix} 1 & x \\ 1 & 1 \end{vmatrix} = 0 \qquad (9b)$$

hence solving the secular determinant gives,

$$x(x^2 - 1) - 1(x - 1) + 1(1 - x) = 0 \qquad (9c)$$

$$\text{therefore,} \qquad x^3 - 3x + 2 = 0 \qquad (9d)$$

$$\text{so,} \qquad (x - 1)(x - 1)(x + 2) = 0 \qquad (9e)$$

and the roots of this polynomial are therefore,

$$x = 1 \quad \text{or} \quad x = 1 \quad \text{or} \quad x = -2$$

substituting for $x = 1$ gives,

$$\frac{H_{11} - H_{00} - E}{H_{12}} = 1 \qquad \Rightarrow \quad H_{11} - H_{00} - E = H_{12}$$

$$\Rightarrow \quad E = H_{11} - H_{00} - H_{12}$$

and substituting for x = -2 gives,

$$\frac{H_{11} - H_{00} - E}{H_{12}} = -2 \qquad \Rightarrow \quad H_{11} - H_{00} - E = -2H_{12}$$

$$\Rightarrow \quad E = H_{11} - H_{00} + 2H_{12}$$

so the three solutions of the secular determinant are,

$$E = H_{11} - H_{00} - H_{12} \text{ (twice)} \qquad \text{and} \qquad E = H_{11} - H_{00} + 2H_{12} \tag{10}$$

When the total Hamiltonian, H, of the system is split,

$$H = H_1 + H_2 + H_3 + \sum_{i<j}^{3} \theta_{ij} \tag{11}$$

H_{11} can be written,

$$H_{11} = \langle x_1' x_2 x_3 | H_1 + H_2 + H_3 + \sum_{i<j}^{3} \theta_{ij} | x_1' x_2 x_3 \rangle$$

$$\Rightarrow H_{11} = \langle x_1' x_2 x_3 | H_1 + H_2 + H_3 + \theta_{12} + \theta_{13} + \theta_{23} | x_1' x_2 x_3 \rangle$$

expanding out the terms in the equation gives,

$$H_{11} = \langle x_1' | H_1 | x_1' \rangle \langle x_2 x_3 | x_2 x_3 \rangle + \langle x_2 | H_2 | x_2 \rangle \langle x_1' \, x_3 | x_1' \, x_3 \rangle$$
$$+ \langle x_3 | H_3 | x_3 \rangle \langle x_1' \, x_2 | x_1' \, x_2 \rangle + \langle x_1' \, x_2 | \theta_{12} | x_1' \, x_2 \rangle \langle x_3 | x_3 \rangle$$
$$+ \langle x_1' \, x_3 | \theta_{13} | x_1' \, x_3 \rangle \langle x_2 | x_2 \rangle + \langle x_2 x_3 | \theta_{23} | x_2 x_3 \rangle \langle x_1' | x_1' \rangle$$

rearranging gives,

$$H_{11} = \langle x_1' | H_1 | x_1' \rangle \langle x_2 | x_2 \rangle \langle x_3 | x_3 \rangle + \langle x_2 | H_2 | x_2 \rangle \langle x_1' | x_1' \rangle \langle x_3 | x_3 \rangle$$
$$+ \langle x_3 | H_3 | x_3 \rangle \langle x_1' | x_1' \rangle \langle x_2 | x_2 \rangle + \langle x_1' \, x_2 | \theta_{12} | x_1' \, x_2 \rangle \langle x_3 | x_3 \rangle$$
$$+ \langle x_1' \, x_3 | \theta_{13} | x_1' \, x_3 \rangle \langle x_2 | x_2 \rangle + \langle x_2 x_3 | \theta_{23} | x_2 x_3 \rangle \langle x_1' | x_1' \rangle$$

and since x_n and x_n' are orthonormal, $\langle x_i | x_j \rangle$ is equal to unity when $i = j$ and is equal to zero when $i \neq j$, simplifying gives,

$$H_{11} = \langle x_1' | H_1 | x_1' \rangle + \langle x_2 | H_2 | x_2 \rangle + \langle x_3 | H_3 | x_3 \rangle$$
$$+ \langle x_1' \, x_2 | \theta_{12} | x_1' \, x_2 \rangle + \langle x_1' \, x_3 | \theta_{13} | x_1' \, x_3 \rangle$$
$$+ \langle x_2 x_3 | \theta_{23} | x_2 x_3 \rangle \qquad (12)$$

Similarly,

$$H_{00} = \langle x_1 x_2 x_3 | H_1 + H_2 + H_3 + \theta_{12} + \theta_{13} + \theta_{23} | x_1 x_2 x_3 \rangle$$

$$\Longrightarrow H_{00} = \langle x_1 | H_1 | x_1 \rangle + \langle x_2 | H_2 | x_2 \rangle + \langle x_3 | H_3 | x_3 \rangle +$$
$$\langle x_1 x_2 | \theta_{12} | x_1 x_2 \rangle + \langle x_1 x_3 | \theta_{13} | x_1 x_3 \rangle + \langle x_2 x_3 | \theta_{23} | x_2 x_3 \rangle \qquad (13)$$

and,

$$H_{12} = \langle x_1' \, x_2 x_3 | H_1 + H_2 + H_3 + \theta_{12} + \theta_{13} + \theta_{23} | x_1 x_2' \, x_3 \rangle$$

expanding out the terms in the equation gives,

$$H_{12} = \langle x_1' | H_1 | x_1 \rangle \langle x_2 x_3 | x_2' x_3 \rangle + \langle x_2 | H_2 | x_2' \rangle \langle x_1' x_3 | x_1 x_3 \rangle +$$
$$\langle x_3 | H_3 | x_3 \rangle \langle x_1' x_2 | x_1 x_2' \rangle + \langle x_1' x_2 | \theta_{12} | x_1 x_2' \rangle \langle x_3 | x_3 \rangle +$$
$$\langle x_1' x_3 | \theta_{13} | x_1 x_3 \rangle \langle x_2 | x_2' \rangle + \langle x_2 x_3 | \theta_{23} | x_2' x_3 \rangle \langle x_1' | x_1 \rangle$$

rearranging gives,

$$H_{12} = \langle x_1' | H_1 | x_1 \rangle \langle x_2 | x_2' \rangle \langle x_3 | x_3 \rangle + \langle x_2 | H_2 | x_2' \rangle \langle x_1' | x_1 \rangle \langle x_3 | x_3 \rangle +$$
$$\langle x_3 | H_3 | x_3 \rangle \langle x_1' | x_1 \rangle \langle x_2 | x_2' \rangle + \langle x_1' x_2 | \theta_{12} | x_1 x_2' \rangle \langle x_3 | x_3 \rangle +$$
$$\langle x_1' x_3 | \theta_{13} | x_1 x_3 \rangle \langle x_2 | x_2' \rangle + \langle x_2 x_3 | \theta_{23} | x_2' x_3 \rangle \langle x_1' | x_1 \rangle$$

and simplifying as in equation 12 leaves only one term,

$$H_{12} = \langle x_1' x_2 | \theta_{12} | x_1 x_2' \rangle = V_{12} \qquad (14)$$

The solutions of the secular determinant (Equation 10) can now be rewritten in terms of H_{00}, H_{11} and H_{12} (Equations 12 - 14) to give the eigenvalues E_{A_2}, E_E1 and E_E2 (where E_E1 and E_E2 are degenerate in D_3 symmetry),

$$E = H_{11} - H_{00} - H_{12} \qquad (10)$$

substituting for H_{11}, H_{00} and H_{12} gives,

$$E = \langle x_1' | H_1 | x_1' \rangle + \langle x_2 | H_2 | x_2 \rangle + \langle x_3 | H_3 | x_3 \rangle$$
$$+ \langle x_1' x_2 | \theta_{12} | x_1' x_2 \rangle + \langle x_1' x_3 | \theta_{13} | x_1' x_3 \rangle + \langle x_2 x_3 | \theta_{23} | x_2 x_3 \rangle$$
$$- \langle x_1 | H_1 | x_1 \rangle - \langle x_2 | H_2 | x_2 \rangle - \langle x_3 | H_3 | x_3 \rangle - \langle x_1 x_2 | \theta_{12} | x_1 x_2 \rangle$$
$$- \langle x_1 x_3 | \theta_{13} | x_1 x_3 \rangle - \langle x_2 x_3 | \theta_{23} | x_2 x_3 \rangle - \langle x_1' x_2 | \theta_{12} | x_1 x_2' \rangle$$

rearranging gives,

$$E = \langle x_1' | H_1 | x_1' \rangle - \langle x_1 | H_1 | x_1 \rangle + \langle x_2 | H_2 | x_2 \rangle - \langle x_2 | H_2 | x_2 \rangle$$
$$+ \langle x_3 | H_3 | x_3 \rangle - \langle x_3 | H_3 | x_3 \rangle + \langle x_1' x_2 | \theta_{12} | x_1' x_2 \rangle - \langle x_1 x_2 | \theta_{12} | x_1 x_2 \rangle$$
$$+ \langle x_1' x_3 | \theta_{13} | x_1' x_3 \rangle - \langle x_1 x_3 | \theta_{13} | x_1 x_3 \rangle + \langle x_2 x_3 | \theta_{23} | x_2 x_3 \rangle$$
$$- \langle x_2 x_3 | \theta_{23} | x_2 x_3 \rangle - \langle x_1' x_2 | \theta_{12} | x_1 x_2' \rangle$$

now taking the pairs of terms 3 and 4, 5 and 6 and 11 and 12, these cancel to zero; the pairs of terms 7 and 8 and 9 and 10 represent the difference between the static multipole moments of the excited states of the molecules and the static multipole moments of the ground states of the molecules and it has been assumed that this difference is small and can be neglected. The first pair of terms are $E_1' - E_1$ which is equal to ΔE_1, the transition energy of the long-axis polarised $\pi \rightarrow \pi^*$ transition of 2,2′-bipyridine molecule 1 and the last term is equal to V_{12}, the interaction between the transition dipole moments of 2,2′-bipyridine molecules 1 and 2. The first and second solutions of the secular determinant (Equation 10) reduce to,

$$E = \Delta E_1 - V_{12}$$

and by a similar method, the third solution of the secular determinant (Equation 10) reduces to,

$$E = \Delta E_1 + 2V_{12}$$

and the eigenvalues E_{A_2}, $E_E 1$ and $E_E 2$ are equal to,

$$E_{A_2} = \Delta E_1 + 2V_{12}, \qquad E_E{}^1 = E_E 2 = \Delta E_1 - V_{12} \tag{15}$$

To find the mixing coefficients, C_j, in the Hückel secular equation (Equation 7), substitute for x = -2 in the Hückel secular determinant,

$$-2C_1 + C_2 + C_3 = 0 \qquad (15a)$$

$$C_1 - 2C_2 + C_3 = 0 \qquad (15b)$$

$$C_1 + C_2 - 2C_3 = 0 \qquad (15c)$$

subtracting Equation 15b from 15a gives,

$$-3C_1 + 3C_2 = 0$$

hence $C_1 = C_2$, and substituting for C_2 in equation 15a gives,

$$-2C_1 + C_1 + C_3 = 0$$

hence $C_1 = C_3$ and hence $C_1 = C_2 = C_3$

normalising gives,

$C_1^2 + C_2^2 + C_3^3 = 1$, but $C_1 = C_2 = C_3$, therefore,

$3C_1^2 = 1$, therefore $C_1 = C_2 = C_3 = \frac{1}{\sqrt{3}}$

hence $\Psi_{A_2} = \frac{1}{\sqrt{3}} (x_1' x_2 x_3 + x_1 x_2' x_3 + x_1 x_2 x_3')$,

Substituting for x = 1 in the secular determinant gives,

$C_1 + C_2 + C_3 = 0$, $C_1 + C_2 + C_3 = 0$ and $C_1 + C_2 + C_3 = 0$

As the levels are degenerate, this gives 1 equation and three unknowns which is impossible to solve hence an arbitrary choice for one of the coefficients must be made, that is let $C_1 = 0$ hence,

$$C_2 + C_3 = 0 \qquad \text{therefore } C_2 = -C_3$$

normalising gives,

$$C_1^2 + C_2^2 + C_3^2 = 1, \qquad \text{hence } 2C_2^2 = 1, \qquad \text{hence } C_2 = \frac{1}{\sqrt{2}}$$

$$\text{and } C_3 = -C_2 = -\frac{1}{\sqrt{2}}, \qquad \text{hence,}$$

$$\Psi_E 2 = \frac{1}{\sqrt{2}} (x_1 x_2' x_3 - x_1 x_2 x_3')$$

To solve for $\Psi_E 1$, use the orthogonality relations,

$$\langle \Psi_{A_2} | \Psi_E 2 \rangle = \langle \Psi_{A_2} | \Psi_E 1 \rangle = \langle \Psi_E 2 | \Psi_E 1 \rangle = 0$$

and let $\Psi_E 1 = a\Phi_1 + b\Phi_2 + c\Phi_3$, hence as $\langle \Psi_A 2 | \Psi_E 1 \rangle = 0$, substituting for Ψ_{A_2} and $\Psi_E 1$ using Equation 5 gives,

$$\frac{1}{\sqrt{3}} \langle \Phi_1 + \Phi_2 + \Phi_3 | a\Phi_1 + b\Phi_2 + c\Phi_3 \rangle = 0$$

the only non-zero terms are,

$$\frac{a}{\sqrt{3}} \langle \Phi_1 | \Phi_1 \rangle + \frac{b}{\sqrt{3}} \langle \Phi_2 | \Phi_2 \rangle + \frac{c}{\sqrt{3}} \langle \Phi_3 | \Phi_3 \rangle = 0, \text{ hence}$$

$$\frac{a}{\sqrt{3}} + \frac{b}{\sqrt{3}} + \frac{c}{\sqrt{3}} = 0, \qquad \text{hence,} \qquad a + b + c = 0 \qquad (15d)$$

and $\langle \Psi_E 2 | \Psi_E 1 \rangle = 0,$

substituting for $\Psi_E 2$ and $\Psi_E 1$ using Equation 5 gives,

$$\frac{1}{\sqrt{2}} \langle \Phi_2 - \Phi_3 | a\Phi_1 + b\Phi_2 + c\Phi_3 \rangle = 0$$

the only non zero terms are,

$$\frac{b}{\sqrt{2}} \langle \Phi_2 | \Phi_2 \rangle - \frac{c}{2} \langle \Phi_3 | \Phi_3 \rangle = 0$$

hence $\frac{b}{\sqrt{2}} - \frac{c}{\sqrt{2}} = 0,$ hence $b = c$

Substitute $b = c$ in Equation 15d giving, $a + 2b = 0$, hence $b = \frac{-a}{2}$

Normalising gives

$$a^2 + b^2 + c^2 = 1, \quad \text{hence,} \quad a^2 + 2\left(-\frac{a}{2}\right)^2 = 1$$

$$\text{hence} \quad \frac{3}{2} a^2 = 1, \quad \text{hence,} \quad a = \frac{\sqrt{2}}{\sqrt{3}}$$

and so $b = c = -\frac{1}{\sqrt{6}}$

$$\text{hence} \quad \Psi_E 1 = \frac{\sqrt{2}}{\sqrt{3}} (\Phi_1) - \frac{1}{\sqrt{6}} (\Phi_2 + \Phi_3) = \frac{1}{\sqrt{6}} (2\Phi_1 - \Phi_2 - \Phi_3)$$

$$\text{hence} \quad \Psi_E 1 = \frac{1}{\sqrt{6}} (2x_1' x_2 x_3 - x_1 x_2' x_3 - x_1 x_2 x_3')$$

APPENDIX 2

As before (Appendix 1), expanding Equation 8 gives the secular determinant which, for non-trivial solutions to the simultaneous equations, is set to zero,

$$\begin{vmatrix} H_{11} - ES_{11} & H_{12} - ES_{12} & H_{13} - ES_{13} \\ H_{21} - ES_{21} & H_{22} - ES_{22} & H_{23} - ES_{23} \\ H_{31} - ES_{31} & H_{32} - ES_{32} & H_{33} - ES_{33} \end{vmatrix} = 0 \qquad (20a)$$

For a hetero-trischelated complex where ligand 1 = 2 ≠ 3, $H_{11} = H_{22} \neq H_{33}$ and $H_{12} = H_{21} \neq H_{13} = H_{31} = H_{23} = H_{32}$, so the secular determinant (20a) can be simplified to,

$$\begin{vmatrix} H_{11} - E & H_{12} & H_{13} \\ H_{12} & H_{11} - E & H_{13} \\ H_{13} & H_{13} & H_{33} - E \end{vmatrix} = 0 \qquad (20b)$$

In order that the ground-state interactions may be considered and so that the energies may be expressed as transition energies, the term $H_{00} = \langle \Psi_0 | H | \Psi_0 \rangle$ is subtracted off the diagonal terms in Equation 20b,

$$\begin{vmatrix} H_{11} - H_{00} - E & H_{12} & H_{13} \\ H_{12} & H_{11} - H_{00} - E & H_{13} \\ H_{13} & H_{13} & H_{33} - H_{00} - E \end{vmatrix} = 0 \qquad (20c)$$

Substituting $a = H_{11} - H_{00} - E$, $b = H_{33} - H_{00} - E$, $c = H_{12}$ and $d = H_{13}$ into Equation 20 c gives,

$$\begin{vmatrix} a & c & d \\ c & a & d \\ d & d & b \end{vmatrix} = 0 \qquad (20d)$$

The secular determinant can be manipulated by adding and subtracting pairs of rows and columns and dividing by two, as follows,

$$\begin{vmatrix} a & c & d \\ c & a & d \\ d & d & b \end{vmatrix} = \tfrac{1}{2} \begin{vmatrix} a+c & c-a & d \\ c+a & a-c & d \\ 2d & 0 & b \end{vmatrix} = \tfrac{1}{4} \begin{vmatrix} 2(a+c) & 0 & 2d \\ 0 & 2(a-c) & 0 \\ 2d & 0 & b \end{vmatrix} = \tag{20e}$$

and as the secular determinant is equal to zero, Equation 20 e can be simplified to,

$$\begin{vmatrix} 2(a+c) & 0 & 2d \\ 0 & 2(a-c) & 0 \\ 2d & 0 & b \end{vmatrix} = 0 \tag{20f}$$

Now if any two rows or two columns in the matrix are interchanged, the sign of the secular determinant is reversed, therefore exchanging columns 1 and 2 in Equation 20f gives,

$$- \begin{vmatrix} 0 & 2(a+c) & 2d \\ 2(a-c) & 0 & 0 \\ 0 & 2d & b \end{vmatrix} = 0 \tag{20g}$$

and exchanging rows 1 and 2 in Equation 20g gives,

$$\begin{vmatrix} 2(a-c) & 0 & 0 \\ 0 & 2(a+c) & 2d \\ 0 & 2d & b \end{vmatrix} = 0 \tag{20h}$$

The matrix in Equation 20h can be rewritten as,

$$2(a - c) \begin{vmatrix} 2(a + c) & 2d \\ 2d & b \end{vmatrix} = 0 \qquad (20i)$$

Substituting back into Equation 20i for a, b, c and d gives,

$$2(H_{11} - H_{00} - E - H_{12}) \begin{vmatrix} 2(H_{11} - H_{00} - E + H_{12}) & 2H_{13} \\ 2H_{13} & H_{33} - H_{00} - E \end{vmatrix} = 0 \qquad (21)$$

and substituting for H_{11}, H_{00}, H_{12} and H_{13} (Appendix 1, Equations 11 to 14) and eliminating the factor of 2 outside the determinant gives,

$$(\Delta E_1 - V_{12} - E) \begin{vmatrix} 2(\Delta E_1 + V_{12} - E) & 2V_{13} \\ 2V_{13} & \Delta E_3 - E \end{vmatrix} = 0 \qquad (25)$$

The solutions to the secular determinant are therefore,

$$\Delta E_1 - V_{12} - E = 0 \qquad \text{which gives } E = \Delta E_1 - V_{12} = E_A \qquad (26)$$

$$\text{and} \quad \begin{vmatrix} 2(\Delta E_1 + V_{12} - E) & 2V_{13} \\ 2V_{13} & \Delta E_3 - E \end{vmatrix} = 0 \qquad (26a)$$

which gives,

$$2(\Delta E_1 + V_{12} - E).(\Delta E_3 - E) - 4V_{13}^2 = 0 \qquad (26b)$$

expanding out the equation and eliminating a factor of 2 gives,

$$\Delta E_1 \Delta E_3 - \Delta E_1 E + \Delta E_3 V_{12} - V_{12} E - \Delta E_3 E + E^2 - 2V_{13}^2 = 0 \qquad (26c)$$

which upon rearringing gives,

$$E^2 + E(-\Delta E_1 - \Delta E_3 - V_{12}) + (\Delta E_1\Delta E_3 + \Delta E_3 V_{12} - 2V_{13}^2) = 0 \qquad (26d)$$

The factors of E for an equation of this form are given by,

$$\frac{-b \pm (b^2 - 4(a.c))^{\frac{1}{2}}}{2a} \quad \text{where in this case, } a = 1$$

$$b = (-\Delta E_1 - \Delta E_3 - V_{12}) \text{ and } C = (\Delta E_1\Delta E_3 + \Delta E_3 V_{12} - 2V_{13}^2)$$

Therefore the solutions to Equation 26d are,

$$E = \frac{\Delta E_1 + \Delta E_3 + V_{12} + \left\{(-\Delta E_1 - \Delta E_3 - V_{12})^2 - 4(\Delta E_1\Delta E_3 + \Delta E_3 V_{12} - 2V_{13}^2)\right\}^{\frac{1}{2}}}{2}$$

$$= E_B^+ \qquad (27)$$

and,

$$E = \frac{\Delta E_1 + \Delta E_3 + V_{12} - \left\{(-\Delta E_1 - \Delta E_3 - V_{12})^2 - 4(\Delta E_1\Delta E_3 + \Delta E_3 V_{12} - 2V_{13}^2)\right\}^{\frac{1}{2}}}{2}$$

$$= E_B^- \qquad (28)$$

Note that the conservation laws for both dipole strength and rotational strength hold, as shown by,

$$D_A + D_B^+ + D_B^- = 2p_1^2 + p_3^2 = p_1^2 + p_2^2 + p_3^2 \qquad (41)$$

For the proof, substitute for $D_A + D_B^+ + D_B^-$ (Equations 35, 37 and 39) in Equation 41,

$$\frac{1}{2}p_1^2 + (C_1^+)^2\frac{3}{2}p_1^2 + (C_2^+)^2 p_3^2 + C_1^+C_2^+\sqrt{2}p_1p_3 + (C_1^-)^2\frac{3}{2}p_1^2 +$$

$$(C_2^-)^2p_3^2 + C_1^-C_2^-\sqrt{2}p_1p_3 = 2p_1^2 + p_3^2 \qquad (41a)$$

but $C_1^+C_2^+ = -C_1^-C_2^-$, therefore cancelling terms in 41a gives,

$$\frac{1}{2}p_1^2 + (C_1^+)^2\frac{3}{2}p_1^2 + (C_1^-)^2\frac{3}{2}p_1^2 + (C_2^+)^2p_3^2 + (C_2^-)^2p_3^2 = 2p_1^2 + p_3^2 \qquad (41b)$$

rearranging gives,

$$\frac{1}{2}p_1^2 + \frac{3}{2}p_1^2\left[(C_1^+)^2 + (C_1^-)^2\right] + p_3^2\left[(C_2^+)^2 + (C_2^-)^2\right] = 2p_1^2 + p_3^2 \qquad (41c)$$

Now the left-hand side will equal the right-hand side if

$$\left[(C_1^+)^2 + (C_1^-)^2\right] = 1 \quad \text{and} \quad \left[(C_2^+)^2 + (C_2^-)^2\right] = 1$$

so substituting for C_1^+ and C_1^- (Equations 32 and 33) gives,

$$\left\{\frac{-\sqrt{2}V_{13}}{(2V_{13}^2 + L^2)^{\frac{1}{2}}}\right\}^2 + \left\{\frac{L}{(2V_{13}^2 + L^2)^{\frac{1}{2}}}\right\}^2 = 1 \qquad (41d)$$

therefore,

$$\frac{2V_{13}^2}{2V_{13}^2 + L^2} + \frac{L_2}{2V_{13}^2 + L^2} = 1 \qquad (41e)$$

adding the two terms gives,

$$\frac{2V_{13}^2 + L^2}{2V_{13}^2 + L^2} = 1 \qquad (41f)$$

and $[(C_1^+)^2 + (C_1^-)^2] = [(C_2^+)^2 + (C_2^-)^2]$

therefore the left-hand side of Equation 41c equals the right-hand side, and so $D_A + D_B^+ + D_B^- = p_1^2 + p_2^2 + p_3^2$ (41)

For the proof of equation 42, substitute for R_A, R_B^+ and R_B^- (Equations 36, 38 and 40 respectively),

$$-\frac{1}{\sqrt{2}}\pi \bar{v}_1 r_1 p_1^2 + (C_1^+)^2 \frac{1}{\sqrt{2}}\pi \bar{v}_1 r_1 p_1^2 + C_1^+ C_2^+ \pi \bar{v}_1 r_1 p_1 p_3 +$$

$$C_1^+ C_2^+ \pi \bar{v}_3 r_3 p_1 p_3 + (C_1^-)^2 \frac{1}{\sqrt{2}}\pi \bar{v}_1 r_1 p_1^2 + C_1^- C_2^- \pi \bar{v}_1 r_1 p_1 p_3 +$$

$$C_1^- C_2^- \pi \bar{v}_3 r_3 p_1 p_3 = 0 \qquad (42a)$$

and as $C_1^+ C_2^+ = -C_1^- C_2^-$, cancelling terms leaves,

$$-\frac{1}{\sqrt{2}}\pi \bar{v}_1 r_1 p_1^2 + (C_1^+)^2 \frac{1}{\sqrt{2}}\pi \bar{v}_1 r_1 p_1^2 + (C_1^-)^2 \frac{1}{\sqrt{2}}\pi \bar{v}_1 r_1 p_1^2 = 0 \qquad (42b)$$

rearranging gives,

$$\frac{1}{\sqrt{2}}\pi \bar{v}_1 r_1 p_1^2 [(C_1^+)^2 + (C_1^-)^2 - 1] = 0 \qquad (42c)$$

but from Equation 41f, $[(C_1^+)^2 + (C_1^-)^2] = 1$, therefore Equation 42c is satisfied and $R_A + R_B^+ + R_B^- = 0$ (42)

APPENDIX 3

The concentration of $\underline{I}$ when $\underline{I}^-$, $\underline{I}^{2-}$ and $\underline{I}^{3-}$ are electrogenerated can be calculated using the Nernst equation:

$$E = E^\circ - \frac{RT}{nF} \ln \frac{a_{ox}}{a_{red}} \qquad (47)$$

$$\Rightarrow E = E^\circ - \frac{RT}{nF} (\ln a_{ox} - \ln a_{red}) \qquad (47a)$$

rearranging and dividing through by $\frac{RT}{nF}$ gives,

$$\ln a_{ox} = (E - E^\circ) \frac{nF}{RT} + \ln a_{red} \qquad (47b)$$

The calculation of a_{ox} is now straightforward providing the following simplifying assumptions are made;

i) the concentration of the complex in the solution is low and so will be approximately equal to the activity of the complex in the solution,

ii) the system is completely reversible and so $E_{\frac{1}{2}} = E^\circ$.

The concentration of $\underline{I}$ when $\underline{I}^-$ is electrogenerated is calculated substituting E = -1.78 V, E° = -1.58 V, n = 1 $moll^{-1}$, F = 9.6487×10^4 C mol^{-1}, R = 8.314 JK^{-1} mol^{-1}, T = 293K and $a_{red} = a_{\underline{I}^-} = 5 \times 10^{-4}$ $moll^{-1}$ into Equation 47b, hence;

$$\ln a_{\underline{I}} = \frac{(-1.78 - (-1.58)) \times 1 \times 9.6487 \times 10^4}{293 \times 8.314} + \ln 5 \times 10^{-4}$$

$$\Rightarrow \ln a_{\underline{I}} = -7.92 + (-7.60)$$

$$\Rightarrow \ln a_{\underline{I}} = -15.52$$

$$\Rightarrow a_{\underline{I}} = 1.81 \times 10^{-7} \text{moll}^{-1}$$

The concentration of $\underline{I}$ when $\underline{I}^{2-}$ is electrogenerated is calculated substituting E = - 2.00 V and E° = - 1.58 V into Equation 47b,

$$\ln a_{\underline{I}} = \frac{(-2.00 - (-1.58)) \times 1 \times 9.6487 \times 10^4}{293 \times 8.314} + \ln 5 \times 10^{-4}$$

$$\Rightarrow \ln a_{\underline{I}} = -16.64 + (-7.60)$$

$$\Rightarrow \ln a_{\underline{I}} = -24.24$$

$$\Rightarrow a_{\underline{I}} = 2.98 \times 10^{-11} \text{ moll}^{-1}$$

The concentration of $\underline{I}$ when $\underline{I}^{2-}$ is electrogenerated is calculated substituting E = -2.30 V and E° = -1.58 V into Equation 47b,

$$\ln a_{\underline{I}} = \frac{(-2.30 - (-1.58)) \times 1 \times 9.6487 \times 10^4}{293 \times 8.314} + \ln 5 \times 10^{-4}$$

$$\Rightarrow \ln a_{\underline{I}} = -28.52 + (-7.60)$$

$$\Rightarrow \ln a_{\underline{I}} = -36.12$$

$$\Rightarrow a_{\underline{I}} = 2.06 \times 10^{-16} \text{ moll}^{-1}$$

REFERENCES

1 Blau F; Ber dt chem Ges, 1888, 21, 1077

2 Blau F; Sber Akad Wiss Wien Abt II^b Chemie, 1898, 107, 767

3 Werner A; Z anorg Chem, 1893, 3, 267

4 Werner A; Ber dt chem Ges, 1911, 44, 1887

5 Werner A; Ber dt chem Ges, 1912, 45, 433

6 Chapman R P, Hammett L P and Walden G H; J Am Chem Soc, 1931, 53, 3908

7 Brandt W W, Dwyer F P and Gyarfas E C; Chem Rev, 1954, 54, 959

8 Burstall F H; J Chem Soc, 1936, 173

9 Burstall F H; Dwyer F P and Gyarfas E C; J Chem Soc, 1950, 953

10 Dwyer F P and Gyarfas E C; J Proc R Soc N S W, 1949, 83, 174

11 Jaeger F M and van Dijk J A; Chem Abstr, 1935, 29, 1733

12 Dollimore L S and Gillard R D; J Chem Soc, Dalton Trans, 1973, 933

13 Mason S F, Peart B J and Waddell R E; J Chem Soc, Dalton Trans, 1973, 944

14 Demas J N and Flynn C M Jr; J Am Chem Soc, 1974, 96, 1959

15 Palmer R A and Piper T S; Inorg Chem 1966, 5, 864

16 Felix F, Ferguson J, Güdel H U and Ludi A; Chem Phys Lett, 1979, 62, 153

17 Felix F, Ferguson J, Güdel H U and Ludi A; J Am Chem Soc, 1980, 102, 4096

18 Decurtins S, Felix F, Ferguson J, Güdel H U and Ludi A; J Am Chem Soc, 1980, 102, 4102

19 Ferguson J and Herren F; Chem Phys Lett, 1982, 89, 371

20 Kalyanansundaram K; Co-ord Chem Rev, 1982, 46, 159

21 McCaffery A J, Mason S F and Norman B J; J Chem Soc (A), 1969, 1428

22 Mason S F and Peart B J; J Chem Soc, Dalton Trans, 1973, 949

23 Harding M J, Mason S F and Peart B J; J Chem Soc, Dalton Trans, 1973, 955

24 Belser P, Daul C and Von Zelewsky A; Chem Phys Lett, 1981, 79, 596

25 Ferguson J, Herren F and McLaughlin G M; Chem Phys Lett, 1982, 89, 376

26 Brandt W W and Paris J P; J Am Chem Soc, 1959, 81, 5001

27 Porter G B and Schläfer H L; Ber Bunsen-Ges Phys Chem, 1964, 68, 316

28 Crosby G A, Perkins W G and Klassen D M; J Chem Phys, 1965, 43, 1498

29 Crosby G A and Klassen D M; J Chem Phys, 1968, 48, 1853

30 Hercules P M and Lytle F E; J Am Chem Soc, 1969, 91, 253

31 Crosby G A and Demas J N; J Am Chem Soc, 1971, 93, 2841

32 Crosby G A and Harrigan R W; J Chem Phys, 1973, 59, 3468

33 Crosby G A and Elfring W H; J Phys Chem, 1976, 80, 2206

34 Creutz C and Sutin N; Adv Chem Ser, 1978, 168, 1

35 Crosby G A and Elfring W H, J Am Chem Soc, 1981, 103, 2683

36 Jones D S, Levy H A and Rillema D P; J Chem Soc Chem Commun, 1979, 849

37 Fujita I and Kobayashi H; Inorg Chem, 1973, 12, 2758

38 Carlin C M, DeArmond M K and Huang W L; Inorg Chem, 1980, 19, 62

39 Hipps K W; Inorg Chem 1980, 19, 1390

40 Dallinger R F and Woodruff W H; J Am Chem Soc, 1979, 101, 4391

41 Forster M and Hester R E; Chem Phys Lett, 1981, 81, 42

42 Bradley P G, Dallinger R F, Hornberger B A, Kress N and Woodruff W H; J Am Chem Soc, 1981, 103, 7441

43 Gratzel M, Infelta P P and Lachish U; Chem Phys Lett, 1979, 62, 317

44 Balzani B, Bensasson R V and Salet C; C R Seances Acad Sci Ser B, 1979, 289, 41

45 Chou M, Creutz C, Netzel T L, Okumura M and Sutin N; J Am Chem Soc, 1980, 102, 1309

46 Braterman P S, Harriman A, Heath G A and Yellowlees L J; J Chem Soc, Dalton Trans, 1983, 1801

47 Carlin M and DeArmond M K; Chem Phys Lett, 1982, 89, 297

48 Ferguson J and Krausz E R; Chem Phys Lett, 1982, 93, 21

49 Ferguson J and Herren F; Chem Phys, 1983, 76, 45

50 Gallhuber E, Kunkely H, Vogler A and Yersin H; J Am Chem Soc, 1983, 105, 4155

51 Gallhuber E and Yersin H; J Am Chem Soc, 1984, 106, 6582

52 Braterman P S; Inorg Chem, 1986, 25, 1732

53 Ferguson J, Krausz E R and Maeder M; J Phys Chem, 1985, 89, 1852

54 Ferguson J and Krausz E; Chem Phys Lett, 1986, 127, 551

55 Gold J S, Kliger D S and Milder S J; J Phys Chem, 1986, 90, 548

56 Bard A J and Tokel N E; J Am Chem Soc, 1972, 94, 2862

57 Bard A J, Hemingway R E and Tokel-Takvoryan N E; J Am Chem Soc, 1973, 95, 6582

58 Aoyagui S and Saji T; J Electroanal Chem Interfacial Chem, 1975, 58, 401

59 DeArmond M K, Hanck K W, Morris D E, Neveux Jr P E, Ohsawa Y and Whitten D G; J Am Chem Soc, 1983, 105, 6522

60 DeArmond M K, Hanck K and Motten A G; Chem Phys Lett, 1981, 79, 541

61 DeArmond M K, Hanck K W and Morris D E; J Am Chem Soc 1983, 105, 3032

62 DeArmond M K, Hanck K W and Morris D E; Inorg Chem, 1985, 24, 977

63 Braterman P S, Heath G A and Yellowlees L J; J Chem Soc, Chem Commun, 1981, 287

64 Angel S M, DeArmond M K, Donohoe R J, Hanck K W and Wertz D W; J Am Chem Soc, 1984, 106, 3688

65 Angel S M, DeArmond M K, Donohoe R J and Wertz D W; J Phys Chem, 1985, 89, 282

66 Braterman P S, Heath G A and Yellowlees L J; Chem Phys Lett, 1982, 92, 646

67 Ohsawa Y, DeArmond M K, Hanck K W and Moreland C G; J Am Chem Soc, 1985, 107, 5383

68 Braterman P S, Heath G A and Yellowlees L J; J Chem Soc, Dalton Trans, 1985, 1081

69 DeArmond M K, Hanck K W and Wertz D W, Coord Chem Rev, 1985, 64, 65

70 Konig E and Kremer S; Chem Phys Lett, 1970, 5, 87

71 Bruin F, Bruin M, Heineken F W and Zahlan A; J Chem Phys 1962, 37, 683

72 Henning J C M; J Chem Phys, 1966, 44, 2139

73 Bolton J R, Dos Santos Veiga J and Reynold W L; J Chem Phys, 1966, 44, 2214

74 Fischer H and Konig E; Z Naturforsch, A: Astrophys, Phys Phys Chem, 1962, 17, 1063

75 Mason S F and Norman B J; Chem Phys Lett, 1968, 2, 22

76 Mason S F; Inorg Chim Acta Rev, 1968, 2, 89

77 Mason S F and Norman B J; J Chem Soc (A), 1969, 1442

78 Bosnich B; Inorg Chem, 1968, 7, 2379

79 Bosnich B; Acc Chem Res, 1969, 2, 266

80 Fresnel A; Annales chimie physique, 1825, 28, 147

81 Darlak R S, Newman M S and Tsai L; J Am Chem Soc, 1967, 89, 6191

82 Eyring H, Kauzmann W J and Walter J E; Chem Rev, 1940, 26, 339

83 Moscowitz A; Adv Chem Phys, 1962, 4, 67

84 Schellman J A; J Chem Phys, 1966, 44, 55

85 Schellman J A; Acc Chem Res, 1968, 1, 144

86 Kuhn W; Z Phys Chem, 1929, B4, 14

87 Kuhn W; Trans Faraday Soc, 1930, 26, 293

88 Kuhn W; Annu Rev Phys Chem, 1958, 9, 417

89 Kirkwood J G; J Chem Phys, 1937, 5, 479

90 Moffitt W; J Chem Phys, 1956, 25, 467

91 Grinter R and Mason S F; Trans Faraday Soc, 1964, 60, 274

92 Larsen E, Mason S F and Searle G H; Acta Chem Scand, 1966, 20, 191

93 Mason J (Banus) and Mason S F; Tetrahedron, 1967, 23, 1919

94 McCaffery A J, Mason S F and Norman B J; Proc Chem Soc, 1964, 259

95 Day P and Sanders N; J Chem Soc (A), 1967, 1530

96 Day P and Sanders N; J Chem Soc (A), 1967, 1536

97 Kemp C M and Mason S F; Chem Commun, 1965, 559

98 Kemp C M and Mason S F; Tetrahedron, 1966, 22, 629

99 Roberts J L and Sawyer D T; Experimental Electrochemistry For Chemists, P54, Wiley-Interscience, New York, 1974

100 Winfield J M; J Fluorine Chem, 1984, 25, 91

101 Coetzee J F; Recommended Methods for Purification of Solvents and Tests for Impurities, P32, Pergamon Press 1982

102 Ta-shue Chou, Jeh-jing Yuan and Chung-huang Tsao; J Chem Res (S), 1985, 18

103 Harrington J S, Van Houten J and Watts R J, J Am Chem Soc, 1977, 99, 2179

104 Meyer T J and Sullivan B P; J Chem Soc, Chem Commun, 1984, 403

105 Stewart B; PhD Thesis, King's College London, 1976

106 Elschner B and Herzog S; Archives Sciences, 1958, 11, (Fasc Spec), 160

107 Reynolds W L; J Phys Chem, 1963, 67, 2866

108 Kaim W; Chem Ber, 1981, 114, 3789

109 Kaim W; J Am Chem Soc, 1982, 104, 3833

110 Gustav K and Herzog S; Z Anorg Allg Chem, 1966, 346, 150

111 Mahon C and Reynolds W L; Inorg Chem, 1967, 6, 1927

112 Pappalardo R; Inorg Chim Acta, 1968, 2, 209

113 Konig E and Lindner E; Spectrochim Acta Part A, 1972, 28, 1393

114 Orgel L E; J Chem Soc, 1961, 3, 3683

115 Bellamy L J; Advances in Infrared Group Frequencies, Chapman and Hall Limited, 1975

116 Nakamoto K; Infrared Spectra of Inorganic and Co-ordination Compounds, John Wiley and Sons Inc, 2nd Edition, 1970

117 Strukl J S and Walter J L; Spectrochim Acta, Part A, 1971, 27, 209

118 Gondo Y and Kanda Y; Bull Chem Soc Jpn, 1965, 38, 1187

119 Merritt L L Jr and Schroeder E D; Acta Crystallographica, 1956, 9, 801

120 Fielding P E and LeFèvre R J W; J Chem Soc, 1951, 2, 1811

121 Hatada K, Okamoto Y and Takada T; Chem Lett, 1984, 757

122 Mason S F; Theory II in Optical Rotatory Dispersion and Circular Dichroism in Organic Chemistry, Ed by Snatzke G, Heyden and Sons Limited, 1967

123 Nernst W H; Z phys Chem, 1888, 2, 613

124 Nernst W H; Z phys Chem, 1889, 4, 129

125 Bard A J and Faulkner L R; Electrochemical Methods. Fundamentals and Applications, John Wiley and Sons, 1980

126 Yellowlees L J; PhD Thesis, University of Edinburgh, 1982

127 Peacock R D and Stewart B; Co-ord Chem Rev, 1982, 46, 129

128 Ballard R E, McCaffery A J and Mason S F, J Chem Soc 1965, 2, 2883

129 Mason S F, Peacock R D and Prosperi T; J Chem Soc Dalton Trans, 1977, 1, 702

130 McWhinnie W R and Miller J D; Adv Inorg Chem Radiochem, 1969, 12, 135

131 CRC Handbook of Chemistry and Physics, 63rd Edition, 1982-83, Ed by Weast R C and Astle M J

132 Kahl J L, Hanck K and DeArmond K; J Inorg Nucl Chem, 1979, 41, 495

133 Kahl J L, Hanck K W and DeArmond K; J Phys Chem, 1978, 82, 540

134 Coombe V T, Heath G A, MacKenzie A J and Yellowlees L J; Inorg Chem, 1984, 23, 3423

135 Noble B C, BSc Thesis, University of Glasgow, 1983

136 Braterman P S, Heath G A, MacKenzie A J, Noble B C, Peacock R D and Yellowlees L J; Inorg Chem, 1984, 23, 3425

137 Kettle S F A, Murrell J N and Tedder J M; Valence Theory, John Wiley and Sons Limited, 2nd Edition, 1966